Probing Local Environments in Ionic Liquids

by

TATIANA A. FADEEVA

A Dissertation submitted to the

Graduate School-New Brunswick

Rutgers, The State University of New Jersey

in partial fulfillment of the requirements

for the degree

of Doctor of Philosophy

Graduate Program in Chemistry and Chemical Biology

written under the direction of

Edward W. Castner Jr.

and approved by

_____

_____

_____

_____

_____

New Brunswick, New Jersey

October 2011

ABSTRACT OF THE DISSERTATION

Probing Local Environments in Ionic Liquids

by TATIANA A. FADEEVA

Dissertation Director:
Edward W. Castner Jr.

The polarity and solvation properties were investigated for four ionic liquids with non-aromatic cation. The four ionic liquids studied were: *N*-methyl-*N*-butylpyrrolidinium bis(trifluoromethylsulfonyl)-imide ($Pyrr_{14}^{+}/NTf_2^{-}$), *N*-methyl-*N*-ethoxyethylpyrrolidinium bis(trifluoromethylsulfonyl)-imide ($Pyrr_{1(202)}^{+}/NTf_2^{-}$), *N*-methyl-tri-*N*-butylammonium bis(trifluoromethylsulfonyl) -imide (N_{1444}^{+}/NTf_2^{-}) and *N*-hexyl-tri-*N*-butylammonium bis(trifluoromethylsulfonyl) -imide (N_{6444}^{+}/NTf_2^{-}). The ammonium based ILs exhibit slightly higher polarity than pyrrolidinium based ILs. The solvation dynamics of the fluorescence probe molecule Coumarin 153 exhibits multi-exponential character in all four ILs. The observed solvation dynamics occur on timescales orders of magnitude longer than for most organic solvents. The reorientational dynamics investigated by method of time-resolved fluorescence anisotropy decay is faster than predicted by hydrodynamic theory.

The ionic liquid/water interaction were characterized for hydrophobic and water-miscible ionic liquids. The two ionic liquids studied were: 1-butyl-1-methyl-pyrrolidinium bis(trifluoromethylsulfonyl)amide ($Pyrr_{14}^{+}/NTf_2^{-}$) and 1-butyl-1-methylpyrrolidinium Triflormethylsulfonate ($Pyrr_{14}^{+}/OTf^{-}$). The concentration

dependence of water proton chemical shift δ_{H2O} reveals different water-anion interaction in these two ILs.

The diffusion properties were investigated in the system IL/water by pulse gradient DOSY experiments. The diffusional behavior of cations and anions is very similar whereas water exhibits anomalously high diffusion rate. The diffusional properties of water are different in two ILs. The ratio D_{H2O} / D_{cation} is higher for more hydrophobic $Pyrr_{14}^{+}$ /NTf_2^{-} that confirms weaker water-anion interaction in this liquid.

Contents

List of Figures

List of Tables

Abbreviations and Terms

BASIL: Biphasic Acid Scavenging utilizing Ionic Liquids

β-BBO: Beta Barium Borate crystal

C153: coumarin 153

C_8mim^+/PF_6^- : 1-methyl-3-octylimidazolium hexafluorophosphate

DBPPSTE: Bipolar Pulse Pair Stimulated Echo Experiment

DOSY: diffusional ordered spectroscopy

DSC: dynamic scanning calorimetry

IL: ionic liquids

K-F: Karl-Fisher titration

MCP-PMT: micro channel plate photomultiplier tube

MD: molecular dynamic simulation method

NMR: nuclear magnetic resonance spectroscopy

OHDRIKES: optical heterodyne detected Raman-induced Kerr effect spectroscopy

OD: outer diameter

PGSE: Pulse Gradient Spin Echo method

$Pyrr_{14}^+/NTf_2^-$: *N*-methyl-*N*-butylpyrrolidinium bis(trifluoromethylsulfonyl)-imide

$Pyrr_{1(202)}^{+}/NTf_2^{-}$: *N*-methyl-*N*-ethoxyethylpyrrolidinium bis(trifluoromethylsulfonyl)-imide

$Pyrr_{14}^{+}/OTf^{-}$: 1-butyl-1-methylpyrrolidinium Trifloromethylsulfonate

N_{1444}^{+}/NTf_2^{-}: *N*-methyl-tri-*N*-butylammonium bis(trifluoromethylsulfonyl)-imide

N_{6444}^{+}/NTf_2^{-}: *N*-hexyl-tri-*N*-butylammonium bis(trifluoromethylsulfonyl)-imide

S-E: Stokes-Einstein hydrodynamic model

S-E-D: Stokes-Einstein-Debye hydrodynamic model

SHG: second-harmonic generation

TAC: time-to-amplitude converter

TDFSS: Time Dependent Fluorescent Stokes Shift

TCSPC: Time Correlated Single Photon Counting

T1: spin-lattice relaxation time

T_2: spin-spin relaxation time

VH: vertical-horizontal angle of detection

VM: vertical-magic angle of detection

VV: vertical- vertical angle of detection

VTF: Vogel-Tammann-Fulcher model

WATERGATE: pulse sequence that suppresses the water peak

α_i : the normalized amplitudes

b_i: amplitude of the time constants characterizing the multi-exponential fit of the solvation function

D_r: rotational diffusion

D: self-diffusion coefficient

d1: relaxation delay time constant

Δ: diffusion time delay

δ_{H2O}: water chemical shift

δ: duration of the gradient pulse

E_a: activation energy

G: field gradient strength

$I(t)$: fluorescence decay transient

$I_{VV}(t)$: fluorescence intensity at vertical-vertical polarization angle

$I_{VH}(t)$: fluorescence intensity at vertical-horizontal polarization angle

$I_{VM}(t)$: fluorescence intensity at vertical-magic polarization angle

I_G: intensity of the signal as a function of G

I_0: the intensity of the signal at G=0,

K(t): isotropic fluorescence decay transient

k_B: Boltzmann constant

M_{H2O}: moles of water

M_{IL}: moles of ionic liquid

R: Boltzmann constant

r: radius of ion or molecule

t: time

τ_i time constant of multiexponential fit of fluorescence decay.

τ_i : the time constant of the multiexponential fit

τ_g: gradient recovery delay

η: viscosity

T: temperature

T_g: glass transition temperature,

T_c: onset temperature for VTF model

$\nu_{em}(t)$: solvation dynamics frequency-shift function

π^*: polarity by empirical solvent polarity scale

(τ_0): rate averaged time constant

($\tau_{1/e}$): effective time constant to reach the 1/*e* point of the decay

$\langle \tau \rangle$): is the averaged solvation time constant

τ_{or} : orientation time constant

γ: gyromagnetic constant

υ: convective flow velocity

x_{H2O}: water mole fraction

Chapter 1

Introduction

1.1 General information about Ionic Liquids

Ionic Liquids (ILs) are an exceptional class of chemical substances: while they consist purely of ions, they are also liquids at ambient temperatures. The combination of words “Ionic Liquid” must sound as strange as “dry water” or “cold fusion.” The explanation of this phenomenon is simple; ions in ILs do not pack into crystal lattices because of their size mismatch, charge delocalization, low symmetry of molecular ions, and conformational disorder. Organic cations that are used in ILs are voluminous compared to alkali halides; because of this property, the interionic distance is larger. Consequentially, Coulombic interaction is reduced between ions, as shown in Fig.1.1.[1]

Examples of common aromatic cations include: alkylpyridinium and alkylimidazolium; and non-aromatic cations include: alkylpyrrolidinium, alkylammonium, and alkylphosphonium. Common anions are bromide, chloride, tetrafluoroborate (BF_4^-), hexafluorophosphate (PF_6^-), bis(trifluoromethylsulfonyl)amide (NTf_2^-), and dicyanamide (DCA^-), as show in Fig.1.2.

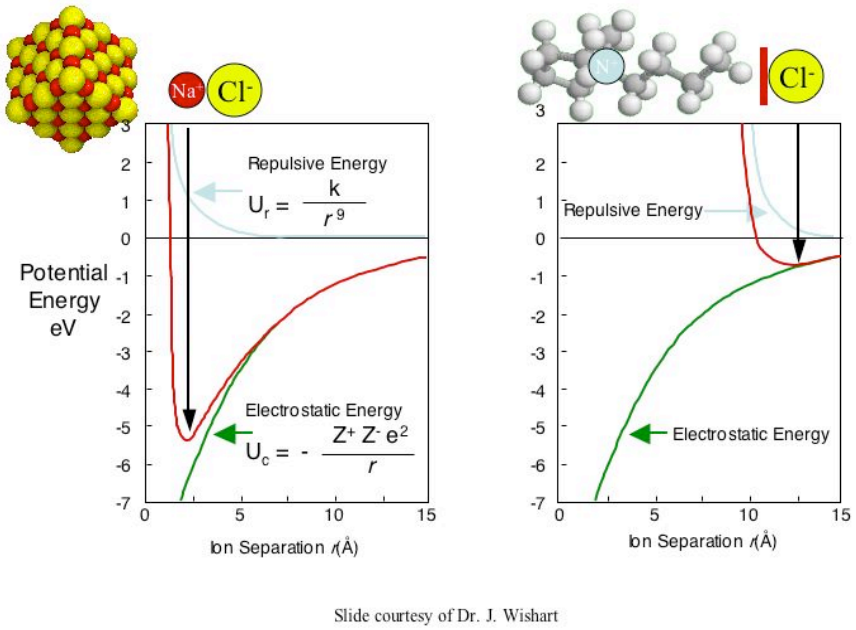

Figure 1.1 The decrease of Coulombic interactions between ions as a function of distance. Left: Na^+Cl^- . Right: 1-butyl-1-methylpyrrolidinium Cl^-

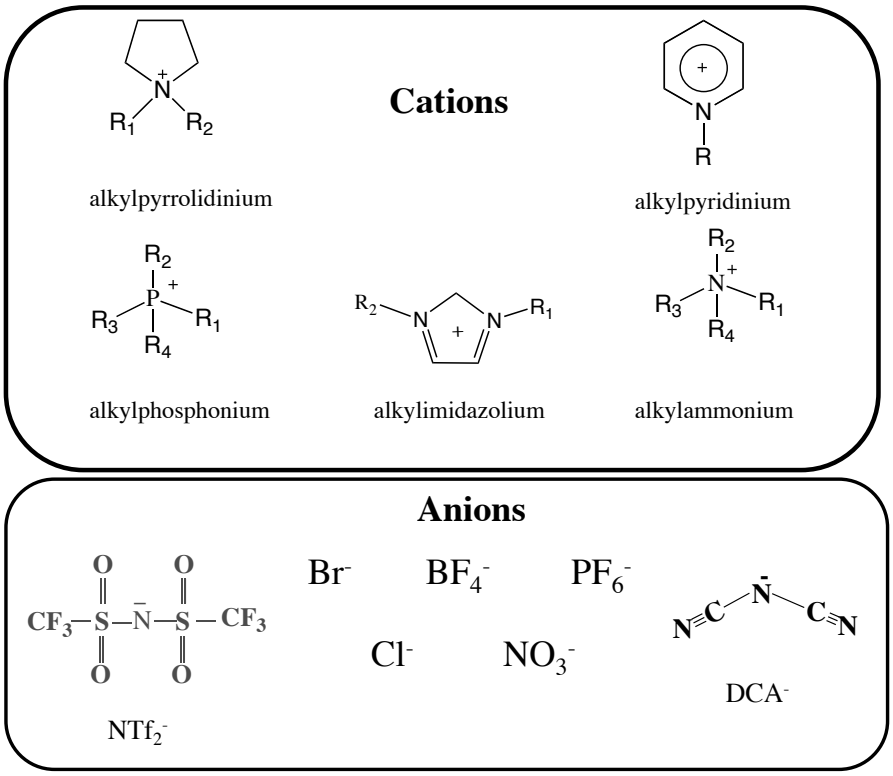

Figure 1.2 Common constituent cations and anions of ionic liquids

Therefore, for better understanding of ILs, we have to consider two peculiar features of ILs that distinguish them from molecular solvents. ILs are **binary liquids** and they consist of **charged species**. The presence of two species, anions and cations, raises a question about their mutual space orientation, interaction, and contribution to local structure.

Another factor that influences the structure of ILs is the presence (or absence) of alkyl chains of varying length on the cation. These two factors, Coulombic forces acting between molecular ions and hydrophobic alkyl chains, provide a huge variety of ILs with different structures. Some of them are more structured, others are amorphous.[2] ILs exhibit structural features not only in the bulk, but also at interfaces.[2] For example, imidazolium sulfate based ILs exhibit a dominating presence of alkyl-functionalized group at the surface as a manifestation of the influence of hydrophobic groups on the structure.[3] The presence of local structure is also confirmed by the heterogeneity of solvation and chemical processes. Properties of ILs vary in broad range because of their diverse structure.

1.1.1 Physical properties of ILs

There are a few properties of ILs that are of particular importance for industrial applications : non-volatility, viscosity, electrochemical properties, thermal stability, polarity and polarizability.

- **Non-volatility**

ILs have negligible vapor pressure because the Coulombic force prevents ions from leaving the surface of the liquid. As a consequence, ILs are non-flammable and there is no vapor loss; this is a very attractive feature for possible use in the chemical industry. However, at high temperatures, ILs can decompose producing flammable gases.[4]

On the other hand, the small value of the vapor pressure in ILs is a drawback, because it does not allow the purification of ILs by distillation. As an exception, some ILs can experience evaporation by way of anion-cation couples leaving the surface in pairs, which allows for distillation at high temperatures.[5-7]

- **Viscosity**

In general, ILs are more viscous than molecular solvents. Their viscosity at room temperature is in the range from tens to thousands of cP.[8, 9] The high viscosity of ILs makes it difficult to work with them in industry; there is much research dedicated to the decrease of viscosity of IL.[10, 11] Many ILs have melting points at or slightly above room temperature; this makes them supercooled liquids at room temperature. Consequently, many ILs at room temperature exhibit glass-like behavior. This is indicated from the temperature dependence of the viscosity deviating from the Arrhenius prediction near the melting point temperature.

- **Electrochemical properties**

ILs have a broad electrochemical window of up to 6 volts.[12] It should be expected that ILs have very high conductivity because they are composed 100% of ions. However, the conductivity of ILs can vary because it depends highly on the transport properties of ions and, consequently, on the size of cations and anions, temperature, and viscosity.[13]

- **Thermal stability**

Thermal stability is another attractive feature of IL. Well-behaved ILs are not chemically decomposing until 250 C.

- **Polarity and polarizability**

Despite the fact that ILs consist of charged species, anions and cations, these charge carriers sometimes manifest their dipolar nature. The voluminous molecular ions have a charge density localized on one part of the molecule and exhibit properties of dipoles. The polarizability of these dipoles influence electrostatic interaction with other charged species.[14] In most cases ILs are moderately polar liquids comparable in polarity with a short-chain alcohols.[15] Though, as Kobrak mentioned in his article:

> "the well-established scenarios for describing dipolar interactions in molecular liquids are not easily transferred to ILs because the net charges of the ions create a fundamentally different environment with partial charge ordering and screening of dipole–dipole interactions by the sea of surrounding ions."[9]

The broad diversity of physical and chemical properties makes ILs very attractive in many fields of research and production. A practically endless number of cation-anion combinations is a source for synthesis of new ILs with desired properties. The term "task specific liquids" was coined when scientists realized that it is possible to design an IL with desired properties by adjusting the structure of constituent anions and cations.[16] One example of a property that can be adjusted is the hydrophobicity of an IL. This can be achieved by altering the length of the alkyl chain on the cation.[17]

Like the hydrophobicity, the viscosity of ILs can also be adjusted by design. For example, the viscosity of the methyl-trimethylsilylmethyl immidazolium / BF_4^- is seven times smaller than the viscosity of an IL which is based on the same anion and the isostructural neopentyl-based cation. The structure of both cations is shown in Fig. 1.3. The fact that the change of only one atom in the structure can reduce the viscosity so dramatically encourages the further research in optimization of ILs by design.[10]

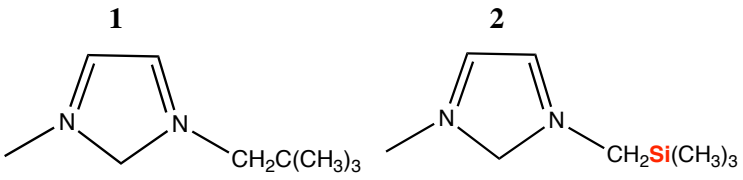

Figure 1.3 The structure of methyl-trimethylsilylmethyl imidazolium (**1**) and neopentyl (**2**) cations

The possibility to adjust the required properties for the needs of research or production is very appealing. However, this requires understanding of how one or another particular property depends on the chemical structure of IL. In an effort to explain the physical and chemical properties of ILs, many researchers turn to investigation of the local structure of ILs using methods such as neutron diffraction, X-ray scattering,[18, 19] neutron scattering,[20] optical heterodyne detected Raman-induced Kerr effect spectroscopy (OHDRIKES)[19, 21] and other methods.

1.2 Applications of IL

Ionic Liquids represent a special type of solvent that offers wide opportunities for chemical synthesis and industrial production. Low vapor pressure, broad electrochemical windows and high conductivity, thermostability, and a large span between melting point and temperature of thermal decomposition make ILs very attractive for use in many fields. A few fields of ILs applications are: energy production, electrochemistry, catalysis and biocatalysis, biomass processing, and many others - from lubricants to dispersants.

One of the biggest successes of the application of ILs in the field of biomass processing is dissolution of the cellulose in the alkyl-imidazolium based ILs.[22, 23] Cellulose is insoluble in water; and processing cellulose involves use of ecologically

harmful solvents. The simple and “green” procedure of dissolution in the IL is not only preferable from the ecological point of view but also allows to recover the cellulose from the solution. The fact that this process is reversible in this way can serve as a base for many technological processes.[22, 23] BASF, the largest chemical company in the world, participates in the further investigation of dissolution of cellulose in ILs, and the introduction of a cellulose-alkyl-imidazolium based process into production.

BASF also is the first company to have introduced ILs into chemical industry. The initial process utilized by BASF was BASIL (*B*iphasic *A*cid *S*cavenging utilizing *I*onic *L*iquids). This process greatly increased efficiency of the reaction.[24]

Application of ILs in the field of energy production and storage is very attractive because of their potentially high conductivity, broad electrochemical window and non-flammability. For instance, ILs can be used as electrolytes in metal-air batteries, and particularly in lithium batteries. Among other advantages the low volatility of ILs will reduce the evaporation of the electrolyte and increase the lifetime of the batteries.[12, 25] Also ILs can be employed in solar cells[26], fuel cells[12, 27], and supercapacitors.[25]

Another application of ILs is in electrochemistry. ILs can be used for the electrodeposition of metals and semiconductors that open perspectives in electroplating and corrosion protection.[25, 28]

Catalysis along with electrochemistry and energy production has broad opportunities for application of ILs. ILs demonstrate the ability to modulate reactivity and selectivity of organic reactions, that allow to use them in organic catalysis.[29] The fact that Ionic liquids *are liquid* within a broad range of temperatures near the ambient temperature makes it possible to use ILs in homogeneous and bi-phasic catalysis as an immobilizing agent in

transition metal catalysis.[30, 31] One of the interesting directions in the field of catalysis is application of paramagnetic ILs in the organic synthesis. Paramagnetic ILs is a relatively new type of ILs based on anions comprising transition-metal coordination complexes.[32, 33] Also, ILs are used in the bio-catalysis and enzymatic catalysis.[34]

The ability of ILs to dissolve high volumes of gases opens one more field of application for ILs. The company Air Products use ILs for storage and transportation of toxic gases such as arsine, trifluoroborane and phosphine. A substantial volume of gas can be dissolved in the IL and then released under negative pressure. Also, ILs have an exceptional ability to dissolve large volumes of carbon dioxide that can be used to capture carbon dioxide from mixtures of gases and for purification of natural gas.[35]

1.3 Research Objectives

For all applications involving ILs as a solvent or reactive component, understanding of physico-chemical processes in the system is very important. Planning my research I focused on solvation processes, solvent-solute interaction, and transport properties of ILs. There are three major objectives of my research:

1. Investigation of the temperature dependent solvation dynamic for a series of four ILs with non-aromatic cations.
2. Interaction between ILs and water.
3. Orientational and translational diffusion in the IL.

1.3.1 Investigation of the temperature dependent solvation dynamics

One of the notable features of ILs is their ability to dissolve a wide variety of molecular and ionic compounds. This feature makes ILs appealing as a reaction medium for many synthetic and industrial applications. Understanding of chemical processes involved in these applications requires detailed knowledge of the solvation dynamics. Investigation of solvation dynamics can elucidate the chemical reactivity, kinetics of reaction, transport properties and many other properties of the system.[2]

Solvation dynamics can be investigated by time-resolved fluorescent spectroscopy. One of the methods often used for investigation of solvation dynamics is the Time Dependent Fluorescent Stokes Shift (TDFSS).[36-38] The TDFSS characterizes reorganization of solvent molecules around a fluorescent probe.[2, 39] As an instrument for the TDFSS, many researchers use Time Correlated Single Photon Counting (TCSPC). One of the most often used solvatochromic probes is coumarin 153 (C153)[40]; the structure of C153 is shown in Fig. 1.3.1.

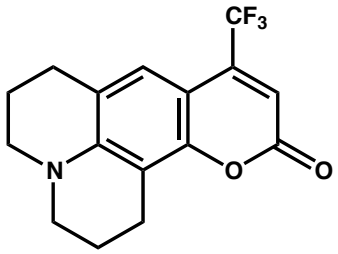

Figure 1.3.1 The structure of Coumarin 153 molecule.

The dipole moment of C153 is approximately 7 D in the ground state and 14 D in the excited state.[41] The large difference between dipole moments of ground state and excited

state makes C153 attractive for investigation of solvation processes, because of the substantial perturbation experienced by surrounding ions.

The solvent reorganization in ILs investigated by TDFSS reveals two regimes: fast reorganization on the sub-picosecond and picosecond scale; and slower reorganization on the nanosecond scale. The immediate reorientation of the closest neighboring ions accounts for at least 10-20% of the total reorganization energy. The fastest relaxation process cannot be registered by TCSPC set up because instrument response of TCSPC is not fast enough. The slower solvent reorganization on the nanosecond time scale involves the collective movement not only of closest neighbors but also of more distant ions.[39]

Solvation dynamics in ILs usually exhibit multi-exponential character. One of the possible explanations of this phenomenon is the binary nature of ILs. Cations and anions in ionic liquids have different shapes and dipole moments; this might influence the solvation dynamics. The presence of local structure in some ILs can be another reason for non-exponential solvation dynamics. Also, the inhomogeneous character of the dynamics of solvent reorganization can be stipulated by the glassy character of IL at the ambient temperatures. Complex cooperative movements of the ions in ionic liquids can cause non-exponential solvation dynamics.[9, 10]

1.3.2. Interaction between ILs and water

Many applications of ILs involve water as a product or byproduct of the reaction, or as an impurity. For example, ILs employed in the hydrogen fuel cells and in cellulosic biomass processing may contain an amount of water close to saturation. Also, there are various proteins that can be dissolved only in the mixture of water with IL, but not in pure

ILs.[42]

The hydrophobicity of ILs may vary in the broad range from total miscibility with water to relatively high hydrophobicity when water concentration at saturation did not exceed $x_{water} = 0.3$, as for example, in the NTf_2^- based ILs.[43]

In general, the degree of hydrophobicity of ILs is governed by the nature of the anion.[44] Usually, the presence of fluorine in the anion increases hydrophobicity, especially when few fluorine atoms surround the other electronegative atom. For example, the ILs containing PF_6^- and NTf_2^- anions are more hydrophobic than ILs containing Cl^-, Br^-, NO_3^- anions. However, the term 'hydrophobic' should not be accidently interpreted as totally water-free. Even seemingly immiscible ILs can contain a substantial amount of water. For example, relatively hydrophobic 1-methyl-3-octylimidazolium hexafluorophosphate (C_8mim^+/PF_6^-) can contain up to 1.36 wt% of water at the 298 K.[45] As Kobrak mentioned in his 2008 review, the concentration of water expressed in the weight percent may lead to underestimation of the water content.[14] The molecular weight of ILs is much higher than molecular weight of water and even low weight percent water concentration is getting substantial when converted into mole fractions. The water concentration of 1.36 wt% in the saturated C_8mim^+/PF_6^- is equivalent to $x_{H2O} = 0.205$; this indicates that there is one water molecule per 4 anion-cation couples. The laboratory experiments and industrial processes with ILs require precautions, because even hydrophobic ILs actively absorb water from air.

The properties of ILs are substantially modified with added water. The addition of water decreases viscosity and lowers the temperature of the melting point and glass formation.[46] Also, some chemical reactions conducted in ILs might be affected by presence of water. For example, some catalysts can be deactivated by even a trace of

water.[47]

Thus, we can summarize that in general, nearly all ILs can contain some amount of water and the properties of ILs and processes conducted in ILs are substantially influenced by a presence of water. Investigation of interaction between water and IL may elucidate properties of IL/water systems.

In IL/water mixtures with a small water concentration, water is associated with the anion. Hydrogen bonds link the anion to water as “anion--H-O-H” agglomerates.[44] The polarity of hydrogen bonds between a molecule of water and the anion determine the strength of these bonds and, consequently, influence mutual solubility of water and the IL, transport properties in the system IL/water and chemical reactivity of water and the anion. In turn, polarity of hydrogen bonds depends on the nature of the anion; this stipulates the variety of chemical properties of water in different ILs.

Investigation of the chemical shift of the water allows us to estimate the polarity of water-anion bond. The ^{1}H NMR chemical shift of water δ_{H2O} depends on the degree of deshielding of water protons that in turn can provide information on the polarity of hydrogen bonds. There is much research on the concentration and temperature dependence of the water chemical shift δ_{H2O} in common organic solvents[48-50] , but there are just few articles related to the water chemical shift δ_{H2O} in the IL/water system. [51, 52]

1.3.3 Orientational and translational diffusion components in the IL

Understanding diffusive processes in ILs is very important for many applications of ILs. The diffusion rate determines transport properties in the system that in turn influences

reaction kinetics. Investigation of diffusion in ILs complementarily replenishes the investigation of solvation dynamics and elucidates the specificity of the reaction processes in viscous and glass-like ILs. The knowledge of diffusive properties of IL/solute system is also required for estimation of conductivity in ILs.

Diffusivity can be characterized by two components: reorientational diffusion and translational diffusion. These components are interconnected and depend on the local friction experienced by the molecule or ion under question. Therefore, diffusivity can characterize some properties of a system on the micro-scale. This includes microviscosity experienced by diffusing species, the interaction between the anion, cation, and solute, and the presence of hydrogen bonds.

Investigation of diffusion in ILs is more complicated and more interesting than in common solvents because they are binary liquids. The difference in size, shape and charge distribution between the cation and anion can lead to different diffusivity of these species. Investigation of diffusion is even more complicated if there is neutral solute in the system.

The translational diffusion can be described as a flux of particles through the section of particular area. In a case where there is no gradient of concentration of diffusing species, the diffusion is called self-diffusion. The self-diffusion coefficient is expressed in units of area over time (m^2s^{-1}, cm^2s^{-1}).

The rough prediction of the diffusivity can be made based on the viscosity of the IL. The Stokes-Einstein (S-E) hydrodynamic model for translational diffusion describes dependence of self-diffusion coefficient on viscosity, radius of diffusing specie and temperature, as given in equation 1.3.3.1 There are a few assumptions inherent in the S-E model. One assumption is that the diffusing molecule has a spherical shape. Then the liquid

is considered as a continuous fluid medium, not as a molecular liquid. To describe the character of translational motion in the S-E model one can introduce “stic” or “slip” conditions that depend on the difference in sizes between solute and solvent.

$$D_{trans} = \frac{k_B T}{c\pi\eta r} \qquad (1.3.3.1)$$

where D_{trans} is translational self-diffusion coefficient , k_B is Boltzmann constant, T is the temperature (K), c is “stick”or “slip” constant varying between 4 and 6, η is the viscosity and r is the radius of the diffusing ion or molecule.

Rotational or orientational diffusion is the counterpart of translational diffusion, which maintains the equilibrium statistical distribution of position of molecules or ions in space. One of the methods of investigation of orientational diffusion is the method of time-resolved fluorescence anisotropy. The decay of emission polarization reflects the local rotational friction experienced by the solvatochromic probe.[38] The reorientational diffusion is described by the Stokes-Einstein-Debye (S-E-D) hydrodynamic model, as given in equation 1.3.3.2

$$D_{or} = \frac{k_B T}{8\pi\eta r^3} \qquad (1.3.3.2)$$

Here all symbols are the same as in equation 1.3.3.1 except r, which is the radius of solvatochromic probe instead of radius of diffusing ions.

The diffusion in pure ILs and in IL/solute systems may deviate from S-E and S-E-D models.[53] One of possible reasons is that both models assume the diffusing species

to be a spherical rotor and the real shape of ions may require the corrections of estimated diffusion. Other possible reasons are strong Coulombic interaction between ions, charge-delocalization and complex dynamical asymmetry. Thereby, investigation of diffusion in ILs requires alternative experimental methods.

A very useful method for determination of self-diffusion coefficients is diffusional ordered spectroscopy (DOSY).[54] The Pulse Gradient Spin Echo method (PGSE) allows monitoring translational motion of nuclear spins.[55, 56]

An increasing number of results have been reported for the study of cation and anion self-diffusion in ionic liquids.[57-60] Pioneering work from the Watanabe group demonstrates that in general diffusion in ILs agrees with hydrodynamic theory predictions.[61] However, the cation diffuses faster than the anion, even in cases when the radius of the cation is larger than the radius of the anion.[62, 63] This was also predicted by MD simulations.[64] These deviations imply that the behavior of ILs is not adequately explained by Stokes –Einstein hydrodynamic model because of complex anion-cation interactions. One of the possible explanations for deviation from Stokes-Einstein model might be existence of the long-range order in ILs that determines the cooperative motion of ions in the ILs.[53]

Relatively viscous ILs often exhibit the Vogel-Tammann-Fulcher (VTF) temperature dependence of viscosity. Taking into consideration that self-diffusion coefficient D correlates inversely with viscosity, it is not surprising that D exhibit VTF temperature dependence at low temperatures.[62]

The introduction of water into the system raises the question of whether or not neutral and H-bond donating and accepting species will have similar transport properties

relative to the constituent cations and anions in the IL. Several research groups have addressed the anomalous self-diffusion of water in ILs both experimentally with PGSE NMR methods and with computational chemistry approaches.[63, 65, 66]

1.4 Summary

The interest of the scientific community in ILs continues to develop in many different directions ranging from biology to nuclear research. Unique properties of ILs promote them into many industrial fields. The specific nature of ILs leads to significant difference between molecular solvents and ILs. Patterns of relationship between structures and properties for ILs deviate from the same patterns of molecular solvents. ILs are relatively new solvents and because of that many details of their structure and properties were not yet studied in detail. This dissertation is dedicated to investigation of solvation dynamics in ILs, interaction between water and ILs, and diffusive properties in the system water/IL. The trends investigated for particular ILs may help understanding the properties of the systems with other ionic liquids.

References

1. *Ionic Liquids IIIB: Fundamentals, Progress, Challenges, and Opportunities: Transformations and Processes*, ed. R.D. Rogers and K.R. Seddon 2002, New York: ACS.
2. E.W. Castner Jr., C.J. Margulis, M. Maroncelli, J.F. Wishart, *Ionic Liquids: Structure and Photochemical Reactions.* Annu. Rev. Phys. Chem., 2011. **62**: p. 85.
3. C. S. Santos, S. Baldelli, *Alkyl Chain Interaction at the Surface of Room Temperature Ionic Liquids: Systematic Variation of Alkyl Chain Length (R) C1-C4, C8) in both Cation and Anion of [RMIM][R-OSO3] by Sum Frequency Generation and Surface Tension.* J. Phys. Chem. B, 2009. **113**: p. 923.
4. M. Smiglak, W. M. Reichert, J. D. Holbrey, J. S. Wilkes, L. Sun, J. S. Thrasher, K. Kirichenko, S. Singh, A. R. Katritzky, R. D. Rogers, , *Combustible ionic liquids by design: is laboratory safety another ionic liquid myth?* Chem. Commun., 2006. **(24)**: p. 2554.
5. E. F. Borra, O. Seddiki, R. Angel, D. Eisenstein, P. Hickson, K. R. Seddon, S. P. Worden, *Deposition of metal films on an ionic liquid as a basis for a lunar telescope.* Nature, 2007. **447**: p. 979.
6. K. R. J. Lovelock, A. Deyko, P. Licence, R. G. Jones, *Vaporisation of an ionic liquid near room temperature.* Phys. Chem. Chem. Phys., 2010. **12**: p. 8893.
7. J.P. Armstrong, C. Hurst, R. G. Jones, P. Licence, K. R. J. Lovelock, C. J. Satterley, I. J. Villar-Garcia, *Vapourisation of ionic liquids.* Phys. Chem. Chem. Phys., 2007. **9 (8)**: p. 982.
8. S. Zhang, N. S. Xuezhong, H. X. Lu, X. Zhang, , *Physical Properties of Ionic Liquids: Database and Evaluation.* J. Phys. Chem. Ref. Data, 2006. **35**: p. 1475.
9. M. N. Kobrak, *Electrostatic Interactions of a Neutral Dipolar Solute with a Fused Salt: A New Model for Solvation in Ionic Liquids.* J. Phys. Chem. B, 2007. **111**: p. 4755.
10. H. Shirota, E. W. Castner, Jr., *Why Are Viscosities Lower for Ionic Liquids with -CH2Si(CH3)3 vs -CH2C(CH3)3 Substitutions on the Imidazolium Cations?* J. Phys. Chem. B, 2005. **109(46)**: p. 21576.
11. J. N. C. Lopes, M. F. C. Gomes, P. Husson, A. A. H. Padua, L. P. N. Rebelo, S. Sarraute, M. Tariq, , *Polarity, Viscosity, and Ionic Conductivity of Liquid Mixtures Containing [C4C1im][Ntf2] and a Molecular Component.* J. Phys. Chem. B, 2011: p. 6088.
12. M. Armand, F. Endres, D. MacFarlane, H. Ohno, B. Scrosati, *Ionic-liquid materials for the electrochemical challenges of the future.* Nature mater. , 2009. **8**: p. 621.
13. D. R. MacFarlane, K. R. Seddon, , *Ionic liquids - Progress on the fundamental issues.* Aust. J. Chem. , 2007. **60**: p. 3.
14. M. N. Kobrak, *The chemical environment of ionic liquids: links between liquid structure, dynamics, and solvation.* Adv. Chem. Phys., 2008. **139**: p. 85.

15. C. Chiappe, M. Malvaldi, C. S. Pomelli, , *Ionic liquids: Solvation ability and polarity.* Pure Appl. Chem., 2009. **81**: p. 767.
16. A. E. Visser, R. P. Swatloski, W. M. Reichert, R. Mayton, S. Sheff, A. Wierzbicki, J. H. Davis Jr, R. D. Rogers, , *Task-specific ionic liquids for the extraction of metal ions from aqueous solutions.* Chem. Commun., 2001(2): p. 135.
17. J. G. Huddleston, A. E. Visser, W. M. Reichert, H. D. Willauer, G. A. Broker, R. D. Rogers, , *Characterization and comparison of hydrophilic and hydrophobic room temperature ionic liquids incorporating the imidazolium cation.* Green Chem., 2001. **3**: p. 156-164.
18. H. K. Kashyap, C. S. Santos, H. V. R. Annapureddy, N. S. Murthy, C. J. Margulis, E. W. Castner, Jr., *Temperature-dependent structure of ionic liquids : X-ray scattering and simulations.* Faraday, 2011. **134(6)**: p. 064501.
19. O. Russina, A. Triolo, L. Gontrani, R. Caminiti, D. Xiao, L. G. Hines Jr., R. A. Bartsch, E. L. Quitevis, N. Pleckhova, K. R. Seddon, , *Morphology and intermolecular dynamics of 1-alkyl-3-methylimidazolium bis(trifluoromethane)sulfonylamide ionic liquids: structural and dynamic evidence of nanoscale segregation.* J. Phys. Cond. Matter, 2009. **21**: p. 424121.
20. C. Hardacre, J. D. Holbrey, C. L. Mullan, T. G. A. Youngs, D. T. Bowron, , *Small angle neutron scattering from 1-alkyl-3-methylimidazolium<p>hexafluorophosphate ionic liquids Cnmim-PF6, n=4, 6, and 8.* J. Chem. Phys., 2010. **133**: p. 1842.
21. E. W. Castner Jr., J. F. Wishart, H. Shirota, *Intermolecular Dynamics, Interactions, and Solvation in Ionic Liquids.* Acc. Chem. Res., 2007. **40 (11)**: p. 1217.
22. R. P. Swatloski, S. K. Spear, J. D. Holbrey, R. D. Rogers, , *Dissolution of Cellulose with Ionic Liquids.* J. Am. Chem. Soc., 2002. **124**: p. 4974.
23. D. A. Fort, R. C. Remsing, R. P. Swatloski, P. Moyna, G. Moyna, R. D. Rogers, , *Can ionic liquids dissolve wood? Processing and analysis of lignocellulosic materials with 1-n-butyl-3-methylimidazolium chloride.* Green Chem., 2007. **9**: p. 63-69.
24. K. R. Seddon, *Ionic liquids: A taste of the future.* Nature Mater., 2003. **2**: p. 363.
25. D.R. Macfarlane, M. Forsyth, P. C. Howlett, J. M. Pringle, G. Annat, W. Neil, E. Izgorodina,, *Ionic Liquids in Electrochemical Devices and Processes: Managing Interfacial Electrochemistry.* Acc. Chem. Res. , 2007. **40**: p. 1165.
26. S. M. Zakeeruddin, M. Graetzel, , *Solvent-Free Ionic Liquid Electrolytes for Mesoscopic Dye-Sensitized Solar Cells.* Adv. Funct. Mater., 2009. **19**: p. 2187.
27. R. F. de Souza, J. C. Padilha, R. S. Gonßcalves, J. Dupont, *Room temperature dialkylimidazolium ionic liquid-based fuel cells.* Electrochem. Comm., 2003. **5**: p. 728.
28. A. P. Abbott, K. J. McKenzie, *Electrodeposition of Metals using ionic Liquids.* Phys. Chem. Chem. Phys., 2006. **8**: p. 4265.
29. A. K. Chakraborti, S. R. Roy, *On Catalysis by Ionic Liquids.* J. Am. Chem. Soc., 2009. **131**: p. 6902.
30. J. Dupont, R. F. de Souza, P. A. Z. Suarez, *Ionic Liquid (Molten Salt) Phase Organometallic Catalysis.* Chem. Rev., 2002. **102**: p. 3667.

31. P. J. Dyson, T. J. Geldbach, *Applications of ionic liquids in synthesis and catalysis.* Electrochem. Soc. Interface, 2007. **16**: p. 50.
32. S. Hayashi, H.-O. Hamaguchi, *Discovery of a magnetic ionic liquid [bmim]FeCl4.* Chem. Lett., 2004. **33**: p. 1590.
33. S. Hayashi, S. Saha, H.-O. Hamaguchi, *A new class of magnetic fluids: bmim[FeCl4] and nbmim[FeCl4] ionic liquids.* IEEE Transactions on Magnetics, 2006. **42**: p. 12.
34. A. J. Walker, N. C. Bruce, *Cofactor-dependent enzyme catalysis in functionalized ionic solvents.* Chem. Comm., 2004: p. 2570.
35. M. J. Muldoon, S. N. V. K. Aki, J. L. Anderson, J. K. Dixon, J. F. Brennecke, *Improving Carbon Dioxide Solubility in Ionic Liquids.* J. Phys. Chem. B, 2007. **111 (30)**: p. 9001.
36. E. W. Castner Jr., M. Maroncelli, G. R. Fleming, , *Subpicosecond resolution studies of solvation dynamics in polar aprotic and alcohol solvents.* J. Chem. Phys., 1987. **86**: p. 1090.
37. M. Maroncelli, G. R. Fleming, , *Picosecond solvation dynamics of coumarin 153: the importance of molecular aspects of solvation.* J. Chem. Phys., 1987. **86(11)**: p. 6221.
38. B. Valeur, *Molecular Fluorescence: Principles and Applications* 2002: Wiley-VCH.
39. A. Samanta, *Solvation Dynamics in Ionic Liquids: What We Have Learned from the Dynamic Fluorescence Stokes Shift Studies.* J. Phys. Chem. Let. , 2010. **1**: p. 1557.
40. M.-L. Horng, J. A. Gardecki, M. Maroncelli, , *Rotational Dynamics of Coumarin 153: Time-Dependent Friction, Dielectric Friction, and<p>Other Nonhydrodynamic Effects.* J. phys. Chem. A, 1997. **101**: p. 1030.
41. R. J. Cave, E. W. Castner, Jr., *Time-Dependent Density Functional Theory Investigation of the Ground and Excited States of Coumarins 102, 152, 153, and 343.* J. Phys. Chem. A, 2002. **106(50)**: p. 12117.
42. K. Fujita, D. R. MacFarlane, M. Forsyth, *Protein solubilising and stabilising ionic liquids.* Chem. Comm., 2005: p. 4804.
43. J. Jacquemin, P. Husson, A. A. H. Padua, V. Majer, *Density and viscosity of several pure and water-saturated ionic liquids.* Green Chem., 2006. **8(2)**: p. 172.
44. L. Cammarata, S. G. Kazarian, P. A. Salter, T. Welton, *Molecular states of water in room temperature ionic liquids,.* Phys. Chem. Chem. Phys., 2001. **3**: p. 5192.
45. M. G. Freire, C. M. S. S. Neves, P. J. Carvalho, R. L. Gardas, A. M. Fernandes, I. M. Marrucho, M. N. B. F. Santos, A. P. Coutinho, *Mutual Solubilities of Water and Hydrophobic Ionic Liquids.* J. Phys. Chem. B, 2007. **111**(45): p. 13082.
46. K. R. Seddon, A. Stark, M. Torres, *Influence of chloride, water, and organic solvents on the physical properties of ionic liquids.* Pure Appl. Chem., 2000. **72**: p. 2275.
47. T. Welton, *Room-Temperature Ionic Liquids. Solvents for Synthesis and Catalysis.* Chem. Rev., 1999. **99**: p. 2071.
48. K. Mizuno, Y. Miyashita, Y. Shindo, H. Ogawa, *NMR and FT-IR Studies of Hydrogen Bonds in Ethanol-Water Mixtures?* J. Phys. Chem., 1995. **99**: p. 3225.

49. G. R. Fulmer, A. J. M. Miller, N. H. Sherden, H. E. Gottlieb, A. Nudelman, B. M. Stoltz, J. E. Bercaw, K. I. Goldberg, , *NMR Chemical Shifts of Trace Impurities: Common Laboratory Solvents, Organics, and Gases in Deuterated Solvents Relevant to the Organometallic Chemist.* Organometallics, 2010. **29**: p. 2176.
50. V. Balevicius, K. Aidas, *Temperature dependence of 1H and 17O NMR shifts of water: Entropy effect*
. Appl. Magn. Reson., 2007. **32**: p. 363.
51. T. Singh, A. Kumar, *Cation-anion-water interactions in aqueous mixtures of imidazolium based ionic liquids.* Vibrational Spectroscopy, 2011. **55**: p. 119.
52. J. Dwan, D. Durant, K. Ghandi, *Nuclear Magnetic Resonance Spectroscopic Studies of the Trihexyl (Tetradecyl) Phosphonium Chloride Ionic Liquid Mixtures with Water.* Cent. Eur. J. Chem., 2008. **6(3)**: p. SI1.
53. K. R. Harris, *The fractional Stokes-Einstein equation: Application to Lennard-Jones,<p>molecular, and ionic liquids.* J. Chem. Phys., 2009. **131**: p. 054503.
54. D. Wu, A. Chen, C. S. Jonson, Jr., *An Improved diffusion-ordered spectroscopy experiment incorporating bipolar-gradient pulses.* . J. Magn. Reson., 1995 **115**: p. 260.
55. E. O. Stejskal, *Use of spin echoes in a pulsed magnetic-field gradient to study anisotropic, restricted diffusion and flow.* J. Chem. Phys., 1965. **43** p. 3597.
56. J. E. Tanner, *Use of the stimulated echo in NMR diffusion studies.* J. Chem. Phys., 1970. **52 (5)**: p. 2523.
57. R. Giernoth, D. Bankmann, N. Schlosrer, *High performance NMR in ionic liquids.* Green Chem., 2005. **7**: p. 279.
58. K. Hayamizu, S. Tsuzuki, S. Seki, Y. Ohno, H. Miyashiro, Y. Kobayashi,, *Quaternary Ammonium Room-Temperature Ionic Liquid Including an Oxygen Atom in Side Chain/Lithium Salt Binary Electrolytes: Ionic Conductivity and 1H, 7Li, and 19F NMR Studies on Diffusion Coefficients and Local Motions.* J. Phys. Chem. B, 2008. **112**: p. 1189.
59. K. Hayamizu, S. Tsuzuki, S. Shiro, *Molecular Motions and Ion Diffusions of the Room-Temperature Ionic Liquid 1,2-Dimethyl-3-propylimidazolium Bis(trifluoromethylsulfonyl)amide (DMPImTFSA) Studied by 1H, 13C, and 19F NMR.* J. Phys. Chem. A, 2008. **112**: p. 12027.
60. A. Wulf, K. Fumino, D. Michalik, R. Ludwig, *IR and NMR Properties of Ionic Liquids: Do They Tell Us the Same Thing?* European Journal of Chemical Physics and Physical Chemistry 2007. **8**: p. 2265.
61. A. Noda, K. Hayamizu, M. Watanabe, *Pulsed-Gradient Spin−Echo 1H and 19F NMR Ionic Diffusion Coefficient, Viscosity, and Ionic Conductivity of Non-Chloroaluminate Room-Temperature Ionic Liquids.* J. Phys. Chem. B, 2001. **105**: p. 4603.
62. H. Tokuda, K. Hayamizu , K. Ishii, M. A. B. H. Susan , M. Watanabe, *Physicochemical Properties and Structures of Room Temperature Ionic Liquids 2. Variation of Alkyl Chain Length in Imidazolium Cation.* J. Phys. Chem. B, 2005. **109**: p. 6103.
63. A. Menjoge, J. Dixon, J. F. Brennecke, E. J. Maginn, S. Vasenkov, *Influence of Water on Diffusion in Imidazolium-Based Ionic Liquids: A Pulsed Field Gradient NMR study.* J. Phys. Chem. B, 2009. **113**(18): p. 6353.

64. S. K. Manish, W. Shi, E. J. Maginn, , *Determining the Accuracy of Classical Force Fields for Ionic Liquids: Atomistic Simulation of the Thermodynamic and Transport Properties of 1-Ethyl-3-methylimidazolium Ethylsulfate ([emim][EtSO4]) and Its Mixtures with Water.* Ind. Eng. Chem. Res., 2008. **47**: p. 9115.
65. A. L. Rollet, P. Porion, V. Michel, B. Isabelle, D. Michael, B. Catherine, J. Laurence, *Anomalous Diffusion of Water in [BMIM][TFSI] Room-Temperature Ionic Liquid.* J. Phys. Chem. B, 2007. **111**(41): p. 11888.
66. M. Moreno, F. Castiglione, A. Mele, C. Pasqui, G. Raos, , *Interaction of Water with the Model Ionic Liquid [bmim][BF4]: Molecular Dynamics Simulations and Comparison with NMR Data.* J. Phys. Chem. B, 2008. **112**: p. 7826.

Chapter 2

Experimental Methods

Overview

Spectroscopic methods used to characterize physico-chemical properties of ILs include up-conversion femtosecond fluorescence spectroscopy,[1, 2] OHDRIKES,[3-6] NMR spectroscopy,[7, 8] and many other methods. One of the frequently used methods for investigating dynamics in ILs is time-resolved fluorescence spectroscopy.[9, 10] This method was used for the investigation of solvation dynamics and local friction in the Ionic Liquids. The investigation of polarity of ILs was conducted by steady state fluorescence spectroscopy. The NMR spectroscopy methods were used for investigation of diffusional properties of ILs.

Thereby, the experimental methods are grouped in two sections:

1 The investigation of the polarity, solvation and local friction in the Ionic Liquids by the fluorescence spectroscopy of the Coumarin 153 solvatochromic probe.

2 The investigation of the interaction between water and IL and diffusive properties of IL/water system by the NMR spectroscopy.

2.1 Investigation of polarity, solvation and local friction in the Ionic Liquids by fluorescence spectroscopy of the Coumarin 153 solvatochromic probe.

2.1.1. Preparation of samples of ILs with C153 for time resolved fluorescence measurements.

2.1.1.1 Materials

The ionic liquids investigated are: *N*-methyl-*N*-butylpyrrolidinium bis(trifluoromethylsulfonyl)-imide $Pyrr_{14}^{+}/NTf_2^{-}$, *N*-methyl-*N*-ethoxyethylpyrrolidinium bis(trifluoromethylsulfonyl)-imide $Pyrr_{1(202)}^{+}/NTf_2^{-}$, *N*-methyl-tri-*N*-butylammonium bis(trifluoromethylsulfonyl)-imide N_{1444}^{+}/NTf_2^{-}, and *N*-hexyl-tri-*N*-butylammonium bis(trifluoromethylsulfonyl)-imide N_{6444}^{+}/NTf_2^{-}. Pyrrolidinium based ILs $Pyrr_{14}^{+}/NTf_2^{-}$ and $Pyrr_{1(202)}^{+}/NTf_2^{-}$ were kindly provided by Dr. James F. Wishart (Brookhaven National Laboratory) and prepared as described by Funston, et al.[11] Ammonium based ILs N_{1444}^{+}/NTf_2^{-} and N_{6444}^{+}/NTf_2^{-} were kindly provided by Dr. Pedatsur Neta of NIST, and prepared as described by Skrzypczak and Neta.[12, 13]

Coumarin 153 (C153) from Acros Organics was used as received for each of the samples.

2.1.1.2 Preparation of samples of ILs with C153

Coumarin 153 has limited solubility in the ammonium based ILs N_{1444}^{+}/NTf_2^{-}, N_{6444}^{+}/NTf_2^{-} and in the $Pyrr_{1(202)}^{+}/NTf_2^{-}$. The solution of the C153 in methanol was used to introduce coumarin in these ILs. The concentration of the C153 in the ILs was adjusted for the absorbance to be approximately 0.1 at 420 nm. This was done by adding 20-100 μL of the concentrated solution of C153 to a small amount of the IL, then diluting with neat IL until absorbance reaches the required value. The methanol was removed under vacuum before spectroscopic characterization of the sample. The $Pyrr_{14}^{+}/NTf_2$ sample was prepared by addition of solid C153 to the IL, followed by dilution with neat IL until a suitable value of absorbance was achieved at 420 nm. Absorption spectra were measured by the Cary-Varian model 50 spectrophotometer with a fixed 1.5 nm optical bandpass. All spectra were baseline-corrected.

Each of our IL/C153 samples was dried at 313 K under vacuum (approximately 0.01 Torr) for 24 h prior to spectroscopy measurements.

Ionic Liquids are quite hydroscopic; even the most hydrophobic ILs can rapidly absorb atmospheric moisture.[14-16] Because water in ILs changes the observed physical properties, care was taken to minimize exposure of the sample to H_2O. Samples were kept in the fused silica cuvettes tightly closed with plastic caps, but not flame sealed. Therefore, samples may have absorbed atmospheric moisture. The series of experiments for investigation of one sample requires 8-10 h or more of the instrument time at ambient condition for about 2-5 days. In between experiments, samples were kept in the desiccator. In order to determine the average water content in our samples I emulated the conditions of our experiment. Samples were prepared using the 24-h vacuum oven drying, waited 5

days, and then measured the water content by Karl Fischer titration using a Mettler-Toledo DL39 Coulometric titrator. The water content of each sample was measured three times. The average and standard deviation values were reported. The water contents (in units of ppm by mass) for the IL samples are as follows: 496 ± 21 ppm for $Pyrr_{14}^{+}/NTf_2^{-}$; 220 ±8 ppm for $Pyrr_{1(202)}^{+}/NTf_2^{-}$; 227±25 ppm for N_{1444}^{+}/NTf_2^{-} and 409±67 ppm N_{6444}^{+}/NTf_2^{-}.

2.1.2 Steady-state Excitation and Emission Spectroscopy

For measuring steady state spectra I used 5x10 mm fused silica sample cuvettes from NSG Precision Cells with four polished windows. Absorption spectra were measured in a geometry having a 5 mm optical path, whereas all steady state and time-resolved emission spectra were measured with a 10 mm optical path for excitation. I have measured steady state fluorescence emission and excitation spectra of C153 in each of the four ionic liquids using Spex Fluoromax-3 fluorometer supplied with Glan-Thompson calcite-prism polarizers with transmission range from 215 to 2000 nm. The slits on the Fluoromax-3 instrument were set for 1.0 nm optical bandpass for both the excitation and emission monochromators. The increment was 0.5 nm and time integration was set at 2 s. The C153 fluorescence maximum was observed at approximately 520 nm for excitation at 420 nm. The emission and excitation spectra for all samples were measured for the set of temperatures 278.2, 293.2, 308.2, 323.2, 338.2, and 353.2 K. The sample temperature was controlled to ± 0.1 K using a Wavelength Electronics thermoelectric temperature controller. The sample equilibration time at each temperature was 10 min.

2.1.3 Time-Resolved Fluorescence Spectroscopy

Time-Resolved Fluorescence Spectroscopy was used as a method for two parts of my research: investigation of the temperature dependent solvation dynamics by the Time Dependent Fluorescence Stokes Shift (TDFSS) and investigation of reorientational dynamics in the ILs by the time-resolved fluorescent anisotropy decay. The time-correlated single-photon counting (TCSPC) method on a laboratory built setup was used to collect the time-resolved fluorescence emission data.[11, 17-21]

2.1.3.1 Time Dependent Fluorescence Stokes Shift

The method of the Time Dependent Fluorescence Stokes Shift (TDFSS) was used for investigation of the temperature dependent solvation dynamics. The fluorescence decay transients were measured by the TCSPC laboratory-built setup. Details of the TCSPC setup has been described in many other articles,[11, 17-21] and only a brief description will be given here. Fig. 2.1.3.1 presents the scheme of the TCSPC set up. A Spectra-Physics Ti-sapphire Tsunami laser is used for photoexcitation. It is capable of generating pulses of 0.5W average power at 82 MHz pulse repetition frequency. The Tsunami laser was tuned to 840 nm. The Beta Barium Borate (β-BBO) doubling crystal was used to generate the second-harmonic generation (SHG). The SHG beam of the fundamental laser frequency with a wavelength 420 nm was vertically polarized using a calcite polarizer and directed at the sample in the fused silica cuvette. Emitted photons from the sample were detected by a Hamamatsu R3809-50U micro channel plate photomultiplier tube (MCP-PMT).

In order to provide synchronization between the fundamental beam and the SHG beam, these beams were spatially separated by a prism. Then, the fundamental beam was sent to a photodiode to dispatch a signal to the time-to-amplitude converter (TAC). Finally, the emission decay is recorded when the multichannel analyzer Becker and Hickl TCSPC SPC-630 builds up a histogram of voltage from the MCP-PMT over time. The measured instrument temporal response width was 70 ps at full-width-half-maximum. For each fluorescence transient, the emission decay was measured using 4096 data points. The full time window was 70 ns. A shorter time window would not capture enough of the long time dynamics while a longer time window would be unnecessary considering that the fluorescence lifetime of the coumarin 153 is only 5 ns.

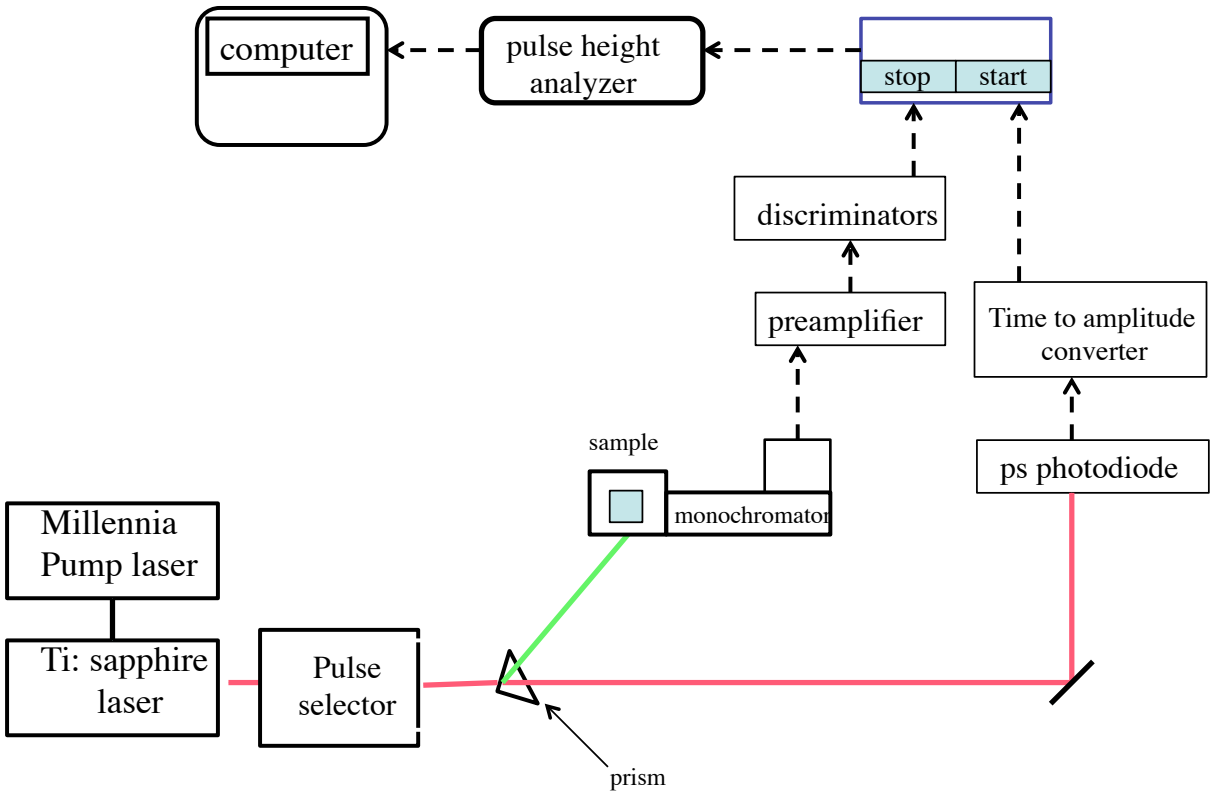

Figure 2.1.3.1 Scheme of the TCSPC laboratory built setup

All fluorescence transients were measured at the isotropic polarization. The emission was detected at the "magic" polarization angle of 54.7° relative to 0° vertically polarized excitation. In order to collect the instrument time response I used a sample prepared as a suspension of a non-dairy creamer in water. The emission decay transients were collected at 14 particular emission frequencies in the range of 16250-22750 cm^{-1} with 500 cm^{-1} increments. The IgorPro program was used to fit transients using the nonlinear least-squares convolute-and-compare algorithm.[22] Transients were fit to a sum-of-exponentials model according to equation 2.1.3.1.

$$I(t) = \sum_{i=1} \alpha_i \exp\left(\frac{-t}{\tau_i}\right) \qquad (2.1.3.1)$$

where I(t) is fluorescence decay transient, α_i are the normalized amplitudes that sum to unity, t is time, and τ_i is time constant of fluorescence decay.

A Quantum Northwest TLC 50/100 thermoelectric temperature controller was used to control the sample temperature to ±0.1 °C. The temperature equilibration time prior to the start of measurements was 10 min.

2.1.3.2 The reorientational dynamics in the ILs

The method of the fluorescent anisotropy decay was used for investigation of the reorientational dynamics in the ILs.

In order to determine the anisotropy decay we have measured time-resolved emission decay transients at vertical- vertical (VV), vertical-magic (VM), and vertical-

horizontal (VH) polarization angles of detection. At vertical-vertical polarization angle (VV), both, the excitation and the emission beam, were polarized vertically; at vertical-magic polarization angle (VM) the excitation was polarized vertically and the emission beam was polarized at the magic angle 54.7°; and at vertical-horizontal polarization angle (VH), the excitation was polarized vertically and the emission beam was polarized at 90° relative to excitation light. The excitation wavelength was the same as in the TDFSS experiment, 420 nm. Emission was detected at 520 nm, where the short- and long-time perturbations to the transients are minimal.

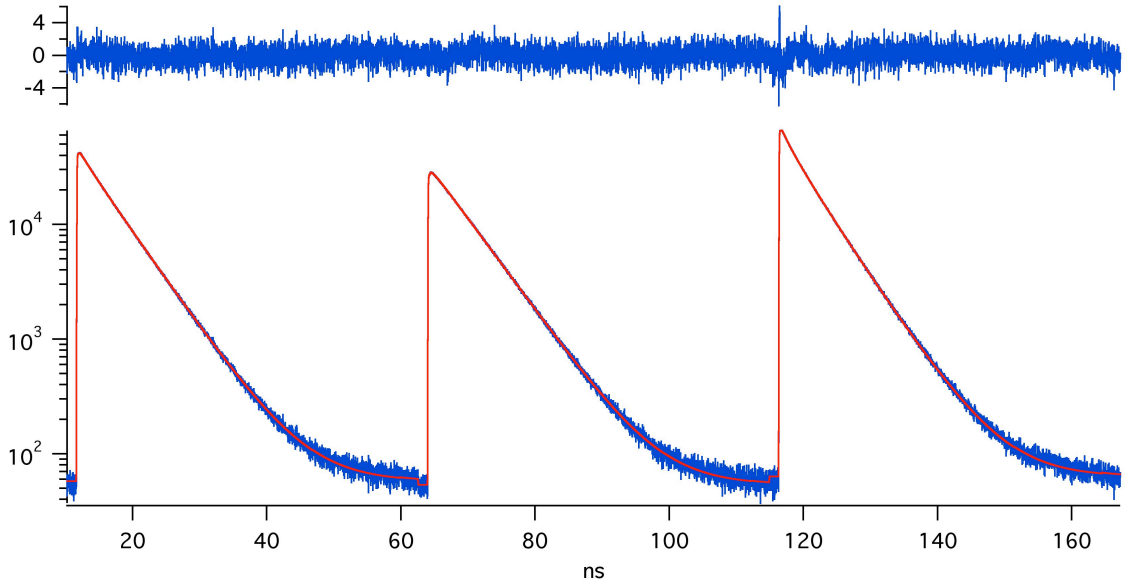

Figure 2.1.3.2 Truncated and concatenated transients for I_{VM}, I_{VV} and I_{VH}

Each transient was measured using a 70 ns data acquisition window. To avoid non-linearities from the edges of the TAC range, I have truncated non-linear regions at the beginning and at the end of the transients. The uncertainty for reorientational dynamics

time constants was estimated to be 5% up to 100 ns and 30% for time constants up to 200 ns.

The $I_{VV}(t)$, $I_{VH}(t)$ and $I_{VM}(t)$ transients were simultaneously fit using the FitAllAtOnce function in IgorPro-5 software.[22] Truncated and concatenated transients $I_{VV}(t)$, $I_{VH}(t)$ and $I_{VM}(t)$ and the reduced residuals from the simultaneous fit are shown in Fig. 2.1.3.2. All three transients were fit at once to equations 2.1.3.2-2.1.3.6. Equation 2.1.3.6 was used to fit the time-resolved decay of polarization anisotropy function r(t) by the sum-of-exponentials model, that allow us to determine component reorientation time constants τ_j and amplitudes r_j for each τ_j . The fit model for each fit was convoluted with the measured instrument response.

$$K(t) = \sum_{i=1} \alpha_i \exp\left(\frac{-t}{\tau_i}\right) \qquad (2.1.3.2)$$

$$I_{VM}(t) = K(t) \qquad (2.1.3.3)$$

$$I_{VV}(t) = \frac{1}{3} K(t)\left(1 + 2r(t)\right) \qquad (2.1.3.4)$$

$$I_{VH}(t) = \frac{1}{3} K(t)\left(1 - r(t)\right) \qquad (2.1.3.5)$$

$$r(t) = \sum_{j=1} r_j \exp\left(\frac{-t}{\tau_{j\_rot}}\right) \qquad (2.1.3.6)$$

where K(t) is isotropic fluorescence decay transient, $I_{VV}(t)$, $I_{VH}(t)$ and $I_{VM}(t)$ are fluorescence intensities at vertical-vertical, vertical-horizontal and vertical-magic polarization angles, respectively, α_i are the normalized amplitudes that sum to unity, t is time, τ_i is the time constant of isotropic fluorescence decay, and τ_j is reorientation time constant.[23-25]

2.2 Investigation of the interaction between water and anion of ILs and diffusional properties in the IL/water system by NMR spectroscopy.

2.2.1 Sample preparation.

2.2.1.2 Materials

The ILs used for these experiments, namely 1-butyl-1-methylpyrrolidinium bis(trifluoromethylsulfonyl)amide ($Pyrr_{14}^+/NTf_2^-$) and 1-butyl-1-methylpyrrolidinium Trifloromethylsulfonate ($Pyrr_{14}^+/OTf^-$), were purchased from Merck/EMD and Iolitech. The ^1H NMR spectra showed the presence of methylene chloride CH_2Cl_2 for ILs bought from Merck/EMD and presence of water for ILs from both vendors. ILs were placed under the vacuum Schlenk line for 48 hours to eliminate these impurities. In order to prepare

samples with particular water concentration we added water to the IL and stirred for 10 hours to ensure homogeneity of the solution. Water concentration was determined using Karl-Fisher titration method. One sample for each liquid was kept as dry as possible: $Pyrr_{14}^{+}/OTf^{-}$ with $x_{H2O} = 0.00023$ and $Pyrr_{14}^{+}/OTf^{-}$ $x_{H2O} = 0.00065$.

2.2.1.3 NMR sample preparation

Investigation of the temperature dependence of the diffusion coefficients requires special preparation of the NMR sample for two reasons. The first reason is the necessity to avoid gas exchange with the atmosphere in order to prevent alteration of the water concentration in the sample. The simplest method is to flame seal the NMR tube. That works for "dry" samples (samples with negligibly small water concentration). But in the case for samples with higher water concentration, water evaporates from the IL and condense at the cold end of the NMR tube. The upper end of the NMR tube is colder because it is further from the temperature controller. Therefore, flame sealed tubes would not completely protect samples of IL/water mixtures from altering the concentration.

A second reason to arrange the special design for NMR samples is the possibility that convection interferes with diffusion. The imperfect design of the temperature controller leads to small fluctuations of the temperature along the sample that cause convection. A possible solution to prevent convection in the sample is to use a shorter sample.[26-28] The smaller length of the sample provides a more even temperature distribution throughout the sample. However, sample length less than 20-25 mm make shimming the magnet difficult, and accurate shimming is necessary for good spectral resolution.

Another way to decrease convection in the sample is the use of a liquid bath to stabilize temperature along the sample.[27]

To avoid these two possible pitfalls, variation of the water concentration in the sample resulting from an exchange with the atmosphere and convection, I designed our samples in the following way. The IL/water mixture samples were flame sealed in the small capsule immediately after determination of the water content by K-F titration. The capsule has a diameter of 3.5 mm and length of approximately 45 mm. The amount of liquid in the capsule was adjusted, so that the length of the sample did not exceed 30 mm. In this case, both a reduced sample length and diameter help to prevent convection effects on the signal. The capsule was placed inside a 5 mm outer diameter NMR tube filled with Krytox oil that served as a liquid bath to eliminate the temperature gradient along the sample. The Krytox is a vacuum lubricant from DuPont consisting of fluorinated hydrocarbons. I chose the Krytox oil as a liquid for the temperature stabilizing bath because it is hydrogen-free, so there are no proton signals in the ^{1}H spectrum to interfere with the spectrum of the $Pyrr_{14}^{+}$ cation. The ^{19}F signal from the Krytox oil does not overlap with the signal from the trifluoromethyl groups of NTf_2^- and OTf^- anions. This encapsulation method was used to prepare all samples including “dry” samples. The images of one of the samples are shown in Fig. 2.2.1.

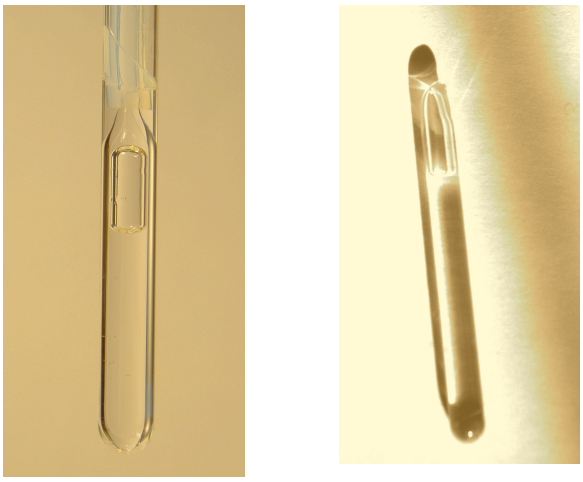

Fig. 2.2.1.1 Left: Photograph of the 3.5 mm OD flame-sealed glass capsule containing the IL/water sample. Right: Photograph of a sample-containing capsule placed inside a standard 5 mm OD NMR tube and covered with Krytox oil.

2.2.1.4 Determination of the water content by Karl-Fisher titration

Water concentration was determined by coulometric Karl-Fisher titration using a Denver Instrument 260 Titration controller. The determination of water concentration by the Karl-Fisher method is based on the oxidation of SO_2 by I_2 according to equation 2.2.1.4.[29, 30] The required iodine is generated at Pt anode by oxidation of iodide contained in the cell solution. Then iodine reacts with H_2O in presence of a nitrogen base, sulfur dioxide and methanol. Thereby, two electrons are required for reaction of one water molecule with one iodine molecule. The amount of water in the sample is determined by electronically integrating the current.

$$I_2 + H_2O + SO_2 + R\text{-}OH + 3R\text{-}N \Rightarrow 2R\text{-}N\text{-}HI + R\text{-}N\cdot HSO_4R \qquad (2.2.1.4)$$

The Hydranal- Coulomat CG reagent was used as a catholyte, and Hydranal-Coulomat AG reagent was used as an anolyte. The accuracy of the method is ±2 μg or 0.5%, the resolution is 0.1 μg of water. The instrument was calibrated prior to each series of experiments by a Hydranal- water standard. The water content of each sample was measured two times. Sample volumes were in the range from 0.5 to 1.5 ml depending on the assumed water concentration.

2.2.1.5 Sample preparation for IL/ D_2O solutions

To study diffusivity of ions in dilute aqueous solutions I prepared samples of $Pyrr_{14}^+/OTf^-$ and $Pyrr_{14}^+/NTf_2^-$ dissolved in D_2O. I chose to dissolve ILs in D_2O and not in H_2O because the peak of water protons almost totally overlaps peaks of the $Pyrr_{14}^+$ cation even with use of the pulse sequence such as WATERGATE that suppresses the water peak. I prepared a sample of $Pyrr_{14}^+/NTf_2^-$ dissolved in D_2O with $x_{pyrr} = 0.0014$ and a sample of $Pyrr_{14}^+/OTf^-$ dissolved in D_2O with $x_{pyrr} = 0.0011$. An aliquot of IL was placed in a weighed amount of D_2O and stirred for 24 hours.

For low viscosity liquids such as D_2O, convection is commonly observed even for small temperature gradients. Therefore, I limited the investigation of diffusion to room temperature measurements. I did not use the ampoules and Krytox™ bath for this samples. These samples were just flame sealed in the NMR tubes.

2.2.2 ^1H, ^{19}F and DOSY NMR measurements

All measurements were performed using the narrow bore Varian DirectDrive spectrometer operating at a proton resonance frequency of 400 MHz. Measurements of ^1H

and ^{19}F spectra and determination of T_1 and T_2 relaxation times were performed using a Varian Auto-X Dual Broadband probe. The field gradient in the pulse field gradient experiments was generated by the model 16-38 diffusion probe from Doty Scientific and gradient amplifier Highlander 10A. In order to avoid error on account of imperfect temperature control I conducted a temperature calibration experiments.

2.2.2.1 Temperature calibration and determination of equilibration time.

One reason for the imperfect temperature control in the NMR experiment can be the difference in temperature of the probe thermometer and temperature of the sample. I employed a temperature calibration method, for which the temperature was measured from the chemical shift of two standard solvent.[27] Methanol was used as a standard for temperatures below ambient, while ethylene glycol was used at temperatures above ambient. I used anhydrous methanol purchased from Sigma Aldrich. Ethylene glycol was dried by CaH_2, and then distilled under vacuum. Both samples were flame sealed in the standard 5mm NMR tubes.

The calibration curve shows small deviations at the high and low temperature regions that do not exceed 0.75 K in the temperature range from 263 to 318 K. These results are shown in the graph in Fig. 2.2.2.1.

The standard sample equilibrated at the room temperature was inserted in the preheated NMR chamber and measurements were conducted with intervals of 30 s each. It was shown that even for high temperatures the equilibration process is fast: at any temperature from 263 to 358 K it takes less than 2 min to completely equilibrate the temperature of the sample.

Nevertheless, samples were equilibrated 15 min after each temperature set up in order to diminish turbulence due to the temperature change.

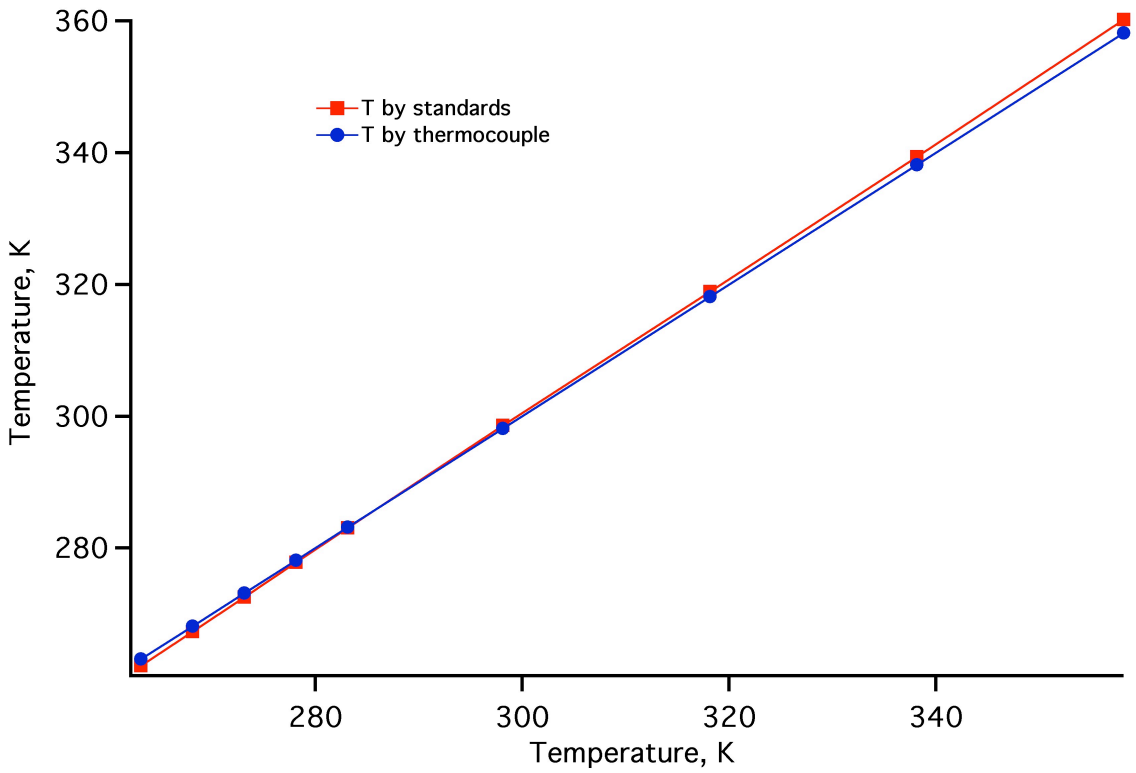

Figure 2.2.2.1 Temperature calibration curve by methanol and ethylene glycol standards. The red line exhibit temperature determined from the chemical shift of the standards; methanol was used below 293 K, ethylene glycol was used above 293 K.

2.2.2.2 Pulse Field Gradient NMR measurements

The NMR method for investigating diffusion in liquids was demonstrated by Stejskal and Tanner in 1965.[31, 32] They introduced the pulsed field gradient method to allow monitoring translational motion of spatially labeled spins. All modern NMR diffusion spectroscopy methods are based on the Pulse Gradient Spin Echo (PGSE) sequence that is shown in Fig. 2.2.2.2.[27, 28]

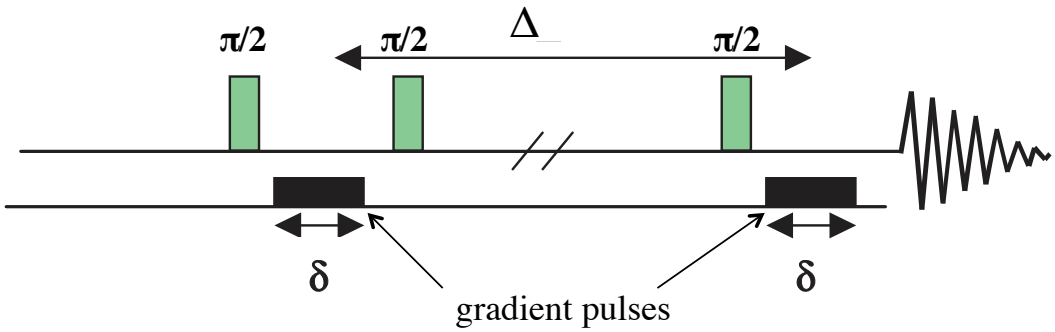

Figure 2.2.2.2 The Pulse Gradient Spin Echo sequence. The gradient pulse duration is given by δ, the time delay between two gradient pulses is given by Δ. [33]

The PGSE sequence operates as follows: The first gradient pulse dephases spins. The second gradient pulse refocus spins; except for those which change coordinates due to diffusion over the time delay Δ between two pulses.[28, 34]

The particular pulse sequence I used is DOSY Bipolar Pulse Pair Stimulated Echo Experiment (DBPPSTE).[35] Instead of each gradient pulse duration of δ there are two equal but opposite gradient pulses of δ/2 duration. Two opposite gradient pulses paired diminish interference associated with eddy currents.[33] The DBPPSTE sequence is shown in Figure 2.2.2.3.

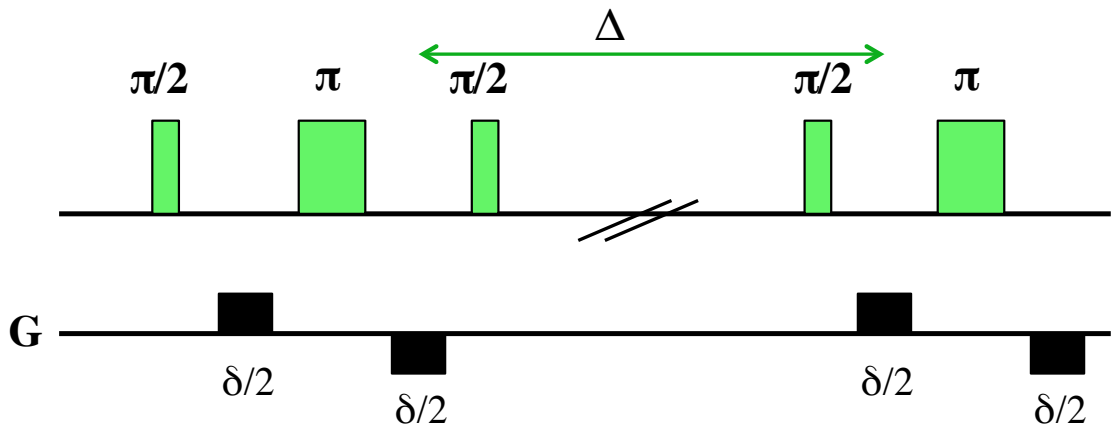

Figure 2.2.2.3 The Bipolar Pulse Pair Stimulated Echo Experiment (DBPPSTE) sequence.[33]

2.2.2.2.1 The spin-lattice and spin-spin relaxation times T_1 and T_2

Some parameters of the DBPPSTE experiment depend on spin-lattice and spin-spin relaxation times T_1 and T_2. The spin-lattice relaxation time T_1 was determined by inversion recovery experiment on the range of temperatures from 263 to 318 K. The T_1 relaxation time varies from 0.5 to 1 s.

The spin-spin relaxation time T_2 was determined by spin echo experiment on the range of temperatures from 263 to 318 K. The T_2 relaxation time varies from 0.05 to 0.15 s.

2.2.2.2.2 The parameters of the DBPPSTE experiment

The choice of the parameters of the DBPPSTE experiment is guided by physical properties of the sample. The duration of the gradient pulse δ is recommended to be

substantially less than T_2, to avoid attenuation of the signal owing to spin-spin relaxation. The duration of the gradient pulse δ was chosen as 0.002 s.

The diffusion time delay Δ is normally set to be less than the T_1 relaxation time in order to avoid signal attenuation resulting from spin-lattice relaxation. Taking into consideration that the T_1 varies from 0.5 to 1 s, it was safe to set the diffusion delay Δ to be 0.07 s.

In order to check for the presence of convection, experiments were run for various values of Δ. The intensity of the PGSE signal has a convection term that depends on Δ according to equation 2.2.2.1[27]

$$I_G \approx \underbrace{I_0 \cos(\gamma \delta G \Delta \upsilon)}_{\textbf{Convection}} * \underbrace{\exp\left(-(\gamma \delta G)^2 D\left(\Delta - \frac{\delta}{3}\right)\right)}_{\textbf{Diffusion}} \qquad (2.2.2.2.1)$$

Here I_G is the intensity of the signal, I_0 is the intensity of the signal at G=0, G is field gradient strength (Gm^{-1}), γ is the gyromagnetic constant ($G^{-1}s^{-1}$), δ is the duration of the gradient pulse (s), Δ is the diffusion delay (s), D is the self-diffusion coefficient (m^2s^{-1}), and υ is the convective flow velocity.

According to equation 2.2.2.2.2, the apparent diffusion coefficient D in the presence of convection will depend on the convective flow velocity υ and on the diffusion delay Δ.

$$D_{app} = D + \frac{\Delta \upsilon^2}{2} \qquad (2.2.2.2.2)$$

where D_{app} is apparent diffusion, D is diffusion without convection, Δ is diffusion delay and υ is the velocity of convective flow.

In order to estimate presence of convection, I measured D for three different diffusion delays: Δ = 0.05, Δ = 0.07 and Δ = 0.1. Measurements were conducted at 318 K, the highest temperature of our temperature series, where the possibility of having temperature gradient and convection is most probable. No sign of convection was observed.

The relaxation delay time constant ***d1*** is recommended to be at least five times longer than T_1 relaxation time, ***d1***≥5* T_1. The relaxation time T_1 varies from 0.5 to 1 s on the range of temperatures 278-318 K. In order to keep the relaxation delay time constant ***d1*** the same at all temperatures, I set it to be 10 s. In this case the degree of relaxation will be very close to 100% at low temperatures as well as at high temperatures.

In order to obtain the best possible signal, the probe was retuned following each temperature change. Calibration of the pulse width *pw* also was conducted following each temperature change. The pulse width was calibrated by checking the pulse width at 90°, 180° and 360° degrees of magnetization vector rotation.

The intensity of the NMR signal was measured as a function of incremental gradient strength G. The gradient strength G was varied from 500-35000 G/m (0.05 - 3.5T/m). The gradient strength array was arranged so that the intensity of the last PGSE signal in the array approximately was equal to 25% of the intensity of the first signal.

The DBPPSTE experiment is time consuming. One experiment including time for temperature equilibration, retuning of the probe, shimming, pulse width calibration, and adjusting the gradient strength array takes on average 1 hour. Limited access to the

instrument equipped with the Doty probe, which is necessary for diffusion measurements, made me cut down the number of experiments and most experiments for the determination of self diffusion coefficients were repeated only two or three times; whereas some experiments were performed only once. The experimental error estimated from standard deviation did not exceed 12%.

2.2.2.3 Determination of self-diffusion coefficient from the exponential decay of the intensity

The intensity of the PGSE signal was measured as a function of incremental gradient strength G. For most experiments an array of 12-15 values of G was used.

The intensity of the signal depends on the square of the field gradient strength exponentially, as given in equation 2.2.2.3.

$$I_G = I_0 \exp\left(-(\gamma\delta G)^2 D\left(\Delta - \frac{\delta}{3} - \frac{\tau_g}{2}\right)\right) \qquad (2.2.2.3)$$

where G is field gradient strength (Gm^{-1}), I_G is the intensity of the signal, I_0 is the intensity of the signal at $G = 0$, γ is gyromagnetic constant ($G^{-1}s^{-1}$), δ is duration of the gradient pulse (s), τ_g is gradient recovery delay, Δ is diffusion delay (s), and D is self-diffusion coefficient (m^2s^{-1}).

The cation self-diffusion coefficient was obtained from the exponential decay of the ^1H NMR signal by Varian software. The self-diffusion coefficients obtained for the seven different ^1H peaks vary insignificantly. Figure 2.2.2.4 presents the typical 2-D

spectrum and it is clear that self-diffusion coefficients for cation peaks are very similar and the only self-diffusion coefficient that differs from others is that for the water peak.

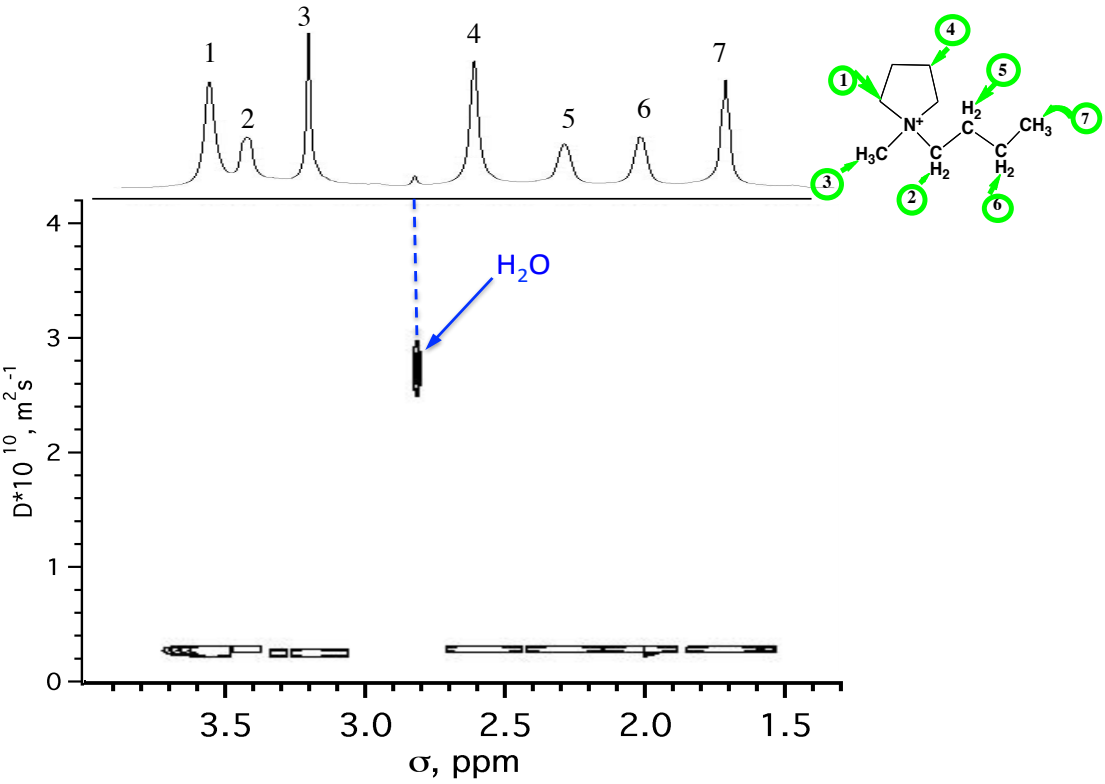

Figure 2.2.2.4 The 2-D DOSY spectrum of $Pyrr_{14}^{+}$ NTf_2^{-}, $x_{H2O} = 0.112$ illustrating that self-diffusion coefficients for the $Pyrr_{14}^{+}$ cation are very close together.

Some peaks exhibit better reproducibility than others. I performed several trials to determine the peak with smallest standard deviation. The ^{1}H peak that belongs to the pyrrolidinium ring proton, labeled as peak "4" in Fig. 2.2.2.4, shows the smallest deviation. Therefore, all cation self diffusion coefficients were reported for this peak.

2.2.2.5 Determination of self-diffusion coefficients of the anion

Neither of our ILs anions, NTf_2^- and OTf^-, have hydrogen atoms in the structure. Because of this the self-diffusion coefficients of the anions were determined from ^{19}F DOSY experiments in the same way as D_{cation} was obtained from ^1H DOSY experiment. For both anions, there is only unique singlet peak in the spectrum arising from the trifluoromethyl groups.

The diffusion coefficient is inversely proportional to the square of the gyromagnetic ratio constant γ, $D \propto 1/\gamma^2$. Hydrogen and fluorine have different gyromagnetic constant γ, $\gamma_{19F} = 40.05$ MHz/T and $\gamma_{1H} = 42.58$ MHz/T. The Varian software calculates the diffusion coefficient based on the $\gamma_{1H} = 42.58$ MHz/T. Therefore, the diffusion coefficient of fluorine calculated by the Varian software must be multiplied by a conversion factor of 1.13, that is the square of γ_{1H}/γ_{19F}.

A possible pitfall in the determination of the anion self-diffusion coefficient is that the sensitivity of the probe to the gradient strength depends on whether the probe is tuned to ^{19}F or ^1H. In order to eliminate this source of error I measured the diffusion of fluorobenzene which has both hydrogen and fluorine in the same molecule. The self-diffusion coefficients of hydrogen and fluorine measured by ^{19}F-DOSY-experiments and ^1H-DOSY-experiment and multiplied by the conversion factor were the same; that proves the validity of the conversion factor equal to 1.13. Therefore, the self diffusion coefficient of the anion as calculated by Varian software was always multiplied by a conversion factor of 1.13.

2.2.2.6 Determination of D_{water} using double exponential fit

The self-diffusion coefficient of the water cannot be calculated using the Varian software for two reasons. The first reason is that the water peak is comparably small, especially in samples with low water concentration, and any distortion of the peak can lead to significant error in the calculation of D_{H2O}. The second reason is that the chemical shift of the water depends on the water concentration and temperature. At some concentrations and temperatures the water peak is partially overlapping with the peak of the methylene group protons on the ring for the $Pyrr_{14}^{+}/NTf_2^{-}$ and methyl group protons attached to the nitrogen for the $Pyrr_{14}^{+}/OTf^{-}$, as shown in Fig. 2.2.2.5.

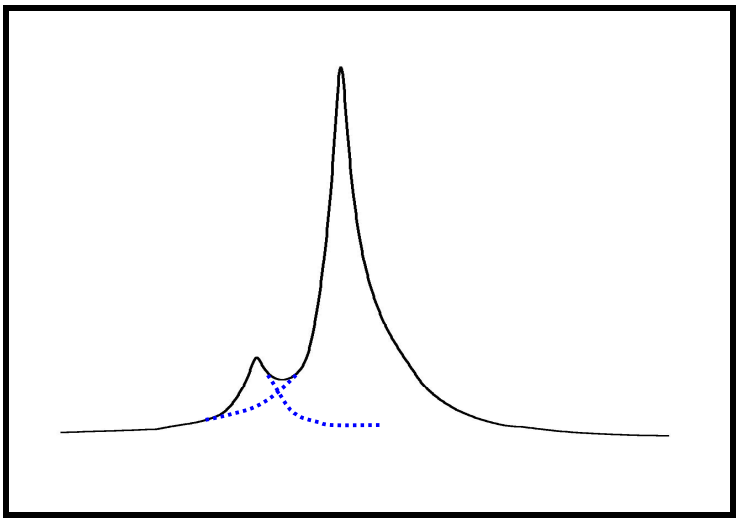

Figure 2.2.2.5 The water peak overlapping with the peak of methyl group attached to the nitrogen for the $Pyrr_{14}^{+}/OTf^{-}$, $x_{H2O} = 0.204$

There are two components contributing to the decay of the water NMR signal: one is real diffusion of water molecules and another is artifact due to overlap with cation peak, which is also decaying because of diffusion of the cation. Fig. 2.2.2.6 presents the logarithmic plot of intensity decay for the water peak and for the ring proton peak of the

cation. The normalized spin echo intensity plotted as a function of the gradient strength squared, as shown in equations 2.2.2.4.

$$\ln\left(\frac{I_G}{I_0}\right) = -(\gamma\delta G)^2 D\left(\Delta - \frac{\delta}{3} - \frac{\tau_g}{2}\right) = KG^2 \qquad (2.2.2.4)$$

In the logarithmic plot the single-exponential decay of the cation peak represented by a straight line, whereas the intensity decay of the water peak is not a straight line due to the artifact of overlap. It is clearly seen in the plot in Fig. 2.2.2.6 that at weak field gradients the water peak is decaying rapidly owing to the fast diffusion of water molecules, and at higher gradients decay is practically parallel to the decay of the cation peak.

The Varian PG-SE analysis software cannot be used for calculations of water self diffusion coefficient because it does not account for the non-exponential decay of the water peak. The self-diffusion coefficient of water can be deduced from the double-exponential fit of the apparent intensity of the water peak I_{H2O_app} as a function of G.[36] The apparent intensity of the water peak as a sum of two components is described by equations 2.2.2.5-2.2.2.8. The self-diffusion coefficient of water D_{H2O} is equal to one of two exponential components in the equation 2.2.2.8, when the other component, D_{cation}, is held constant. The value of D_{cation} is obtained from the exponential fit of equation 2.2.2.7

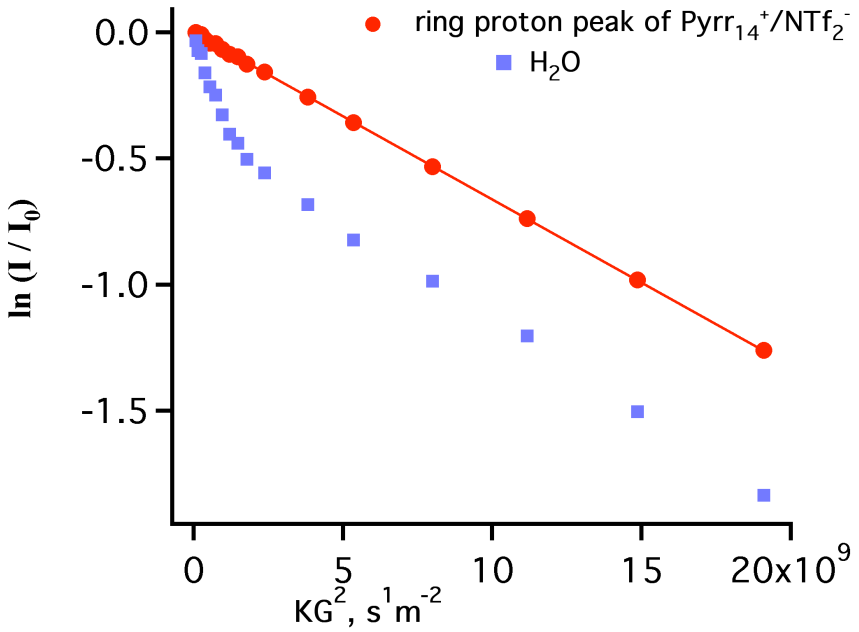

Figure 2.2.2.6 Logarithmic of the normalized spin echo intensity vs. KG^2 illustrating double exponential decay of the water peak. Data are shown for the ring proton peak and the water peak of the sample of $Pyrr_{14}^+/NTf_2^-$, $x_{H2O} = 0.112$ at 318 K.

$$I_{H2O\_app} = A_1 I_{H2O} + A_2 I_{cation} \tag{2.2.2.5}$$

where I_{H2O_app} is the apparent intensity of the water peak overlapping with the cation peak, I_{H2O} is signal intensity due to water protons, $I_{catiion}$ is signal intensity due to cation protons, and A_1, A_2 coefficients characterize the degree of the overlapping.

$$I_{H2O} = I_0 \exp\left(D_{H2O}(-(\gamma\delta G)^2)\left(\Delta - \frac{\delta}{3} - \frac{\tau_g}{2}\right)\right) = I_0 \exp(D_{H2O} M) \tag{2.2.2.6}$$

$$I_{cation} = I_0 \exp\left(D_{cation}(-(\gamma\delta G)^2)\left(\Delta - \frac{\delta}{3} - \frac{\tau_g}{2} \right) \right) = I_0 \exp(D_{cation} M)$$

(2.2.2.7)

where I_0 is the intensity of the signal at G = 0, G is field gradient strength (Gm^{-1}), γ is gyromagnetic constant ($G^{-1}s^{-1}$), δ is duration of the gradient pulse (s), τ_g is gradient recovery delay, Δ is diffusion delay (s), and D is self-diffusion coefficient (m^2s^{-1}).

$$I_{H2O\_app} = A_2 I_0 \exp\left(MD_{H2O}\right) + A_1 I_0 \exp\left(MD_{cation}\right)$$

(2.2.2.8)

2.2.3 Viscosity measurements

Viscosities were measured using the Cambridge Applied Systems ViscoLab 4100 automated viscometer over the temperature range from 281.8 K to 319.9 K for $Pyrr_{14}^+/OTf^-$ and from 279.9 K to 316.9 K for $Pyrr_{14}^+/NTf_2^-$. The Viscolab 4100 system is equipped with a set of calibrated stainless steel pistons of varying diameters that allow the measurement of viscosity in the range from 1 to 10^4 cP. The flow-through temperature control jacket connected to a Lauda Brinkmann RMT-6 recirculating chiller provided temperature control of ± 0.1 K. The viscometer was placed in a Captair pyramidal glove tent that was continuously purged with argon to avoid absorption of water from the air by the IL. The water content in the sample was measured before and after the temperature series of viscosity measurement using the Karl-Fisher titrator. Each temperature series begins at room temperature. Then the viscosity was measured at higher temperatures than

ambient, for which the absorption of water from the air is less likely. Following the above-ambient measurements, I measured viscosity at points below room temperature. The water content was 129 ppm before and 560 ppm after viscosity measurement for $Pyrr_{14}^{+}/OTf^{-}$. The more hydrophobic $Pyrr_{14}^{+}/NTf_2^{-}$ did not absorb a substantial amount of water; the water content was 52 ppm before and 378 ppm after the viscosity measurement.

References

1. H. Shirota, E. W. Castner, Jr., *Solvation in highly nonideal solutions: A study of aqueous 1-propanol using the coumarin 153 probe*. J. Chem. Phys., 2000. **112**: p. 2367.
2. S. Arzhantsev, M. Maroncelli, *Design and Characterization of a Femtosecond Fluorescence Spectrometer Based on Optical Kerr Gating*. Appl. Spectrosc., 2005. **59**: p. 206.
3. E. W. Castner Jr., M. Maroncelli, *Solvent dynamics derived from optical Kerr effect, dielectric dispersion, and time-resolved Stokes shift measurements: an empirical comparison*. Journal of Molecular Liquids 1998. **77(1-3)**: p. 1.
4. H. Shirota, E. W. Castner, Jr., *Physical Properties and Intermolecular Dynamics of an Ionic Liquid Compared with Its Isoelectronic Neutral Binary Solution*. J. Phys. Chem. A, 2005. **109**: p. 9388.
5. H. Shirota, J. F. Wishart, E. W. Castner Jr., *Intermolecular Interactions and Dynamics of Room Temperature Ionic Liquids That Have<p>Silyl- and Siloxy-Substituted Imidazolium Cations*. J. Phys. Chem. B, 2007. **111**: p. 4819.
6. H. Shirota, A. M. Funston, J. F. Wishart, E. W. Castner, *Ultrafast dynamics of pyrrolidinium cation ionic liquids*. J. Chem. Phys., 2005. **122**: p. 184512.
7. A. Noda, K. Hayamizu, M. Watanabe, *Pulsed-Gradient Spin−Echo 1H and 19F NMR Ionic Diffusion Coefficient, Viscosity, and Ionic Conductivity of Non-Chloroaluminate Room-Temperature Ionic Liquids*. J. Phys. Chem. B, 2001. **105**: p. 4603.
8. H. Tokuda, K. Hayamizu , K. Ishii, M. A. B. H. Susan , M. Watanabe, *Physicochemical Properties and Structures of Room Temperature Ionic Liquids 2. Variation of Alkyl Chain Length in Imidazolium Cation*. J. Phys. Chem. B, 2005. **109**: p. 6103.
9. M. Maroncelli, G. R. Fleming, , *Picosecond solvation dynamics of coumarin 153: the importance of molecular aspects of solvation*. J. Chem. Phys., 1987. **86(11)**: p. 6221.
10. Horng, M.L., Gardecki, J. A.; Papazyan, A.; Maroncelli, M., J. Phys. Chem., 1995. **99,** : p. 17311-37.
11. A. M. Funston, T. A. Fadeeva, J. F. Wishart, E. W. Castner, Jr., *Fluorescence Probing of Temperature-Dependent Dynamics and Friction in Ionic Liquid Local Environments*. J. Phys. Chem. B, 2007. **111**: p. 4963.
12. A. Skrzypczak, P. Neta, *Diffusion-Controlled Electron-Transfer Reactions in Ionic Liquids*. J. Phys. Chem. A, 2003. **107**(39): p. 7800.
13. A. Skrzypczak, P. Neta, *Rate constants for reaction of 1,2-dimethylimidazole with benzyl bromide in ionic liquids and organic solvents* Int. J. Chem. Kinet. , 2004. **36**: p. 253.
14. M. N. Kobrak, *The chemical environment of ionic liquids: links between liquid structure, dynamics, and solvation*. Adv. Chem. Phys., 2008. **139**: p. 85.

15. K. R. Seddon, A. Stark, M. Torres, *Influence of chloride, water, and organic solvents on the physical properties of ionic liquids*. Pure Appl. Chem., 2000. **72**: p. 2275.
16. T. Welton, *Room-Temperature Ionic Liquids. Solvents for Synthesis and Catalysis*. Chem. Rev., 1999. **99**: p. 2071.
17. H. Shirota, E. W. Castner Jr., *Solvation in highly nonideal solutions: A study of aqueous 1-propanol using the coumarin 153 probe*. J. Phys. Chem. B, 2000. **112**: p. 2367.
18. C. D. Grant, M. R. DeRitter, K. E. Steege, T. A. Fadeeva, E. W. Castner, Jr., *Fluorescence Probing of Interior, Interfacial, and Exterior Regions in Solution Aggregates of Poly(ethylene oxide)– Poly(propylene oxide)–Poly(ethylene oxide) Triblock Copolymers*. Langmuir 2005. **21**: p. 1745.
19. C. D. Grant, K. E. Steege, M. R. Bunagan, E. W. Castner, Jr., *Microviscosity in Multiple Regions of Complex Aqueous Solutions of Poly(ethylene oxide)–Poly(propylene oxide)–Poly(ethylene oxide)*. J. Phys. Chem. B, 2005 **109**: p. 22273.
20. L. Frauchiger, H. Shirota, K. E. Uhrich, E. W. Castner, Jr., *Dynamic Fluorescence Probing of the Local Environments within Amphiphilic Star-like Macromolecules*. J. Phys. Chem. B, 2002. **106**: p. 7463.
21. K. E. Steege, J. Wang, K. E. Uhrich, E. W. Castner Jr., *Local Polarity and Microviscosity in the Hydrophobic Cores of Amphiphilic Star-like and Scorpion-like Macromolecules*. Macromolecules 2007. **40**: p. 3739.
22. *Wavemetrics Igor Pro 5.04b Edition. Wavemetrics, Inc. Lake Oswego, OR,* , 2005.
23. A. J. Cross, G. R. Fleming, *Analysis of time-resolved fluorescence anisotropy decays*. Biophys. J. , 1984 **46**: p. 45.
24. B. Valeur, *Molecular Fluorescence: Principles and Applications* 2002: Wiley-VCH.
25. J. R. Lakowicz, *Principles of Fluorescence Spectroscopy*1999: Kluwer Academic/ Plenum Publishers.
26. W. S. Price, *NMR studies of translational motion* 2009.
27. T. D. W. Claridge, *High-Resolution NMR Techniques in Organic Chemistry*, ed. J. E. Backvall, J.E. Baldwin, and R.M. Williams 2009: Elsevier.
28. J. B. Lambert, E. P. Mazzola, *Nuclear Magnetic Resonance 5pectroscopy An Introduction to Principles, Applications, and Experimental methods*.2004: Pearson Education, Inc.
29. T. Chandrasekhar, *260-Titration controller operation manual*, 2008, Denver instrument Company.
30. P. A. Bruttel, R. Schlink, , *Water determination by Karl Fischer Titration* 2004: Metrohm AG, .
31. E. O. Stejskal, *Use of spin echoes in a pulsed magnetic-field gradient to study anisotropic, restricted diffusion and flow*. J. Chem. Phys., 1965. **43** p. 3597.
32. J. E. Tanner, *Use of the stimulated echo in NMR diffusion studies*. J. Chem. Phys., 1970. **52 (5)**: p. 2523.
33. E. Schreiber, *VnmrJ Liquids NMR User Guide*. , ed. E. Schreiber 2006.
34. J. Keeler, *Understanding NMR spectroscopy* 2005: Wiley.

35. D. Wu, A. Chen, C. S. Johnson, Jr., *An Improved Diffusion Ordered Spectroscopy Experiment Incorporating Bipolar Gradient Pulses*. J. Magn. Reson. , 1995. **A115**: p. 260.
36. A. Menjoge, J. Dixon, J. F. Brennecke, E. J. Maginn, S. Vasenkov, *Influence of Water on Diffusion in Imidazolium-Based Ionic Liquids: A Pulsed Field Gradient NMR study*. J. Phys. Chem. B, 2009. **113**(18): p. 6353.

Chapter 3

Investigation of polarity, solvation and local friction in the Ionic Liquids

3.1 Overview

Fluorescence spectroscopy of the solvatochromic probe Coumarin 153 (C153) in the Ionic Liquids was used to examine properties of four ionic liquids (ILs) with non-aromatic cations. As a result, polarity, the temperature dependent solvation dynamics, and reorientational dynamics were characterized.The polarity was characterized using the method of steady-state spectroscopy. The temperature dependent solvation dynamics was investigated using the method of time dependent fluorescence Stokes shift (TDFSS). The solvation dynamics was characterized using a time-dependent solvation function and the temperature dependence of the solvation behavior was investigated for all four ILs. Below we present the principal steps of the experiment, where the major point is obtaining the frequency shift of the time-dependent emission spectra.

3.1.1 The TDFSS scheme for studying solvation dynamics

1. Obtain the steady-state spectra of the C153 for all ILs at each temperature

2. Measure fluorescence transients using the time correlated single photon counting (TCSPC) setup
3. Fit the transients to a sum-of-exponentials model
4. Normalize the transients to steady-state spectra
5. Reconstruct spectra at fixed time delays using time slices from the normalized transients
6. Obtain the peak frequency of the reconstructed spectra using log-normal skewed Gaussian fit
7. Construct the solvation time correlation function from the graph of the maximum fluorescence emission wavelength vs. time
8. Fit the solvation time correlation function to the multi-exponential model
9. Characterize the solvation dynamics using the effective time constants (τ_0), ($\tau_{1/e}$) and ($\langle \tau \rangle$)

3.1.2 The scheme of the fluorescence anisotropy experiment

Local friction measured by the solvatochromic probe molecule is a means of characterizing the local friction that is experienced by a reacting molecule in this solvent.[1-3] The temperature dependent reorientational dynamics were investigated using the method of time-resolved fluorescence anisotropy.

1. Measure fluorescence transients at three relative polarization angles; vertical-vertical (VV), vertical-magic (VM), and vertical-horizontal (VH), using vertically polarized excitation.
2. Characterize the reorientational dynamics by the anisotropy decay function r(t) constructed based on VV, VM and VH emission intensity transients
3. Fit r(t) to a sum-of-exponentials model
4. Characterize the reorientation dynamics by three time constants (τ_0), ($\tau_{1/e}$) and ($\langle\tau\rangle$)

3.1.3 Four Ionic Liquids are studied

All fluorescence spectroscopy studies were performed for four ILs:

1. *N*-methyl-*N*-butylpyrrolidinium bis(trifluoromethylsulfonyl)-amide
   $Pyrr_{14}^{+}/NTf_2^{-}$
2. *N*-methyl-*N*-ethoxyethylpyrrolidinium bis(trifluoromethylsulfonyl)-amide
   $Pyrr_{1(202)}^{+}/NTf_2^{-}$
3. *N*-methyl-tri-*N*-butylammonium bis(trifluoromethylsulfonyl)-amide
   N_{1444}^{+}/NTf_2^{-}
4. *N*-hexyl-tri-*N*-butylammonium bis(trifluoromethylsulfonyl)-amide
   N_{6444}^{+}/NTf_2^{-}

The structures of the four ILs are presented on Fig.3.1.3.

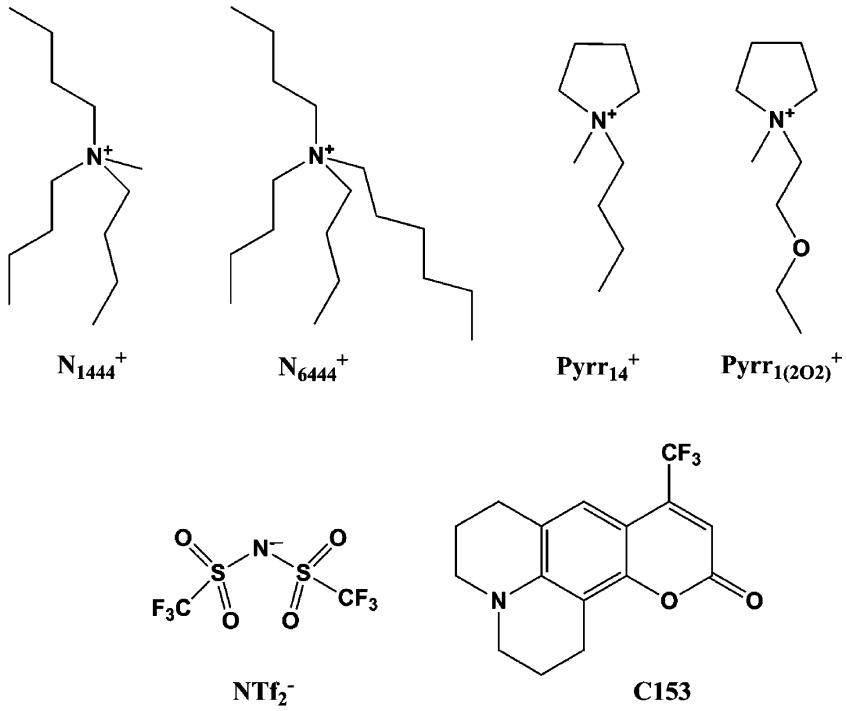

Figure 3.1.3 Structures of the four ionic liquid cations: N_{1444}^+, N_{6444}^+, $Pyrr_{14}^+$, and $Pyrr_{1(202)}^+$, together with the ionic liquid anion NTf_2^- and the fluorescence probe molecule coumarin 153 (C153).[4]

These four ILs have non-aromatic cations in contrast with imidazolium or pyridinium based ILs. Two of these ILs, namely $Pyrr_{14}^+/NTf_2^-$ and $Pyrr_{1(202)}^+/NTf_2^-$, have a pyrrolidinium based cation. The ethoxyethyl substituent makes $Pyrr_{1(202)}^+/NTf_2^-$ even less viscous than $Pyrr_{14}^+/NTf_2^-$.[4] Two other ILs have alkyl-ammonium based cations. Their only difference is the length of the carbon chain of the substituent: methyl for N_{1444}^+/NTf_2^- and hexyl for N_{6444}^+/NTf_2^-. All four ILs mentioned share the same bis(trifluoromethylsulfonyl)-amide (NTf_2^-) anion. The presence of the trifluoromethyl group makes these ILs relatively hydrophobic compared to more water miscible ILs with anions such as NO_3^-, Cl^-, Br^- or trifluoromethylsulfonate.[5] The saturated concentration of water in the bis(trifluoromethylsulfonyl)-amides is typically about $x_{H2O} = 0.24\text{-}0.32$.[6]

The viscosity and the phase behavior of all four ILs were studied by Funston, et al.[4] The calorimetric and viscosity data for the four ionic liquids are shown in Table 3.1.1. The heat capacity data show that ammonium based ILs have melting points around 300 K. Note that all measurements performed at 278.2 and 293.2 K were on supercooled liquids. Pyrrolidinium based ILs exhibit lower melting points. While $Pyrr_{14}^{+}/NTf_2^{-}$ has a melting point at 255 K, $Pyrr_{1(202)}^{+}/NTf_2^{-}$ does not exhibit a melting point at all. Instead of a melting transition, $Pyrr_{1(202)}^{+}/NTf_2^{-}$ displays a small negative change in heat capacity at 235 K.[4] The viscosities for all four ILs can be determined from the Vogel-Tamman-Fulcher (VTF) model as shown in equation 3.1.1.

$$\ln \eta = \ln \eta_0 + \frac{DT_C}{T - T_C} \qquad (3.1.1)$$

where η_0 is a reference viscosity at which the exponential term is 0, *D* is the fragility parameter, T_c is a characteristic temperature at which η diverges.[7, 8]

The parameters for all four ILs are given in the Table 3.1.1, as well as viscosities at 293.2 K. Note that the ammonium based ILs are approximately an order of magnitude more viscous than pyrrolidinium based ILs.[4]

Table 3.1.1 Calorimetric and viscosity data for four Ionic Liquids.[a]

cation	T_g (K)	T_m (K)	η (cP)	ln(η_0)	D	T_c
N_{1444}^+	205	300	787	-4.12	8.45	164.4
N_{6444}^+	206	298	909	-3.51	7.93	165.8
$Pyrr_{14}^+$	184	255	95	-2.28	6.11	154.8
$Pyrr_{1(202)}^+$	182		66	-2.09	5.59	155.1

[a] T_g is a glass transition temperature, T_c is onset temperature for VTF model, η are reported for 293.2 in cP

3.2 Investigation of polarity of ILs by steady-state fluorescence spectroscopy

The steady-state fluorescence emission and excitation spectra of Coumarin 153 were measured for four ILs at six temperatures (278.2 K, 293.2 K, 308.2 K, 323.3 K, 338.2 K and 353.2 K) to characterize polarity of ILs and for the purpose of reconstruction of time dependent emission spectra. All spectra are shown in Fig.3.2.1.

One of the possible pitfalls in the study of the fluorescence emission probes in the IL is the fact that some ILs have non-negligible fluorescent emission of their own.[9, 10] Fortunately, ILs based on non-aromatic cations do not have any significant background emission. The emission spectra of C153 in the ILs were not perturbed by the emission of the neat ILs.[4]

It is clearly seen on Fig. 3.2.1 that there is a difference between emission spectra of the alkylammonium and pyrrolidinium based ILs. For two alkylammonium based ILs,

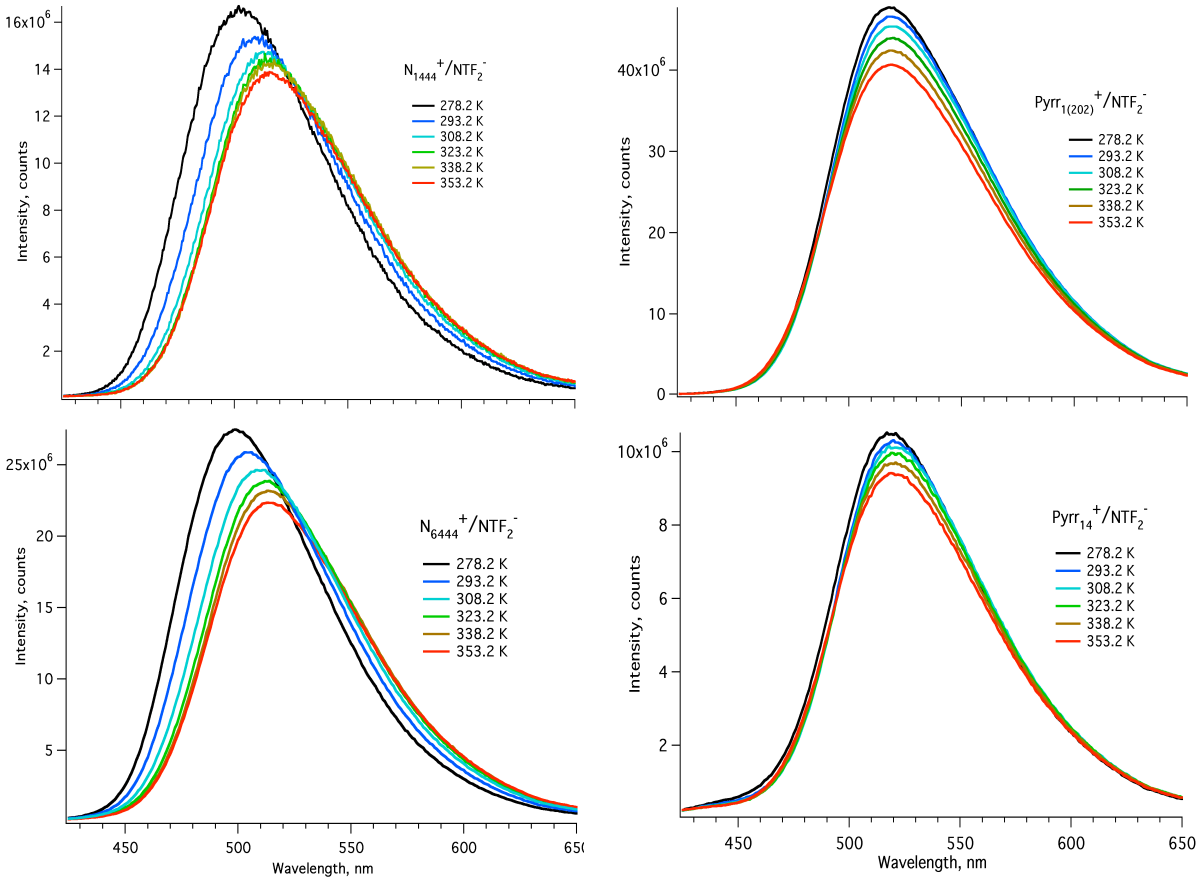

Figure3.2.1 The steady-state fluorescence emission spectra of the Coumarin-153 in the N_{1444}^{+}/NTf_2^{-} N_{6444}^{+}/NTf_2^{-}, $Pyrr_{14}^{+}/NTf_2^{-}$ and $Pyrr_{1(202)}^{+}/NTf_2^{-}$

N_{1444}^{+}/NTf_2^{-} and N_{6444}^{+}/NTf_2^{-}, the maximum emission wavelength shifts to the red with increasing temperature. This effect can be explained by slow solvation dynamics in the viscous and supercooled ILs, taking into consideration that melting points for both ammonium based ILs is near 300 K.

Immediately after excitation, a chromophore emits light at a particular wavelength. The solvation process as a rapid reorientation of IL ions around the chromophore molecule follows the excitation of the chromophore and decreases the energy of emitted light.

Consequently, the maximum emission wavelength shifts to the red edge of the spectrum. The spectrum registered by steady state spectroscopy is an integral sum of the emission starting at the moment from when the molecule is excited. The endpoint of this process depends on the lifetime of the chromophore. If the process of solvation is slow and is not completed during the chromophore lifetime, then emission of totally solvated chromophores (emission at the red edge) is not registered and the spectrum is blue shifted. With an increasing temperature, the viscosity of the IL decreases, and the solvation process gets faster. Therefore, the blue shift is observed at low temperatures and is diminished or not observed at high temperatures.

This effect is much less significant for pyrrolidinium based ILs $Pyrr_{14}^{+}/NTf_2^{-}$ and $Pyrr_{1(202)}^{+}/NTf_2^{-}$. These two ILs are less viscous and have lower T_m. Subsequently, the solvation processes are nearly totally resolved for the lifetime of C153.

The emission spectrum of the some chromophores can be used for determination of the polarity of the solvent. One of the most commonly used empirical solvent polarity scales build on the base of hypsochromic behavior (blue shift) of the betaine-30 dye in the polar solvents. The correlation between red shift of C153 in the polar solvents and the empirical solvent polarity scale was developed by Horng and coworkers for polar aprotic solvents.[11] Equation 3.2.1 shows the relationship for determination of empirical polarity.

$$\nu_{em} = 21217 - 3505 \bullet \pi^* \qquad (3.2.1)$$

where ν_{em} is maximum of C153 emission expressed in wavenumbers, cm^{-1} and π^* is polarity by empirical solvent polarity scale.

The values of π* were estimated for all four ILs for all temperatures, as shown in Table 3.2.1. Obviously, the value of π* estimated for N_{1444}^{+}/NTf_2^{-} and N_{6444}^{+}/NTf_2^{-} at temperatures below 338.2 K, does not reflect true polarity of the IL because the solvation relaxation is not completed during the excited state lifetime of the probe. This case reminds us of the necessity to consider the specificity of solvation dynamics in supercooled ILs. The temperature dependence of π* for four ILs is shown in Fig.3.2.2. The estimated value of π* at the 353.2 characterize N_{1444}^{+}/NTf_2^{-} and N_{6444}^{+}/NTf_2^{-} as being slightly more polar than $Pyrr_{14}^{+}/NTf_2^{-}$ and $Pyrr_{1(202)}^{+}/NTf_2^{-}$ that consists with a literature data.[12-15]

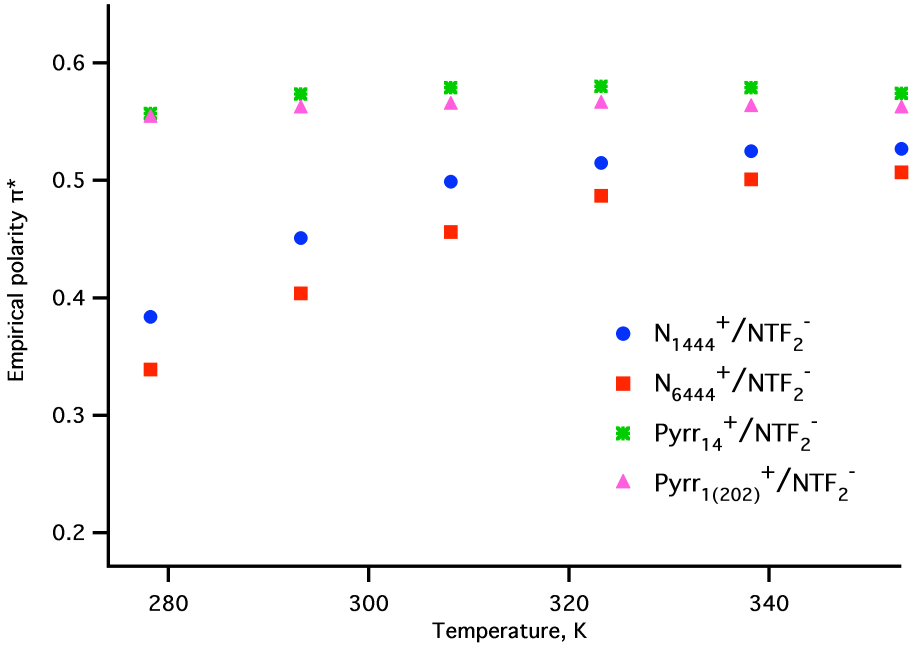

Figure 3.2.2 The plot of empirical polarity estimated from steady-state fluorescence spectra of C153 in ILs vs. temperature. The plot illustrates the artifact of estimated polarity due to slow solvation dynamics in the supercooled ILs.

All steady-state fluorescence spectra were used to reconstruct the time dependent emission spectra in the investigation of the temperature dependent solvation dynamics using the method of Time Dependent Fluorescent Stokes Shift (TDFSS).

Table 3.2.1 C 153 emission maxima and estimated values of π^*.[a]

T (K)	N_{1444}^+ / NTf_2^-		N_{6444}^+ / NTf_2^-		$Pyrr_{14}^+ / NTf_2^-$		$Pyrr_{1(202)}^+ / NTf_2^-$	
	ν_{em_max}	π^*	ν_{em_max}	π^*	ν_{em_max}	π^*	ν_{em_max}	π^*
278.2	19872	0.384	20028	0.339	19265	0.557	19280	0.553
293.2	19637	0.451	19802	0.404	19207	0.574	19249	0.561
308.2	19468	0.499	19620	0.456	19187	0.579	19240	0.564
323.2	19411	0.515	19508	0.487	19186	0.580	19237	0.565
338.2	19376	0.525	19461	0.501	19189	0.579	19247	0.562
353.2	19371	0.527	19439	0.507	19203	0.574	19252	0.561

[a] frequency units are cm^{-1}

3.3 Temperature dependent solvation dynamics for a series of four ILs with non-aromatic cation

3.3.1 The physicochemical background of the TDFSS method

The method of Time Dependent Fluorescent Stokes Shift is widely used for investigation of solvation dynamics in ILs.[1, 12, 13, 15-22]

As the chromophore is excited by light, it rapidly changes its electronic configuration. Then, the part of the excited state energy is relaxed via internal conversion and vibrational relaxation processes. This process has a duration of approximately 2-10 ps and cannot be resolved by TDFSS method. Some energy should be consumed during interaction with a solvent because in the excited state the dipole moment of the molecule is significantly larger than in the ground state, and now dipoles or ions of solvent urge to reorient around the molecule. This occurs on the time scale of nanoseconds.[23] Vibration relaxation and solute-solvent interactions are both responsible for shift of emissions wavelength from the wavelength of the excitations light. The Fig.3.3.1.1 exhibit transition of the C153 chromophore molecule from ground state to excited state, and reorientation of solvent molecules (or ions) around it.

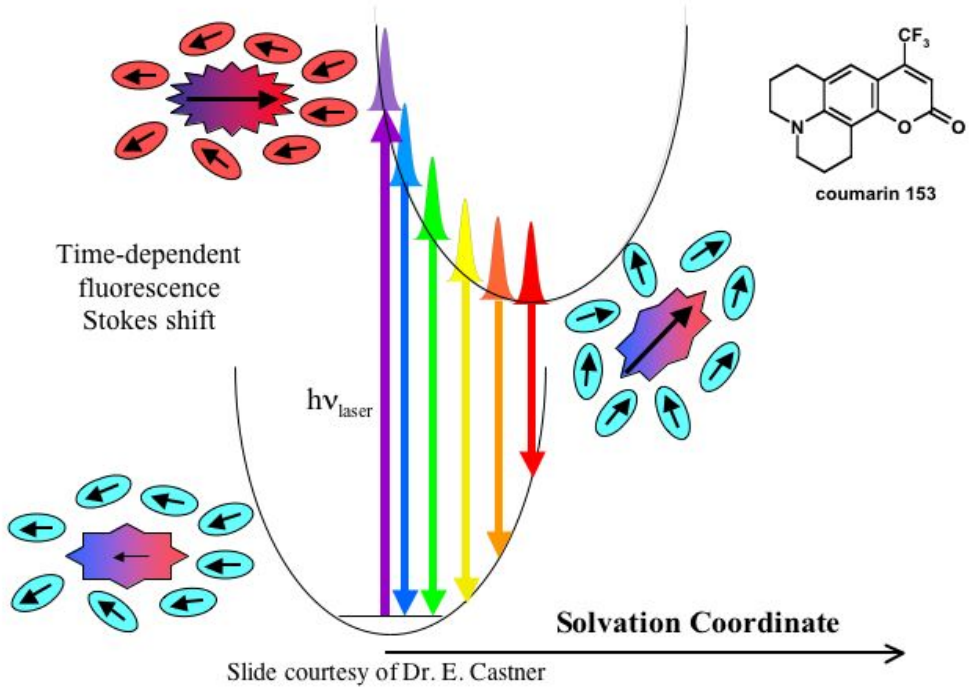

Figure 3.3.1.1 Illustration of the principles of the time-dependent fluorescence Stokes shift.

When the chromophore emits light, emission occurs at longer wavelengths. This shift of the emission wavelength relative to excitation wavelength is called Stokes shift and can be observed by steady state fluorescence.

Obviously, the Stokes shift depends strongly on the polarity of the media and the local environment of the chromophore. Therefore, Stokes shift can be used to determine polarity of the medium or the local environment of the probe.

Another manifestation of the interaction of the chromophore with its local environment can be observed by time resolved spectroscopy. The decay of the fluorescence emission detected at the particular wavelength is not exponential. This is because there are two or more components that contribute to the decay of the population of excited

chromophores having particular energy. In addition to the radiative decay processes, there are also relaxation processes caused by interaction with solvent that consequently leads to the transfer of these chromophores to the population with lower energy, which corresponds to longer wavelength. The multi-exponential time dependence of fluorescence intensity described by equation 3.3.1.[24]

$$I(t) = \sum_{j=1} a_j \exp(-\frac{t}{\tau_j}) \qquad (3.3.1)$$

where τ_j are decay time constants, and a_j are amplitudes.

The pattern of the fluorescence decay is not the same for emission at the different wavelength. In Fig.3.3.1.2 one can observe a rapid decay of blue wavelength changes to be slow at the red wavelengths.

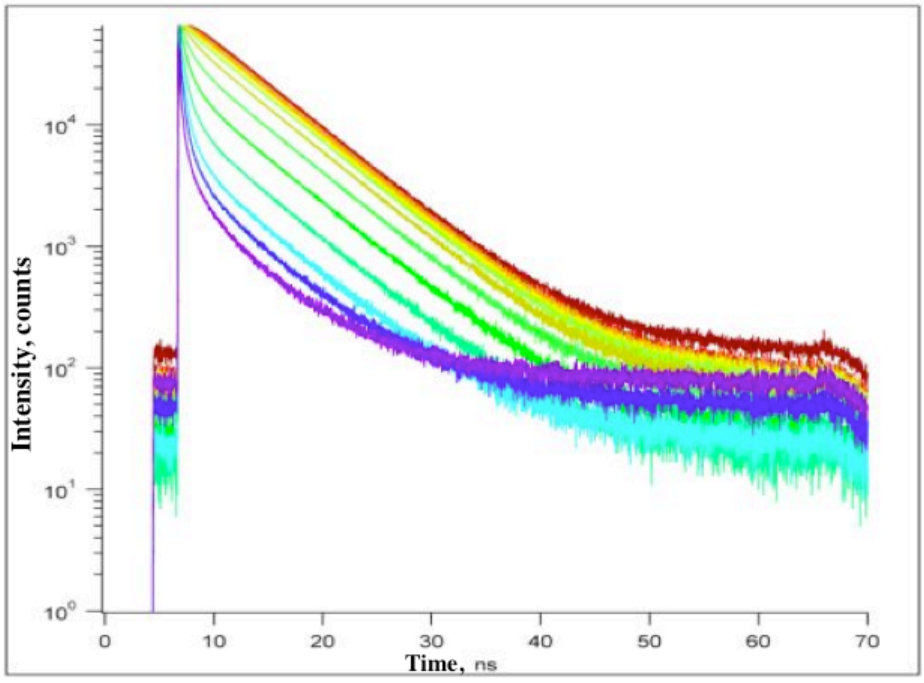

Figure 3.3.1.2 Time-dependent fluorescence transients for C153 in N_{1444}^{+}/NTf_2^{-} at 293.2 K.

3.3.2 Multi-exponential fits of the fluorescence transients

For each IL at each temperature point I measured fluorescence transients at 14 particular emission frequencies in the range from 16250 to 22750 cm^{-1} with 500 cm^{-1} increments. Typical TCSPC transients for C153 in N_{1444}^{+}/NTf_2^{-} at 308.2 K are presented in Fig.3.3.2.1. Three transients have been chosen to represent emission at the red edge, middle and blue edge of the spectrum, which were measured at 22250 cm^{-1}(top), 18750 cm^{-1} (middle) and 16250 cm^{-1} (bottom) emission frequency. All transients were fit to 3, 4 or 5 exponential models using an iterative convolute-and-compare nonlinear least-squares analysis. In general, more exponentials must be included in order to fit the transients measured at the edges of the spectrum. The multi-exponential character of the transients is especially pronounced for emission at the high frequency, such as at 22250 cm^{-1}; this is

clearly seen in Fig. 3.3.2.1, top. These multi-exponential fits were used to reconstruct spectra at particular time delays in order to determine the frequency shift caused by solvation.

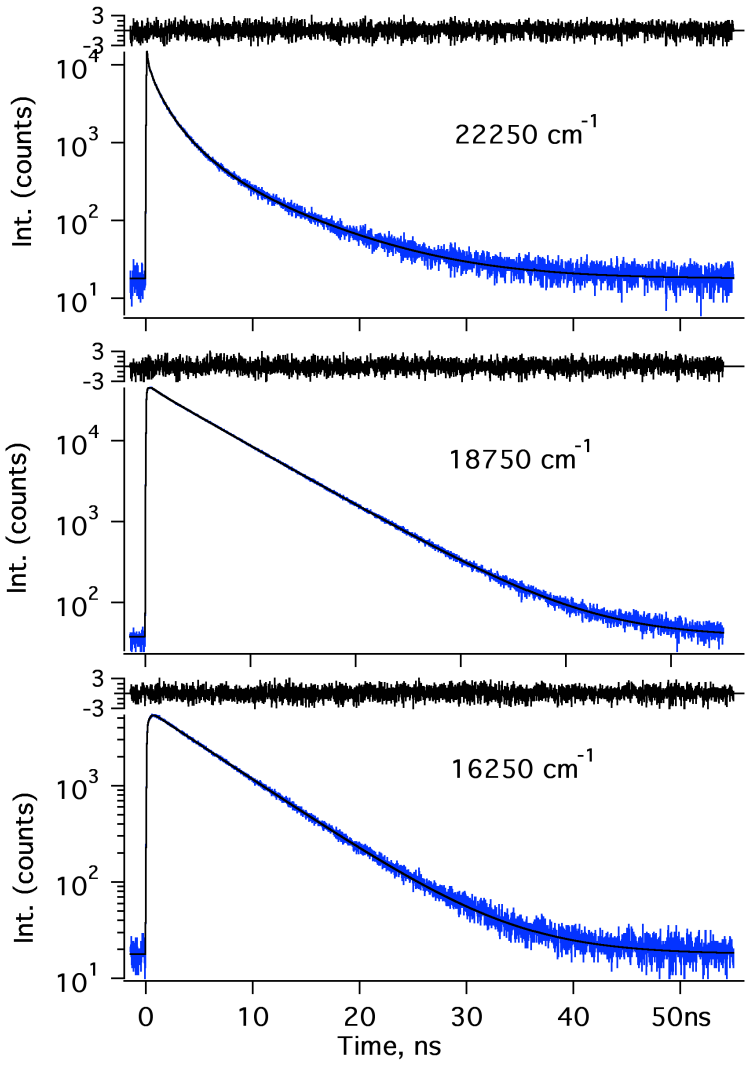

Figure 3.3.2.1 TCSPC transients for C153 in $Pyrr_{14}^{+}/NTf_2^{-}$ at 308.2 K, using 420 nm laser excitation. The TCSPC data are shown in blue, with the best fits to 5-exponential (top, bottom) and 4-exponential (middle) models and reduced residuals shown in black. Note that the emission transient for 22, 250 cm^{-1} is clearly nonexponential over the entire transient.

3.3.3 Reconstruction of spectra at particular time delays

The spectra at particular time delays have been reconstructed by the standard spectral reconstruction method.[11, 25, 26] These spectra can be viewed as "slices" of the 3-dimensional plot where z axis is emission intensity, y axis is emission frequency, and x axis is time. I have calculated the reconstructed spectra for 101 time slices from 1 ps to 100 ns. It should be taken into consideration that the lifetime of the C153 in the ILs is approximately 5 ns, therefore after 30 ns the intensity of the signal is less than 1% of the initial intensity. Time-slices of the normalized TCSPC transients were log-spaced for times ranging from 1 ps to 100 ns; but usually only slices up to 20 ns were processed.

Fig.3.3.2.2 presents a few typical spectra for N_{1444}^{+}/NTf_2^{-} at 338.2 K.

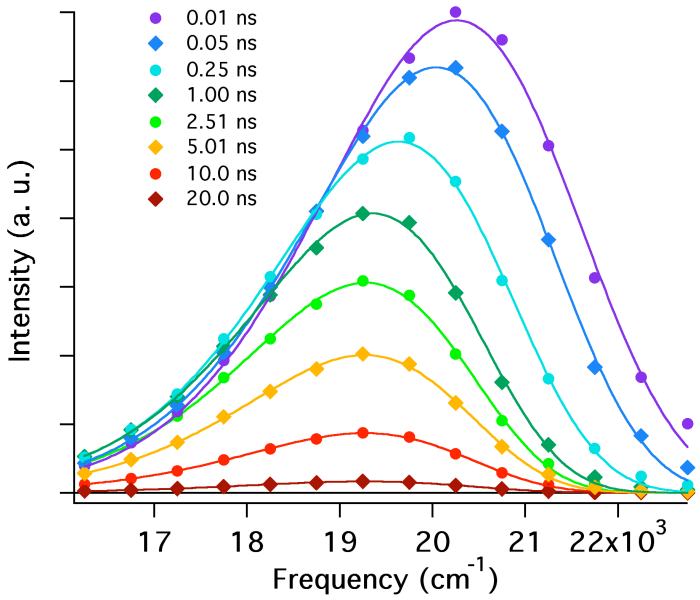

Figure 3.3.2.2 Typical reconstructed emission spectra for C153 in N_{1444}^{+}/NTf_2^{-} at 338.2 K. The circles represent the intensity of the emission at the given time slice, while the solid lines are the log-normal fits to the transient spectra. From top to bottom, the spectra are plotted for time slices at 0.01, 0.05, 0.251, 1.0, 2.51, 5.01, 10.0, and 20.0 ns.

The maximum emission frequency shifts to the red edge with time. This shift represents the solvation dynamics of the chromophore probe owing to movement of ions around the C153 probe molecule.

3.3.4 The solvation dynamics frequency-shift function

The solvation dynamics frequency-shift function was plotted as the maximum emission frequency vs. time for each IL for all temperature points, as shown in Fig. 3.3.4.2. For our ILs, the solvation dynamics frequency-shift function $\nu_{em}(t)$ exhibits non-exponential character and cannot be fit to the single-exponential model. The multi-exponential character of the solvation function $\nu_{em}(t)$ is especially well seen on two upper plots in Fig. 3.3.4.2; the inflection points in the log-log plots of $\nu_{em}(t)$ vs. time for ammonium based ILs indicate that the solvation dynamics are non-exponential.

Each of the solvation dynamics time-correlation functions $\nu_{em}(t)$ has been fit to sums of exponentials. Usually the best fit was obtained with a 3- or 4-exponential model, with a fewer exponentials (sometimes only two) at the higher temperatures. The best fits for all four ILs are presented in tables 3.3.2.1, 3.3.2.2, 3.3.3.3 and 3.3.3.4.

The solvation relaxation is much slower for more viscous N_{1444}^{+}/NTf_2^{-} and N_{6444}^{+}/NTf_2^{-} than for the pyrrolidinium based ILs. Time constants for the pyrrolidinium based ILs are order of magnitude smaller than for ammonium based ILs. Also, ammonium based ILs have more pronounced multi-exponential character of solvation.

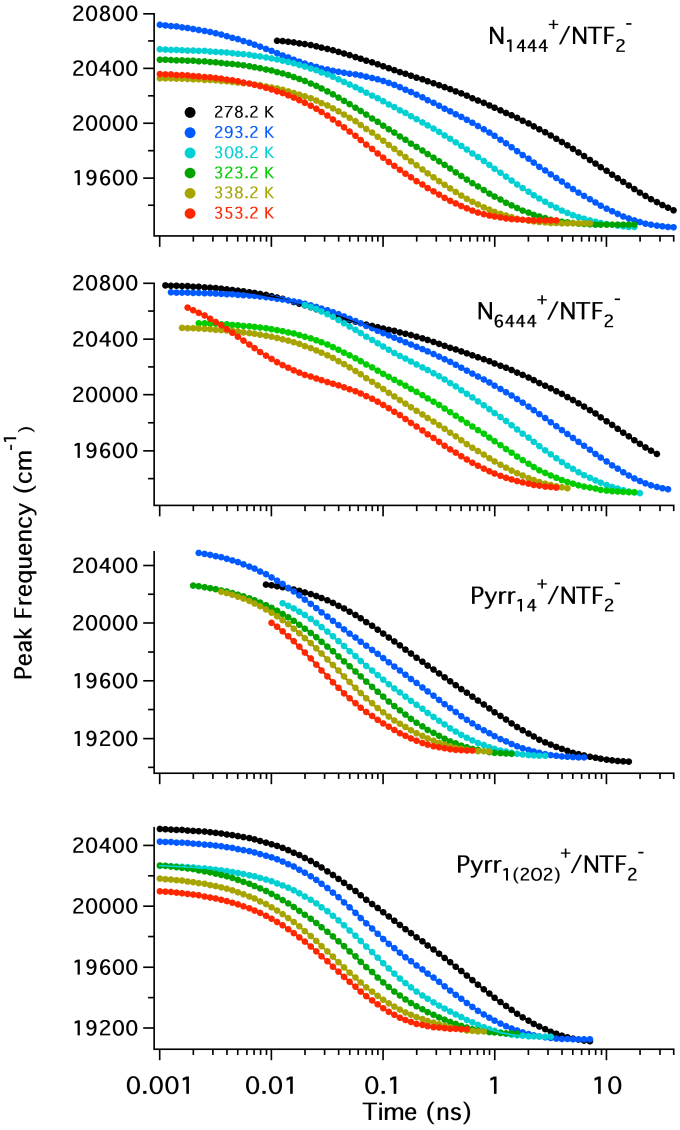

Figure 3.3.4.2 Log-normal plots of the emission frequency time correlation function (from top to bottom): $Pyrr_{14}^{+}/NTf_2^{-}$, $Pyrr_{1(202)}^{+}/NTf_2^{-}$, N_{1444}^{+}/NTf_2^{-} and N_{6444}^{+}/NTf_2^{-} for the set of temperatures 278.2, 293.2, 308.2, 323.2, 338.2, and 353.2 K.

Table 3.3.4.1 Fit parameters for the C153 TDFSS in the N_{1444}^{+}/NTf_2^{-}.[a]

T	$\nu_{em}(t\rightarrow\infty)$	A_1	τ_1	A_2	τ_2	A_3	τ_3	A_4	τ_4	t_{start}	t_{end}	τ_0	$\tau_{1/e}$	$\langle\tau\rangle$
278.2	19276	228	0.0648	243	0.527	358	4.12	544	21.7	0.011	70.8	0.336	5.90	9.79
293.2	19239	324	0.0 093	254	0.217	425	1.46	513	7.65	0.001	44.7	0.0417	1.68	3.04
308.2	19239	278	0.0441	269	0.240	475	1.16	286	4.13	0.001	17.8	0.166	0.826	1.38
323.2	19260	366	0.0457	240	0.195	301	0.532	309	1.48	0.001	17.8	0.122	0.348	0.560
338.2	19269			336	0.0582	404	0.224	328	0.703	0.001	7.10	0.133	0.229	0.319
353.2	19291	15	0.00677	476	0.0464	384	0.204	208	0.466	0.001	3.55	0.0734	0.127	0.183

Table 3.3.4.2 Fit parameters for the C153 TDFSS in the N_{6444}^{+}/NTf_2^{-}.[a]

T	$\nu_{em}(t\rightarrow\infty)$	A_1	τ_1	A_2	τ_2	A_3	τ_3	A_4	τ_4	t_{start}	t_{end}	τ_0	$\tau_{1/e}$	$\langle\tau\rangle$
278.2	19494	255	0.0245	174	0.262	211	1.51	664	13.6	0.011	28.2	0.116	3.70	7.21
293.2	19311	266	0.0577	213	0.338	333	1.72	621	9.26	0.0126	35.5	0.260	2.73	4.47
308.2	19284	412	0.0490	265	0.337	447	1.57	399	5.74	0.0 20	20.0	0.160	1.38	2.04
323.2	19299	311	0.0542	232	0.252	488	1.13	208	3.97	0.00236	17.8	0.174	0.768	1.17
338.2	19322			380	0.0558	363	0.306	429	1.21	0.00158	4.47	0.140	0.365	0.554
353.2	19330	604	0.00545	247	0.112	383	0.329	236	1.01	0.00177	3.55	0.0128	0.170	0.270

Frequencies reported in cm^{-1}, temperature in K, time constants τ_i and fit points t_{start} and t_{end} in ns.

Table 3.3.4.3 Fit parameters for the C153 TDFSS in the $Pyrr_{14}^{+}/NTf_2^{-}$.[a]

T	$\nu_{em}(t\rightarrow\infty)$	A_1	τ_1	A_2	τ_2	A_3	τ_3	A_4	τ_4	t_{start}	t_{end}	τ_0	$\tau_{1/e}$	$\langle\tau\rangle$
278.2	19034	382	0.0786	256	0.290	438	11.07	214	4.19	0.00891	15.9	0.208	0.630	1.140
293.2	19068	422	0.0179	278	0.0722	414	0.263	369	1.02	0.00224	6.31	0.0506	0.194	0.346
308.2	19077			539	0.0364	453	0.199	264	0.588	0.0126	2.82	0.0716	0.173	0.211
323.2	19091	216	0.0174	454	0.0519	356	0.160	189	0.351	0.002	1.41	0.0508	0.0891	0.124
338.2	19107			256	0.0201	540	0.0407	410	0.168	0.00355	0.891	0.0424	0.0631	0.0796
353.2	19116					729	0.0209	484	0.103	0.010	0.631	0.0v306	0.0562	0.0535

Table 3.3.4.4 Fit parameters for the C153 TDFSS in the $Pyrr_{1(202)}^{+}/NTf_2^{-}$.[a]

T	$\nu_{em}(t\rightarrow\infty)$	A_1	τ_1	A_2	τ_2	A_3	τ_3	A_4	τ_4	t_{start}	t_{end}	τ_0	$\tau_{1/e}$	$\langle\tau\rangle$
278.2	19109	323	0.0363	229	0.0953	411	0.441	448	1.68	0.001	7.10	0.113	0.409	0.686
293.2	19125			608	0.0524	452	0.366	254	0.995	0.001	7.10	0.100	0.201	0.342
308.2	19144					694	0.0619	440	0.406	0.001	3.16	0.0921	0.126	0.195
323.2	19163			146	0.00974	636	0.0538	350	0.263	0.001	1.58	0.040	0.0790	0.113
338.2	19174			419	0.0254	341	0.0496	273	0.186	0.001	0.794	0.0416	0.0524	0.0757
353.2	19194					459	0.0257	469	0.0765	0.001	0.562	0.0387	0.0463	0.0514

Frequencies reported in cm^{-1}, temperature in K, time constants τ_i and fit points t_{start} and t_{end} in ns.

To account for the heterogeneity of the TDFSS dynamics the solvation dynamics was characterized by three different time constants (τ_0), ($\tau_{1/e}$) and ($\langle \tau \rangle$), where the rate averaged time constant (τ_0) reflects the solvation dynamics at the early time, ($\tau_{1/e}$) is the effective time constant to reach the 1/*e* point of the decay, and ($\langle \tau \rangle$) is the averaged solvation time constant, which is strongly biased toward the longest time constant, as shown in equations 3.3.4.1, 3.3.4.2.

$$\tau_0 = \left(\sum_{i=1} \frac{1}{\tau_i a_i} \right)^{-1} \qquad (3.3.4.1)$$

$$\tau_{ave} = \sum_{i=1} \tau_i a_i \qquad (3.3.4.2)$$

where τ_i is one of the time constants characterizing the multi-exponential fit of the solvation function, and a_i is the normalized amplitude, as shown in equation 3.3.4.3.

$$a_i = \frac{b_i}{\sum_j b_j} \qquad (3.3.4.3)$$

where b_i is the amplitude of the time constants characterizing the multi-exponential fit of the solvation function.

This approach of describing the solvation dynamics was first used by Horng, et al.[11] As mentioned in their article, all three time constants would be the same for single-exponential model, but for the multi-exponential model the impact of a particular exponent at certain times makes the three time constants different.[11] The rate averaged time constant (τ_0) and the averaged solvation time constant ($\langle \tau \rangle$) have more uncertainty then

($\tau_{1/e}$), because (τ_0) and ($\langle \tau \rangle$) are placed at the edges of our time-scale which is limited by the temporal instrument response (early time) and the lifetime of the probe (long time).

3.3.5 The correlation between solvation rates and shear viscosities

Maroncelli et al. pointed out that reorientation of ions around the chromophore is accomplished largely by translational movement of ions.[1, 27] Consequently, solvation rates in the ILs exhibit strong correlations with shear viscosities. To compare the character of the solvation dynamics for ILs under investigation I have plotted all three effective solvation dynamics time constants (τ_0), ($\tau_{1/e}$) and ($\langle \tau \rangle$) versus the ratio of the shear viscosity to the temperature, η/T, as shown in Fig.3.3.5.1. The rate averaged time constant (τ_0) has values from tens to hundreds of picoseconds. This is on the edge of the resolution of our instrument and consequently has a large uncertainty. The log-log plot of the ($\tau_{1/e}$) shows that solvation rate with regards to η/T is faster for ammonium based ILs than for pyrrolidinium based ILs.

The log-log plot of the ($\langle \tau \rangle$) exhibit the same order of increasing of solvation dynamics regards to the η/T.

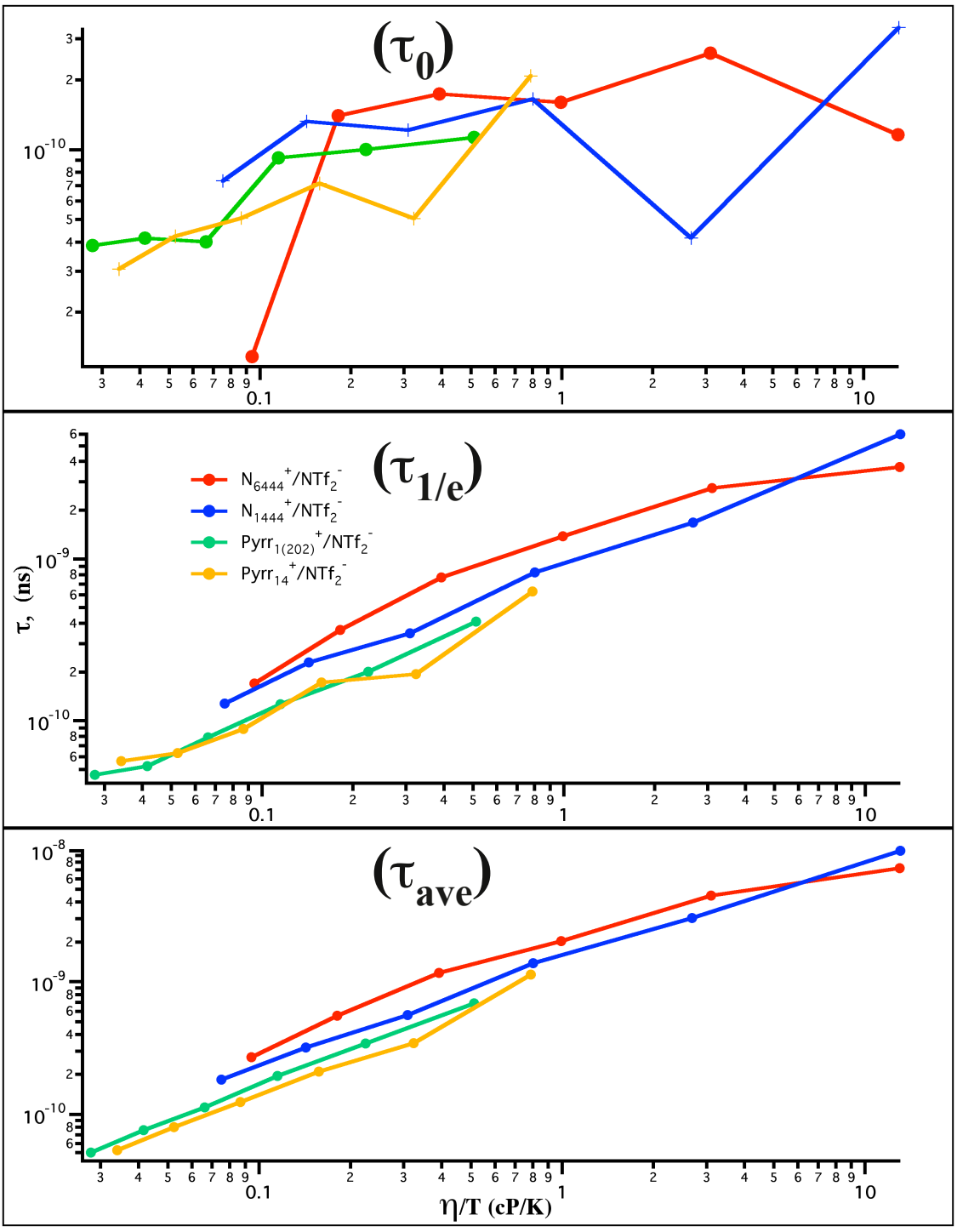

Figure 3.3.5.2 Log-log plot of TDFSS time constants vs. the ratio of viscosity over temperature η/T. Lines are not fits, but are guidance to the eye.

3.3.6 The temperature dependence of the solvation function

At temperatures near or below the ILs melting points, they become supercooled liquids and exhibit glass-like behavior. The temperature dependence of some properties of supercooled ILs such as viscosity, diffusion and solvation dynamics can deviate from the Arrhenius function and be fitted better by Vogel-Tammann-Fulcher (VTF) function, as shown in equation 3.3.6.1, 3.3.6.2.

$$\ln\left(\frac{1}{\tau}\right) = \ln(k_0) - \frac{E_a}{RT} \qquad (3.3.6.1)$$

where τ is an effective time constant, E_a is activation energy, R is Boltzmann constant and T is temperature.

$$\ln\left(\frac{1}{\tau}\right) = \ln(k_0) + \frac{DT_c}{T - T_c} \qquad (3.3.6.2)$$

where D is the constant, T_c is a characteristic temperature at which τ_{rot} diverges.

Note that in the high-temperature limit, when $T >> T_c$, the VTF function approaches the Arrhenius function.

The DSC data shows that ammonium based ILs have T_m at around 300 K; that means that measurements at the 278.2 and 293.2 K were performed on the supercooled liquids. However, pyrrolidinium based ILs exhibit lower melting points. The $Pyrr_{14}^{+}/NTf_2^{-}$

has melting point at 255 K and $Pyrr_{1(202)}^{+}/NTf_2^{-}$ does not exhibit melting transition but instead shows a small negative change in heat capacity at 235 K.

We fit the temperature dependence of the effective solvation time constants (τ_0), ($\tau_{1/e}$) and ($\langle \tau \rangle$) to both - the Arrhenius and VTF functions. The parameters of these fits are shown in table 3.3.6.1. In all cases the VTF function gives a better or an equivalent fit. The parameters for both fits are given in Table 3.3.6.1. Though the VTF model fits better the deviation of the temperature dependence of the time constants from Arrhenius model is not substantial. We used the Arrhenius fit to calculate E_a for all ILs. The energies E_a for all four ILs are shown in table 3.3.6.1. As expected, the E_a for early time dynamics (τ_0) is lower that ($\tau_{1/e}$) and ($\langle \tau \rangle$). The values of E_a for the more viscous ammonium based ILs are larger than for the pyrrolidinium based ILs.

Table 3.3.6.1 VTF and Arrhenius fit parameters for time constants τ_0, $\tau_{1/e}$, and $\langle\tau\rangle$.

		VTF			Arrhenius	
		$\ln(k_0)$	D	T_c	$\ln(k_0)$	E_a/R
N_{1444}^+/NTf_2	τ_0	24.77	-3.897	102.9	25.61	-863.9
	$\tau_{1/e}$	27.70	-4.782	179.7	36.80	-4912
	$\langle\tau\rangle$	29.39	-9.781	146.8	37.24	-5195
N_{6444}^+/NTf_2^-	τ_0	29.33	-68.76	26.55	30.01	-2211
	$\tau_{1/e}$	31.95	-69.25	43.46	33.81	-4081
	$\langle\tau\rangle$	32.18	-74.50	43.04	34.12	-4329
$Pyrr_{14}^+/NTf_2^-$	τ_0	24.12	-0.0566	269.7	29.88	-1993
	$\tau_{1/e}$	25.15	-0.8249	229.8	32.47	-3062
	$\langle\tau\rangle$	26.33	-1.902	208.5	34.60	-3827
$Pyrr_{1(202)}^+/NTf_2$	τ_0	27.42	-11.94	77.73	28.75	-1655
	$\tau_{1/e}$	26.55	-2.367	187.9	32.20	-2911
	$\langle\tau\rangle$	29.31	-11.52	115.8	33.35	-3393

a Units of *T*c and *E*a/R are in K, and *k*0 units are in *s*-1.

3.4 Investigation of reorientation dynamics in the ILs.

The reorientation dynamics of a fluorescence probe molecule is closely related to the solute-solvent interaction and can elucidate some aspects of the chemical reactions in the ILs. A crude estimate of the rotational dynamics can be made using hydrodynamic theory. The Stokes-Einstein-Debye model relates the rate of the rotational diffusion D_r to the size of the molecule, the viscosity and the temperature. But the basic hydrodynamic theory does not consider coupling between solute and solvent molecules, the key question of any chemical system.[28, 29] To investigate the reorientation dynamics in the ILs we used the method of the time-resolved fluorescence polarization anisotropy.

3.4.1 The physicochemical principles of the time-resolved fluorescence polarization anisotropy

The physicochemical principles of the method of time-resolved fluorescence polarization anisotropy are derived from the fact that a chromophore excited by linearly polarized light will always have an emission polarization at a fixed angle relative to the excitation polarization.[24, 30, 31] In the time gap between absorption and emission of the photon the molecule of the chromophore rotates by an angle Θ and consequently the plane of emitted light is rotated by the angle Θ with regards to the plane of exiting light.

The ensemble of molecules will depolarize light in such a way that instead of a plane of polarization, the emitted light has a cone of polarization. Hence, the dynamics of depolarization depends on the dynamics of reorientation of the chromophore.

3.4.2 Multi-exponential fit of the fluorescence anisotropy decay

I have measured the fluorescence anisotropy decay for $Pyrr_{14}^{+}/NTf_2^{-}$, $Pyrr_{1(202)}^{+}/NTf_2^{-}$, N_{1444}^{+}/NTf_2^{-} and N_{6444}^{+}/NTf_2^{-} for six temperature points: 278.2 K, 293.2 K, 308.2 K, 323.3 K, 338.2 K and 353.2 K. Fig. 3.4.2.1 presents typical transients for time-resolved fluorescence anisotropy decay experiments. I used multi-exponential models to fit the fluorescence anisotropy data, because the single-exponential model did not provide a good fit to the data. Tables 3.4.2.1, present the parameters of fluorescent anisotropy transients fit for all four ILs.

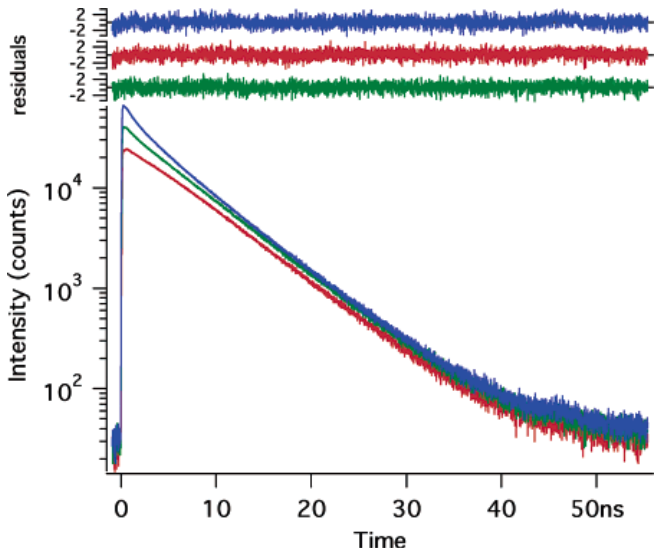

Figure 3.4.2.1 Typical TCSPC fluorescence anisotropy data for C153 in $Pyrr_{1(202)}^{+}/NTf_2^{-}$ at 293.2 K. The data are color-coded by the combination of emission polarizations measured relative to the vertical excitation polarization at 420 nm. The data is shown in blue for the VV transient, green for the VM transient, and red for the VH transient. The corresponding reduced residuals for the simultaneous fit to all three transients are shown at the top.

For all four ILs, the limiting anisotropy r(0) decreases with increasing temperature. A possible explanation is that the fastest component, which has a reorientational time too short to be resolved by TCSPC, was missed.

Typically, the anisotropy decay was fit to a three-exponential model. For some temperatures, pyrrolidinium based ILs were observed to have long time component with a time constant greatly exceeding the C153 lifetime. The 5 ns lifetime of the C153 probe constrains the accuracy of determining the long time constant. These longest time constants have strong covariances with the associated amplitudes, so that the uncertainty of these long time constants was estimated to be higher than 50%. The ammonium based ILs do not show this long time component, except at the temperature point 278.2 K.

Table 3.4.2.1. Anisotropy fit parameters for N_{1444}^{+}/NTf_2^{-}.[a]

T	η	r(0)	r_1	$\tau_{1,rot}$	r_2	$\tau_{2,rot}$	r_3	$\tau_{3,rot}$	$\tau_{0,rot}$	$\tau_{1/e,rot}$	$\langle\tau\rangle_{rot}$
278.2	3634	0.395	0.0199	1.02	0.0695	10.3	0.305	242	14.4	179.5	189
293.2	786.1	0.382	0.0308	.623	0.0630	3.71	0.289	46.4	5.27	33.3	35.7
308.2	247.1	0.349	0.0564	.529	0.0741	3.32	0.219	16.5	2.46	9.35	11.1
323.2	99.91	0.335	0.0387	.135	0.0801	0.983	0.216	5.63	0.825	3.3	3.88
338.2	48.25	0.383	0.0990	0.0526	0.0797	.594	0.204	2.74	0.183	.95	1.60
353.2	26.54	0.292			0.0776	.241	0.214	1.30	0.599	.902	1.02

Table 3.4.2.2. Anisotropy fit parameters for N_{6444}^{+}/NTf_2^{-}.[a]

T	η	r(0)	r_1	$\tau_{1,rot}$	r_2	$\tau_{2,rot}$	r_3	$\tau_{3,rot}$	$\tau_{0,rot}$	$\tau_{1/e,rot}$	$\langle\tau\rangle_{rot}$
278.2	3612	0.363	0.0253	0.692	0.0537	6.76	0.284	132	7.78	99.6	104
293.2	909.3	0.375	0.0426	0.513	0.0877	5.52	0.245	63.4	3.65	36.4	42.7
308.2	306.2	0.367	0.0528	0.392	0.0887	2.89	0.225	25.0	2.10	13	16.1
323.2	126.9	0.346	0.0570	0.166	0.0999	1.37	0.189	8.76	0.787	3.85	5.21
338.2	61.29	0.334	0.0650	0.117	0.0955	0.837	0.174	3.98	0.468	1.78	2.3
353.2	33.27	0.315	0.0778	0.134	0.0870	0.724	0.150	2.19	0.409	1.00	1.27

Temperature are in K, viscosities η in cP, time constants $\tau_{i,rot}$ in ns.

Table 3.4.2.3. Anisotropy fit parameters for $Pyrr_{1(202)}^{+}/NTf_2^{-}$.[a]

T	η	r(0)	r_1	$\tau_{1,rot}$	r_2	$\tau_{2,rot}$	r_3	$\tau_{3,rot}$	r_4	$\tau_{4,rot}$	$\tau_{0,rot}$	$\tau_{1/e,rot}$	$\langle\tau\rangle_{rot}$
278.2	219.1	0.327	0.0141	0.466	0.0502	2.12	0.263	15.5			4.62	12.1	12.8
293.2	94.80	0.372			0.0487	0.658	0.266	5.29	0.0570	220	2.98	6.28	37.6
308.2	48.48	0.333			0.0472	0.358	0.257	2.57	0.0285	85.5	1.43	2.56	9.35
323.2	28.00	0.323			0.0511	0.325	0.248	1.45	0.0242	111	0.981	1.4	9.46
338.2	17.72	0.289			0.0279	0.164	0.138	0.647	0.0123	1.11	0.584	0.75	0.799
353.2	12.03	0.284			0.0494	0.215	0.219	0.564	0.0156	1.27	0.450	0.49	0.542

Table 3.4.2.4. Anisotropy fit parameters for $Pyrr_{14}^{+}/NTf_2^{-}$.[a]

T	η	r(0)	r_1	$\tau_{1,rot}$	r_2	$\tau_{2,rot}$	r_3	$\tau_{3,rot}$	$\tau_{0,rot}$	$\tau_{1/e,rot}$	$\langle\tau\rangle_{rot}$
278.2	142.5	0.402	0.0453	0.884	0.245	8.73	0.112	121	5.02	14.1	39.2
293.2	65.77	0.358	0.0537	0.609	0.250	4.15	0.0543	439	2.41	4.81	69.7
308.2	35.45	0.332	0.0539	0.410	0.240	2.10	0.0382	436	1.35	2.20	51.8
323.2	21.39	0.327	0.0372	0.209	0.245	1.14	0.0447	858	0.833	1.32	118
338.2	14.04	0.342	0.0594	0.185	0.232	.745	0.0505	497	0.541	0.82	74.0
353.2	9.839	0.239	0.0497	0.190	0.189	.505			0.376	0.41	0.440

Temperature are in K, viscosities η in cP, time constants $\tau_{i,rot}$ in ns.

3.4.3. The reorientation dynamics of C153 in four ILs

At the different temperatures best fits to the observed r(t) in our four ILs may require models with different number of exponents. In order to compare reorientational dynamics in all four ILs it was more helpful to use the time constants (τ_0), ($\tau_{1/e}$) and ($\langle \tau \rangle$).

The effective averaged inverse rate (τ_0), the effective time constant for the 1/e point of the decay ($\tau_{1/e}$), and the average time constants ($\langle \tau \rangle$) were calculated the same way as it was done for the TDFSS data. The average time constant ($\langle \tau \rangle$) is strongly biased toward the long time component despite that these long components have relatively small amplitude. Consequently, ($\langle \tau \rangle$) constants have largest uncertainty. I used (τ_0), ($\tau_{1/e}$) and ($\langle \tau \rangle$) time constants to analyze the temperature dependence of the reorientational dynamics by VTF and Arrhenius functions.

3.4.4 The temperature dependence of the reorientation dynamics

The fit parameters for VTF and Arrhenius functions are presented in Table 3.4.2.5. The VTF function provides better fits for most of the time constants, though the Arrhenius fit has only slightly lower quality. The deviation from the Arrhenius fit over the small range of the temperatures is not substantial, therefore it is legitimate to use the Arrhenius function to find the activation energies E_a. The fastest component of the reorientation process (τ_0) has energies, which are smaller than energies for ($\tau_{1/e}$) and ($\langle \tau \rangle$). As expected, the activation energies E_a for ammonium based ILs are higher than for less viscous $Pyrr_{14}^{+}/NTf_2^{-}$ and $Pyrr_{1(202)}^{+}/NTf_2^{-}$.

Table 3.4.2.5 VTF and Arrhenius fit parameters for time constants τ_0, $\tau_{1/e}$, and $\langle\tau\rangle$.

		VTF			Arrhenius	
		$\ln(k_0)$	D	T_c	$\ln(k_0)$	E_a/R
N_{1444}^+/NTf_2	τ_0	26.46	-3.805	192.2	36.65	-5143
	$\tau_{1/e}$	27.61	-5.645	189.7	41.77	-7225
	$\langle\tau\rangle$	27.26	-5.793	186.5	40.54	-6896
N_{6444}^+/NTf_2^-	τ_0	27.54	-8.794	140.2	33.50	-4122
	$\tau_{1/e}$	32.50	-32.38	93.86	38.54	- 6249
	$\langle\tau\rangle$	34.03	- 71.92	55.86	37.47	-5977
$Pyrr_{14}^+/NTf_2^-$	τ_0	27.09	-12.80	106.7	30.58	-3176
	$\tau_{1/e}$	3054	-35.29	72.17	33.74	-4322
	$\langle\tau\rangle$	32.35	-74.26	47.45	34.91	-4961
$Pyrr_{1(202)}^+/NTf_2$	τ_0	26.52	- 7.490	138.3	31.32	- 3376
	$\tau_{1/e}$	27.10	-6.912	156.5	34.15	-4428
	$\langle\tau\rangle$	26.75	- 87.25	32.97	29.08	-3671

a Units of T_c and E_a/R are in K, and k_0 units are in s^{-1}.

3.4.5 The hydrodynamic model

The hydrodynamic theory applied to analyze the reorientational dynamics of C153 may elucidate the mechanism of the interaction between solute-solvent molecules in the ILs.[28, 29] The hydrodynamic model describes the rotation of the molecule analogous to rotation of the macroscopic body immersed in the liquid. The Stokes-Einstein-Debye (S-E-D) model relates the rate of the orientational time constant, τ_{or}, to the size of the molecule, the viscosity and the temperature, as shown in equation 3.4.5.1.

$$\tau_{or} = \frac{\eta V}{k_B T} \qquad (3.4.5.1)$$

where τ_{or} is the orientation time constant, k_B is the Boltzmann constant, T is temperature, η is viscosity of the IL and V is volume of the C153 molecule.

The S-E-D model estimates the time constant for molecular reorientation assuming a spherical rotor. Therefore the shape of the real molecule may invoke the necessity to introducing a proportionality constant in this equation. The molecular volume of C153 is a constant for all four IL/chromophore systems, estimated to be 246 $\AA^3$ from the method of van der Waals increments.[32, 33]

To compare the reorientational behavior of C153 in the four ILs, I plotted the effective time constants (τ_0) and ($\tau_{1/e}$) versus η/T in Fig 3.4.5.1. Along with that, τ_{or} was plotted. As estimated from the hydrodynamic theory with the use of equation 3.4.5.1. The average time constant ($\langle \tau \rangle$) was not plotted because for pyrrolidinium ILs it has an

uncertainty larger than 50%; also for ammonium based ILs, because ($\langle \tau \rangle$) values are very close to the ($\tau_{1/e}$).

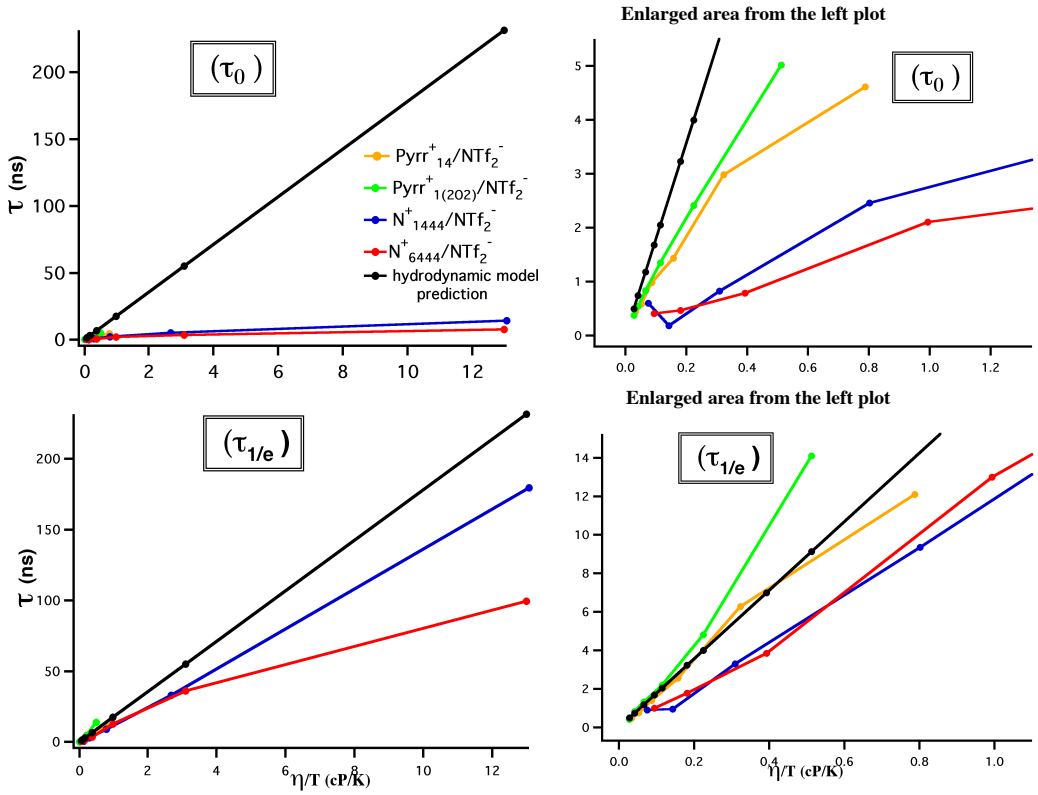

Figure 3.4.5.1. Fluorescence anisotropy effective time constants (τ_0) and ($\tau_{1/e}$) plotted vs the ratio of viscosity over temperature for the ILs N_{1444}^+/NTf_2^-, N_{6444}^+/NTf_2^-, $Pyrr_{14}^+/NTf_2^-$ and $Pyrr_{1(202)}^+/NTf_2^-$.

The slope of the effective averaged inverse rate (τ_0) is smaller than the slope of τ_{or} for all four ILs, as shown in Fig. 3.4.5.1, top. This is not surprising, taking into consideration that (τ_0) is biased toward the fast component of the reorientational dynamics. The slope of the effective time constant for the 1/e point in the decay, ($\tau_{1/e}$), has a value very close to the τ_{or} (only a bit smaller) for pyrrolidinium based ILs and significantly lower for ammonium based ILs. In both cases: for early time dynamics (τ_0) and for ($\tau_{1/e}$), the reorientation is faster than predicted by hydrodynamic theory. One possible explanation is

that the shape of the C153 molecule deviates from the spherical rotor and the prediction by hydrodynamic model is not exact. Another possible reason is that the hydrodynamic model does not reflect the chemical interaction between the molecule of C153 and neighboring molecules of ILs. The shear viscosity of the IL depends on the interaction between component molecular ions.

If the interaction between C153 molecule and ions is weaker than the interaction between ions, then C153 will experience lower dielectric friction and micro-viscosity, that leads to faster reorientation dynamics.[28] For both effective time constants (τ_0) and ($\tau_{1/e}$) the slopes diminish in the following order: $Pyrr_{1(202)}^{+}/NTf_2^{-}$, $Pyrr_{14}^{+}/NTf_2^{-}$, N_{1444}^{+}/NTf_2^{-} and N_{6444}^{+}/NTf_2^{-}. The reorientational dynamics is significantly faster than predicted by hydrodynamic theory for ammonium ILs and just slightly faster in the pyrrolidinium ILs. One of the possible reasons for this difference is the degree of coupling between C153 and IL ions is different for these liquids.

3.5 Conclusion

The polarity, solvation dynamics and reorientational dynamics were investigated for four ILs with non-aromatic cation: $Pyrr_{14}^{+}/NTf_2^{-}$, $Pyrr_{1(202)}^{+}/NTf_2^{-}$, N_{1444}^{+}/NTf_2^{-} and N_{6444}^{+}/NTf_2^{-}. The empirical solvent polarity was estimated for all four IL using the steady-state fluorescence spectra. The ammonium based ILs exhibit slightly higher polarity than pyrrolidinium based ILs.

The solvation behavior of four ILs with non-aromatic cations was investigated by the TDFSS method. The observed solvation dynamics occur on timescales orders of magnitude longer than for most organic solvents. The solvation dynamics of the C153

exhibits multi-exponential character in all four ILs $Pyrr_{14}^{+}/NTf_2^{-}$, $Pyrr_{1(202)}^{+}/NTf_2^{-}$, N_{1444}^{+}/NTf_2^{-} and N_{6444}^{+}/NTf_2^{-}. We used three time constants, (τ_0), ($\tau_{1/e}$) and ($\langle \tau \rangle$), to characterize the solvation dynamics and found that rates of solvation in the ILs correlate with the shear viscosities of these liquids. The temperature dependence of the solvation dynamics was characterized by the VTF and Arrhenius functions, with VTF providing a better fit. The activation energies E_a for solvation in the ILs were estimated using the Arrhenius function. The activation energies E_a are higher for ammonium based ILs than for pyrrolidinium based ILs.

The reorientational dynamics for all four ILs was investigated using the method of time-resolved fluorescence anisotropy decay. The fluorescence anisotropy decay was fit to a multi-exponential model and characterized by three time constants: (τ_0), ($\tau_{1/e}$) and ($\langle \tau \rangle$). The reorientation rates scale according to the shear viscosities of the ILs. The fit of the temperature dependence to the VTF and Arrhenius functions reveals the superiority of the VTF fit. The Arrhenius function was used to estimate the activation energy of reorientation E_a. The activation energies E_a for ammonium based ILs are higher than for less viscous $Pyrr_{14}^{+}/NTf_2^{-}$ and $Pyrr_{1(202)}^{+}/NTf_2^{-}$. The hydrodynamic theory was applied to the reorientation dynamics of C153 in the ILs. The fast component of the reorientation for all ILs is much faster, almost a whole order of magnitude, than the rate predicted by hydrodynamic theory.The ($\tau_{1/e}$) component of the reorientational dynamics is significantly faster than predicted by the hydrodynamic theory for ammonium ILs and just slightly faster in the pyrrolidinium ILs.The heterogeneous solvation dynamics in the ILs designate the broader distribution of solvation rates. One possible consequence of this fact is a more

heterogeneous distribution of chemical reaction rates. This is one more unique feature of Ionic Liquids adding to many other special properties.

References

1. N. Ito, R. Biswas, M. Maroncelli, J. A. Ingram, R. S. Moog, *Solute Rotation and Solvation Dynamics in a Room-Temperature Ionic Liquid.* J. Phys. Chem. B, 2003. **107**: p. 5926.
2. Ito, N.A., S.; Heitz, M.; Maroncelli, M. J. Phys. Chem. B 2004, 108, 5771-5777., J. Phys. Chem. B 2004. **108**: p. 5771-5777.
3. N. Ito, S. Arzhantsev, M. Maroncelli, *The Probe Dependence of Solvation Dynamics and Rotation in the Ionic Liquid 1-Butyl-3-Methyl-Imidazolium Hexafluorophosphate.* Chem. Phys. Lett. , 2004. **396**: p. 83.
4. A. M. Funston, T. A. Fadeeva, J. F. Wishart, E. W. Castner, Jr., *Fluorescence Probing of Temperature-Dependent Dynamics and Friction in Ionic Liquid Local Environments.* J. Phys. Chem. B, 2007. **111**: p. 4963.
5. L. Cammarata, S. G. Kazarian, P. A. Salter, T. Welton, *Molecular states of water in room temperature ionic liquids,*. Phys. Chem. Chem. Phys., 2001. **3**: p. 5192.
6. J. Jacquemin, P. Husson, A. A. H. Padua, V. Majer, *Density and viscosity of several pure and water-saturated ionic liquids.* Green Chem., 2006. **8(2)**: p. 172.
7. C. A. Angell, C. Alba, A. Arzimanoglou, R. Boehmer, J. Fan, Q. Lu, E. Sanchez, H. Senapati, M. Tatsumisago, *Stress and structural relaxation, chemical reaction freezing, crystal nucleation and microemulsion arrest, in relation to liquid fragility*, in *AIP Conference Proceedings* 1992. p. 3.
8. C. A. Angell, *Liquid Fragility and the Glass Transition in Water and Aqueous Solutions.* Chem. Rev., 2002. **102**: p. 2627.
9. Paul A., Mandal P. K., A. Samanta, *On the optical properties of the imidazolium ionic liquids.* Journal of Physical Chemistry B, 2005. **109(18)**: p. 9148.
10. A. Paul, P. K. Mandal, A. Samanta, *How transparent are the imidazolium ionic liquids? A case study with 1-methyl-3-butyl-imidazolium hexafluorophosphate, [BMIM][PF6].* Chem. Phys. Lett., 2005. **402**: p. 375.
11. M. L. Horng, J. A. Gardecki, A. Papazyan, M. Maroncelli *Subpicosecond Measurements of Polar Solvation Dynamics - Coumarin-153 Revisited.* J. Phys. Chem., 1995. **99(48)**: p. 17311.
12. R. Karmakar, A. Samanta *Steady-State and Time-Resolved Fluorescence Behavior of C153 and PRODAN in Room-Temperature Ionic Liquids.* J. Phys. Chem. A. , 2002. **106**: p. 6670.
13. Mandal P. K., Samanta A., *Fluorescence Studies in a Pyrrolidinium Ionic Liquid: Polarity of the Medium and Solvation Dynamics.* J. Phys. Chem. B, 2005. **109**: p. 15172.
14. S. N. V. K. Aki, J. F. Brennecke, A. Samanta, *How polar are room-temperature ionic liquids?* Chem. Comm., 2001(5): p. 413.
15. K. A. Fletcher, I. A. Storey, A. E. Hendricks, S. Pandey, *Behavior of the solvatochromic probes Reichardt's dye, pyrene, dansylamide, Nile Red and 1-pyrenecarbaldehyde within the room-temperature ionic liquid bmimPF6.* Green Chem., 2001(3): p. 210.

16. C. D. Grant, M. R. DeRitter, K. E. Steege, T. A. Fadeeva, E. W. Castner, Jr., *Fluorescence Probing of Interior, Interfacial, and Exterior Regions in Solution Aggregates of Poly(ethylene oxide)- Poly(propylene oxide)-Poly(ethylene oxide) Triblock Copolymers.* Langmuir 2005: p. 1745.
17. R. Karmakar, A. Samanta, *Dynamics of Solvation of the Fluorescent State of Some Electron Donor−Acceptor Molecules in Room Temperature Ionic Liquids, [BMIM][(CF3SO2)2N] and [EMIM][(CF3SO2)2N]*. J. Phys. Chem. A, 2003. **107**: p. 7340.
18. N. Ito, S. Arzhantsev, M. Heitz, M. Maroncelli, , *Solvation and Rotational Dynamics of Coumarin 153 in Alkylphosphonium Ionic Liquids.* Journal of Physical Chemistry B 2004. **108**: p. 5771.
19. S. Saha, P. K. Mandal, A. Samanta, *Solvation dynamics of nile red in a room temperature ionic liquids using streak camera.* Phys. Chem. Chem. Phys., 2004(6): p. 3106.
20. S. Arzhantsev, H. Jin, N. Ito, M. Maroncelli, *Observing the Complete Solvation Response of DCS in Imidazolium Ionic Liquids, from the Femtosecond to the Nanosecond Regimes.* Chem. Phys. Lett., 2006. **417**: p. 524.
21. P. K. Chowdhury, M. Halder, L. Sanders, T. Calhoun, J. L. Anderson, D. W. Armstrong, X. Song, J. W. Petrich, *Dynamic Solvation in Room Temperature Ionic Liquids.* J. Phys. Chem. B 2004. **108**: p. 10245.
22. S. N. Baker, G. A. Baker, M. A. Kane, F. V. Bright, *The cybotactic region surrounding fluorescent probes dissolved in 1-butyl-3-methylimidazolium hexafluorophosphate: effects of temperature and added carbon dioxide.* J. Phys. Chem. B 2001. **105**: p. 9663.
23. A. Samanta, *Solvation Dynamics in Ionic Liquids: What We Have Learned from the Dynamic Fluorescence Stokes Shift Studies.* J. Phys. Chem. Let. , 2010. **1**: p. 1557.
24. B. Valeur, *Molecular Fluorescence: Principles and Applications* 2002: Wiley-VCH.
25. E. W. Castner Jr., M. Maroncelli, G. R. Fleming, , *Subpicosecond resolution studies of solvation dynamics in polar aprotic and alcohol solvents.* J. Chem. Phys., 1987. **86**: p. 1090.
26. E. W. Castner Jr., G. R. Fleming, B. Bagchi, M. Maroncelli, *The Dynamics of Polar Solvation: Inhomogeneous Dielectric Continuum Models.* J. Chem. Phys. . 1988. **89**: p. 3519.
27. S. Arzhantsev, N. Ito, M. Heitz, M. Maroncelli, *Solvation Dynamics of Coumarin 153 in Several Classes of Ionic Liquids: Cation Dependence of the Ultrafast Component,.* Chem. Phys. Lett., 2003. **381**: p. 278.
28. M.-L. Horng, J. A. Gardecki, M. Maroncelli, , *Rotational Dynamics of Coumarin 153: Time-Dependent Friction, Dielectric Friction, and<p>Other Nonhydrodynamic Effects.* J. phys. Chem. A, 1997. **101**: p. 1030.
29. L. Reynolds, J. A. Gardecki, S. J. V. Frankland, M. L. Horng, M. Maroncelli, *Dipole Solvation in Non-Dipolar Solvents: Experimental Studies of Reorganization Energies and Solvation Dynamics.* J. Phys. Chem. , 1996. **100**: p. 10337.

30. J. R. Lakowicz, *Principles of Fluorescence Spectroscopy*1999: Kluwer Academic/ Plenum Publishers.
31. G. R. Fleming, *Chemical Applications of Ultrafast Spectroscopy*1986: Oxford, University Press London.
32. A. Bondi, *Van der Waals volumes and radii.* J. Phys. Chem., 1964. **68**: p. 441.
33. J. T. Edward, *Molecular volumes and the Stokes-Einstein equation.* Journal of Chemical Education, 1970. **47(4)**: p. 261.

Chapter 4

Investigation of the interactions between water and Ionic Liquids

4.1 Overview

Understanding the properties of mixture Ionic Liquids (ILs) with water is important for many processes involving water as a reactant, product or impurity. Examples include processes in hydrogen fuel cells, dissolution of biomass, catalysis, enzymatic catalysis and many others.[1-4]

Two characteristics of IL/water system will be considered in this chapter:

I. The interaction between water molecules and the molecular anions and cations of the IL. The H_2O-IL interactions were investigated by observing the chemical shift of the water proton as a function of the water concentration in the IL and as a function of temperature.

II. The diffusional properties of the IL/water system studied as a temperature dependence of self-diffusion coefficients of cations, anions and water.

The NMR studies were performed for two ILs;1-butyl-1-methylpyrrolidinium bis(trifluoromethylsulfonyl)amide $Pyrr_{14}^{+}/NTf_2^{-}$ and 1-butyl-1-methylpyrrolidinium Trifloromethylsulfonate $Pyrr_{14}^{+}/OTf^{-}$, shown in Fig. 4.1.1.

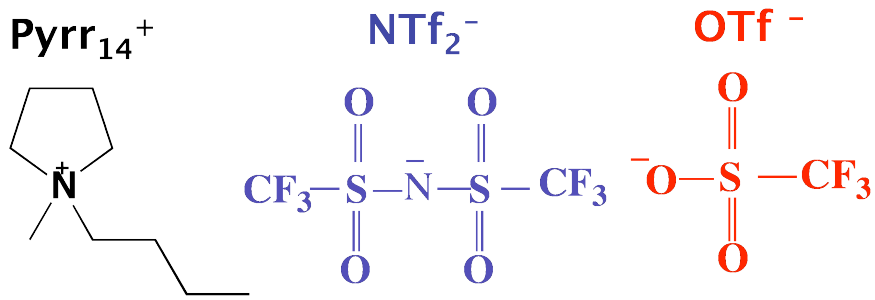

Figure 4.1.1 The structure of component ions of studied ILs.

These ILs share the same non-aromatic cation $Pyrr_{14}^+$, but they have different anions: hydrophobic NTf_2^- and more water miscible OTf^-. Fig. 4.1.1 presents the structure of anions and the cation. The $Pyrr_{14}^+/NTf_2^-$ is more than two times less viscous than $Pyrr_{14}^+/OTf^-$; viscosities at 293.2 K are 97 cP and 217 cP respectively.

4.2 Results and discussion

4.2.1 Temperature dependence and dependence of the water proton NMR chemical shift on the water concentration in the IL

4.2.1.1. ^{1}H spectrum of P_{14}^+/NTf_2^- and $Pyrr_{14}^+/OTf^-$

I have investigated dependence of the water proton chemical shift on the water concentration in the range of concentrations x_{H2O} = 0.00478 - 0.17554 for P_{14}^+/NTf_2^- and x_{H2O} = 0.045254 -0.30086 for $Pyrr_{14}^+/OTf^-$.

The ^{1}H spectrum of "dry" samples (samples with negligibly small water concentration) is the same for both IL - $Pyrr_{14}^{+}/OTf^{-}$ and $Pyrr_{14}^{+}/NTf_2^{-}$. This is because both ILs have the same cation and because the anion does not have any ^{1}H atoms.

Samples of ILs with non-negligible water concentration are different from each other. The typical ^{1}H spectrum of $Pyrr_{14}^{+}/NTf_2^{-}$ containing water is shown in Fig. 4.2.1. The peak labeled "7" originates from the protons of the terminal methyl group on the butyl chain. The peaks "6" and "5" are assigned to the protons of methylene groups on the butyl chain. The peak "2" is assigned to the methylene group attached to the nitrogen. The peak "3" belongs to the methyl group attached to the nitrogen and peaks "1" and "4" are assigned to the protons on the pyrrolidinium ring. The line, which originates from the water protons is marked on the spectrum as "H_2O".

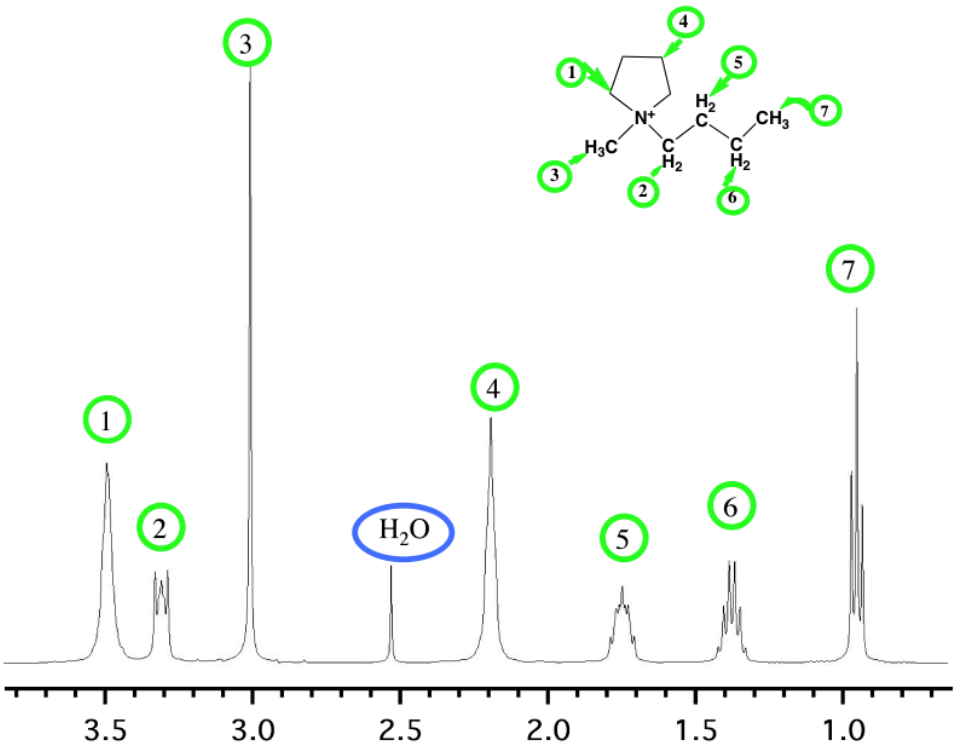

Figure 4.2.1 ^{1}H NMR spectrum of $Pyrr_{14}^{+}/NTf_2^{-}$ for x_{H2O} =0.176. The spectral assignments for the cation are labeled in the inset diagram

The water proton peak is of special interest for us. In bulk water, the proton is deshielded because the e-density around the proton was reduced by the covalent bond to the oxygen and by the H-bond to the oxygen of the neighboring molecules. As a consequence, the water peak is positioned downfield with a chemical shift of δ_{H2O} = 4.8 ppm. When H_2O is dissolved in the IL, the water donates H-bonds to the anion of IL. The degree of deshielding resulting from the water-anion H-bonds depends on the polarity of these bonds. The more polar water-to-anion H-bond more effectively deshields the proton and, consequently, δ_{H2O} is offset further downfield.

At the concentration of water in the IL x_{H2O} = 0.1 the chemical shift of the water δ_{H2O} is approximately 2.44 ppm in the P_{14}^+/NTf_2^-, 3.07 ppm in the $Pyrr_{14}^+OTf^-$ and 4.80 ppm in the bulk water at the temperature 298.2 K. This observation indicates that the polarity of water-OTf^- bonds is higher than water-NTf_2^- bonds, and polarity of water-water bonds is even higher. It is not only the nature of the IL that influences the chemical shift. The water chemical shift varies substantially both as a function of water concentration and as a function of temperature.

4.2.1.2 Concentration dependence of the water proton chemical shift, δ_{H2O}

For water in the two pyrrolidinium ILs, there is a strong downfield chemical shift for water with increasing concentration as shown in Fig. 4.2.1.2. The dependence of the water proton chemical shift δ_{H2O} on the water concentration is also known for other solvents such as ethanol and some organic solvents.[5]

Experimental results exhibit the linear dependence of water chemical shift δ_{H2O} on the observed range of concentrations. In Fig. 4.2.1.2 the concentration is expressed as a mole ratio between H_2O and IL that shows how many anion-cation pairs there are

per one molecule of water. The slope of the water chemical shift as a function of concentration is very different for the two ionic liquids; the slope is 1.33 for $Pyrr_{14}^{+}/OTf^{-}$ and 1.97 for $Pyrr_{14}^{+}/NTf_2^{-}$.

Water dissolved in an IL associates with the anion.[6] One of the possible explanations for the dependence of δ_{H2O} on the water concentration in the IL is the change of proportion between water-water and water-anions bonds with changing water concentration. When the concentration of water is higher, it is more probable for the water molecule to make a bond with another water molecule, leading to a downfield shift.

Another possible explanation is that the H-bond donated from water to the anion changes the polarity of anion. (It is not common to speak about polarity of the charged species, but in case of spacious ions of ILs it is the best way to refer to the distribution of electron density.) When a water molecule makes a bond to the anion it changes the polarity of the anion that, in turn, change the polarity of other ions through the electrostatic interaction. Thereby, change in the water concentration would lead to change of polarity in water-anion bonds. The difference in the slope for linear dependence of the chemical shift δ_{H2O} vs. concentration reflects the different water-anion interactions for $Pyrr_{14}^{+}/OTf^{-}$ and $Pyrr_{14}^{+}/NTf_2^{-}$.

Dependence of water proton chemical shift on the concentration of water in the IL can be used for indirect determination of water concentration in the IL. This method would have the advantage of using small amount of IL and it does not destroy the sample.

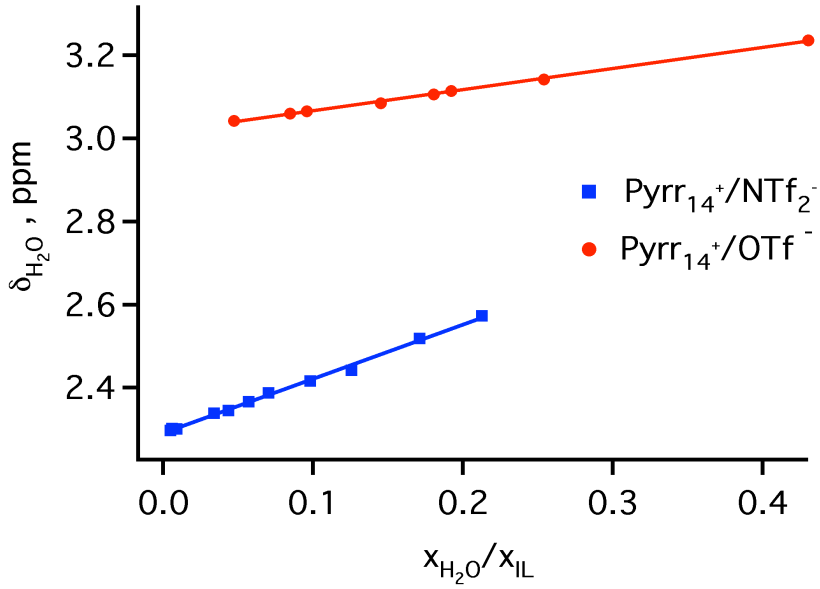

Figure 4.2.1.2 ^{1}H chemical shift for water at 298.2 K plotted versus the mole ratio of water to IL for $Pyrr_{14}^{+}/OTf^{-}$ (red circles) and for water in $Pyrr_{14}^{+}/NTf_2^{-}$ (blue squares).

4.2.1.3 Temperature dependence of the water proton chemical shift

The entropically driven process of H-bond breaking makes the water proton chemical shift δ_{H2O} temperature dependent. Fig. 4.2.1.3 presents an example of chemical shift as a function of temperature for $Pyrr_{14}^{+}/ NTf_2^{-}$ with $x_{H2O} = 0.112$.

I have measured the temperature dependence of the chemical shift of the water proton δ_{H2O} for five samples: two samples of $(Pyrr_{14}/^{+} NTf_2^{-})$/water mixtures with water concentrations $x_{H2O} = 0.112$ and $x_{H2O} = 0.176$ and three samples of $(Pyrr_{14}^{+}/OTf^{-})$/water mixtures with water concentrations $x_{H2O} = 0.078$, $x_{H2O} = 0.126$ and $x_{H2O} = 0.204$. All measurements were performed for the range of temperatures from 268 K to 318 K.

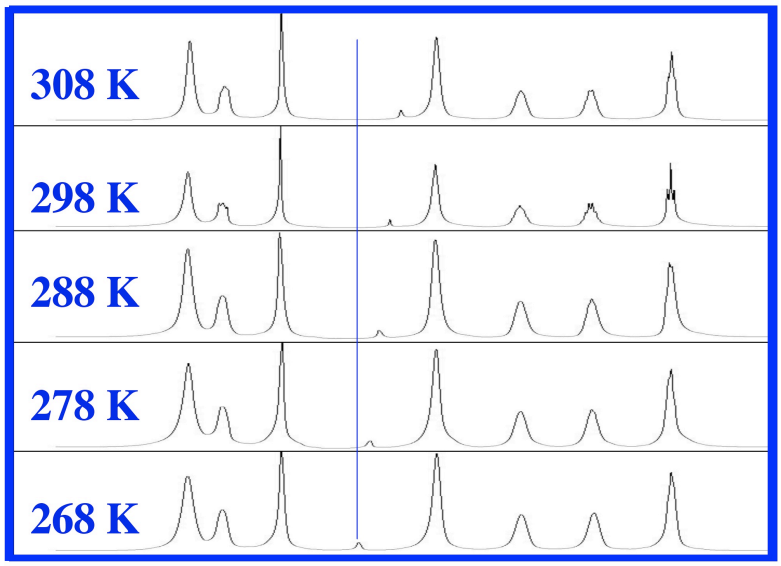

Figure 4.2.1.3 ^{1}H NMR spectrum of $Pyrr_{14}^{+}$/ NTf_2^{-}, $x_{H2O} = 0.112$ as a function of temperature. Note the shift of the water peak to lower ppm.

The sample $Pyrr_{14}^{+}$ /NTf_2^{-} with the highest water concentration $x_{H2O} = 0.176$ exhibits phase separation for temperatures below 278 K. No change in the appearance of the sample was noticed. The phase separation is deduced from the appearance of a bulk-water-like peak at 4.85 ppm that is coincident with a decrease of intensity of the dissolved water peak (water associated with anion) at 2.68 ppm. Because of phase separation, the temperature dependence of δ_{H2O} for $Pyrr_{14}^{+}$ /NTf_2^{-} with $x_{H2O} = 0.176$ was studied only for temperatures above 278 K. It is clearly seen in Fig. 4.2.1.4, that the plot of δ_{H2O} for $Pyrr_{14}^{+}$ /NTf_2^{-} with $x_{H2O} = 0.176$ deviates from linearity at the temperature below 278.2 K.

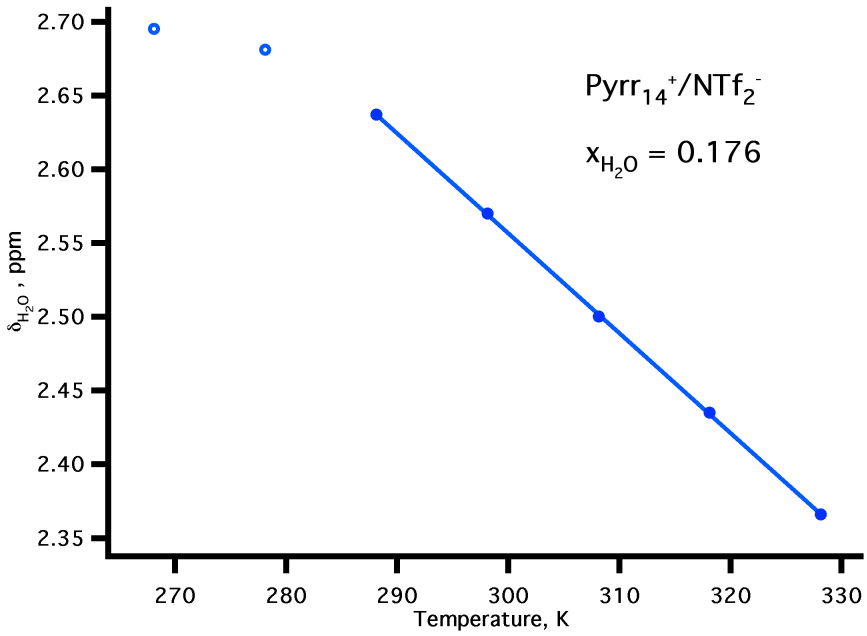

Figure 4.2.1.4 ^{1}H chemical shift for H_2O in $Pyrr_{14}^+/NTf_2^-$ with $x_{H2O} = 0.176$ as a function of temperature.

Fig. 4.2.1.5 shows the temperature dependence of the water proton chemical shift δ_{H2O} for all samples studied. Also, in order to compare the temperature dependence of δ_{H2O} of water dissolved in the IL with behavior of bulk water, we estimated the temperature dependence of δ_{H2O} for bulk water from equation 4.1.[7]

$$\delta_{H2O} = 7.83 - \frac{T}{96.9} \qquad \text{for pH} = 5.5 \qquad (4.1)$$

Experimental data for all five IL samples with added H_2O exhibit linear temperature dependence of the water proton chemical shift δ_{H2O}. However, the slopes of these linear dependencies are different. The values of the slopes are presented in table 4.2.1. The value of a slope reflects the interaction strength between the water molecule and the anion. Slopes are higher for samples with higher water concentration. This is an evidence for increased water-anion interaction with increasing water concentration

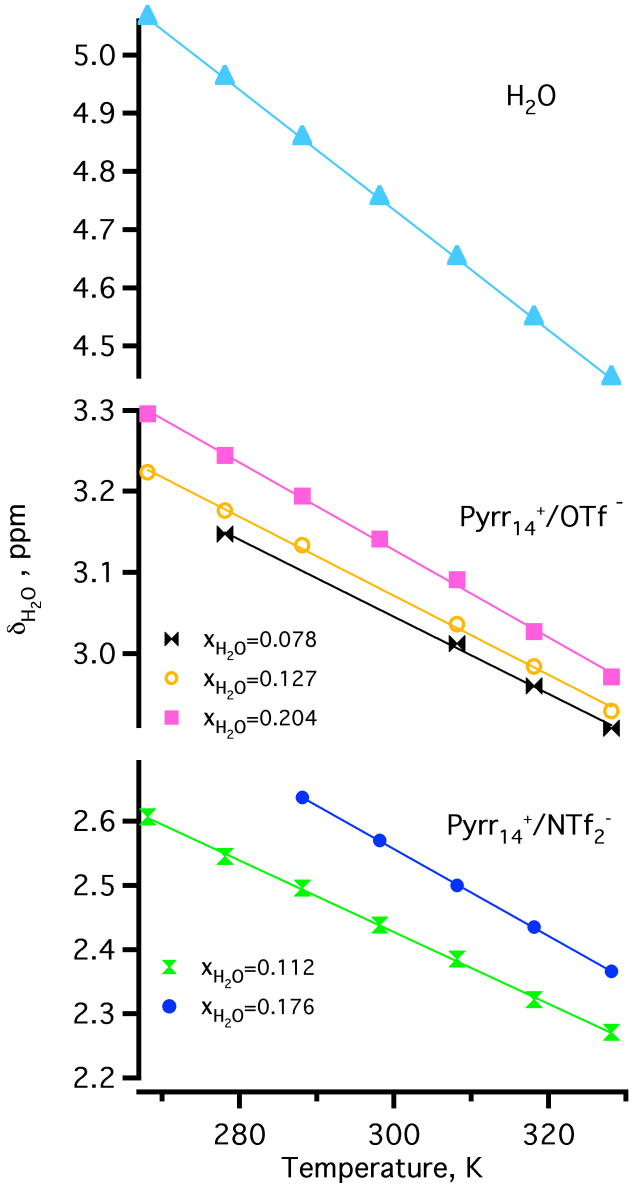

Figure 4.2.1.5 ^{1}H chemical shift for H_2O as a function of temperature. (top) bulk H_2O, (middle) H_2O in $Pyrr_{14}^{+}/OTf^{-}$, (bottom) H_2O in $Pyrr_{14}^{+}/NTf_2^{-}$.

in the IL. This observation is consistent with the fact that water-anion H-bonds became more polar with increasing water concentration. The value of δ_{H2O} is more strongly temperature dependent for bulk H_2O than for H_2O in either of the two ILs.

The values of the slopes that reflects strength of water-anion interaction are slightly higher for $Pyrr_{14}^{+}/NTf_2^{-}$ than for $Pyrr_{14}^{+}/OTf^{-}$ at the approximately equal water concentrations, despite the fact that water-anion bonds are more polar in the

($Pyrr_{14}^+/OTf^-$)/water systems. A possible explanation is that the interaction strength depends not on the concentration in mole fraction, but on the degree of saturation, meaning how close the water concentration is to saturation in the sample.

Table 4.2.1 The slopes of temperature dependencies of water chemical shift δ_{H2O}

Ionic Liquid	Concentration of water, x_{H2O}	Slope, ppm /K
$Pyrr_{14}^+NTf_2^-$	0.112	-0.0056
	0.176	-0.0068
$Pyrr_{14}^+OTf^-$	0.078	-0.0047
	0.127	-0.0049
	0.204	-0.0054
Water	1	-0.0103

4.2.1.4 Viscosity measurements

The viscosities were measured for dry IL samples, $Pyrr_{14}^+/NTf_2^-$, $x_{H2O} = 0.00023$ and $Pyrr_{14}^+/OTf^-$, $x_{H2O} = 0.00065$ over the temperature range 278-320 K. The temperature dependence of viscosity is shown in Fig. 4.2.1.6.

ILs are typically fragile glass-formers. One consequence is that the viscosity temperature dependence is better fit by a Vogel-Tammann-Fulcher (VTF) function than by an Arrhenius function.

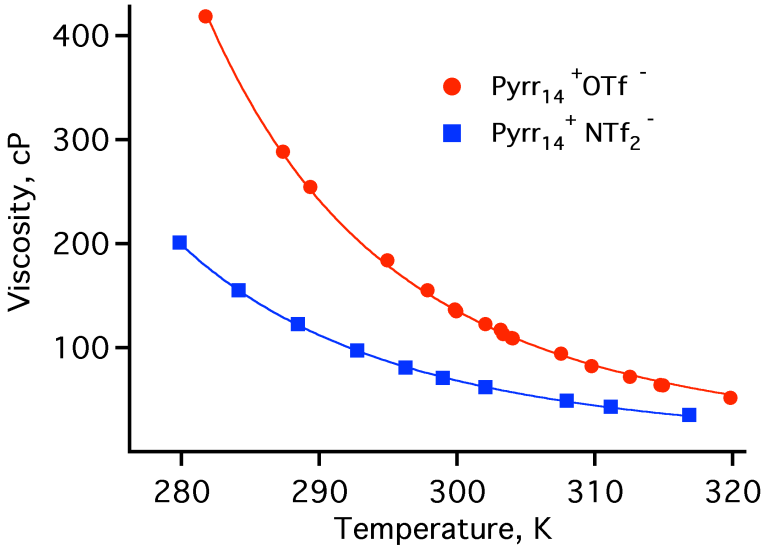

Figure 4.2.1.6 Temperature dependence of the viscosity for $Pyrr_{14}^{+}NTf_2^{-}$, x = 0.00023 and $Pyrr_{14}^{+}OTf^{-}$, x = 0.00065. The solid lines show the VTF fit to the equation 4.2.

I fit the viscosity data to the VTF model using equation 4.2. Following the method of Angell et al., the value for the viscosity at the glass transition temperature T_g was arbitrarily set to 10^{13} cP.[8] Values of T_g were obtained by J. F. Wishart et al., (Brookhaven National Laboratory) from DSC measurements using a scan rate of 10 K/min. [9] The viscosity data presented here for $Pyrr_{14}^{+}/NTf_2^{-}$ are in quantitative agreement with the values obtained by J. F. Wishart, et al., Brookhaven National Laboratory. Parameters for the fit of the viscosity data to the VTF model are found in table 4.2.2.

$$\eta(T) = \left(\eta_0 \exp\left(\frac{DT_c}{T - T_c} \right) \right)^{-1} \qquad (4.2)$$

where η is the viscosity at temperature T, η_0 is a reference viscosity at which the exponential term is 0 (high temperature limit), D is the fragility parameter, T_c is a characteristic temperature for which η diverges.

Table 4.2.2 Fit parameters of the viscosity data to the VTF model for $Pyrr_{14}^{+}/NTf_2^{-}$ x = 0.00023 and $Pyrr_{14}^{+}/OTf^{-}$, x = 0.00065

Ionic Liquid	$\ln(\eta_0)$	T_c	D	T_g
$Pyrr_{14}^{+}/NTf_2^{-}$	-2.375	156.7	-6.032	184
$Pyrr_{14}^{+}/OTf^{-}$	-4.442	129.5	-12.32	173

4.2.2 Determination of self-diffusion coefficients in the system IL/water

4.2.2.1. Physico-chemical background for Diffusional Ordered Spectroscopy

Diffusion in liquids is random translational motion of molecules or ions in three dimensions that arises from thermal energy under conditions of thermodynamic equilibrium. There is no thermal gradient leading to convection, nor concentration gradient.[10]

The NMR pulse-field gradient spin echo method is widely used for investigation of self-diffusion coefficients.[11-15] The specific pulse sequence used in the present research is a type of NMR Diffusion Ordered SpectroscopY (DOSY). When a magnetic field gradient is applied along the z-axis of an NMR tube, nuclear spins with different z-coordinate experience magnetic fields of different strengths and consequently, become dephased. Thus, nuclear spins become spatially labeled, so that their translational motion can be monitored.[10, 16-18] The degree of dephasing depends on the strength

of the applied field gradient, as shown in equation 4.2.2.1. Hence, the intensity of the NMR spin-echo signal was measured as a function of incremental gradient strength.

$$I_G = I_0 \exp\left(-(\gamma\delta G)^2 D\left(\Delta - \frac{\delta}{3}\right)\right) \qquad (4.2.2.1)$$

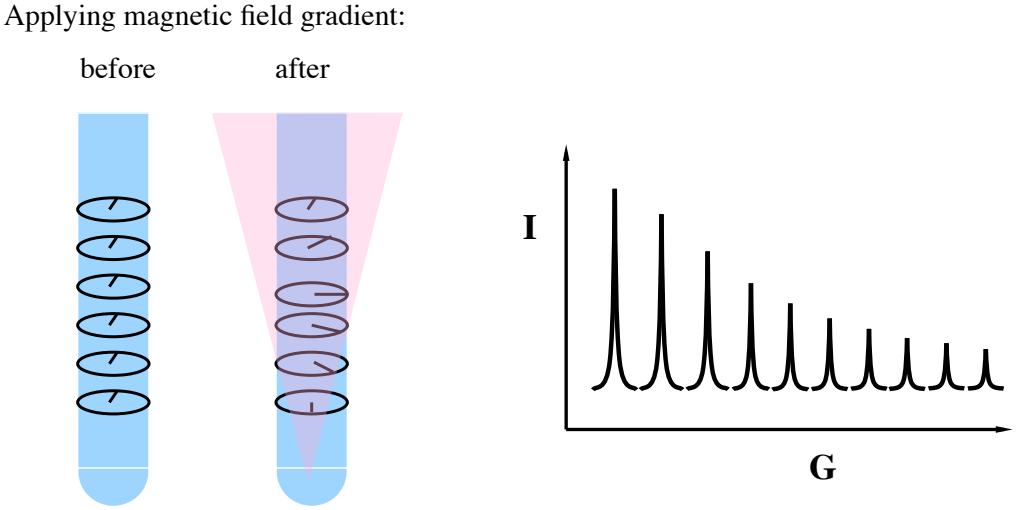

Figure 4.2.2.1 Illustration of Pulse Field gradient NMR method: (left) spins experiencing different strength of magnetic field became dephased. (right) Decay of spin-echo signal intensity with increasing gradient strength

The results of the DOSY experiments are presented in the form of a 2D spectrum with a chemical shift on the horizontal axis and the diffusion coefficient on the vertical axis. The typical 2D spectrum is shown in Figure 4.2.2.2 for the ^{1}H spectrum of $Pyrr_{14}^+/NTf_2^-$ with $x_{water} = 0.112$ (top) with diffusion coefficients for each peak of the ^{1}H spectrum (bottom). It is clearly seen that the diffusion coefficients for all peaks of the $Pyrr_{14}^+$ cation have approximately the same values and that the self-diffusion coefficient for water is much higher.

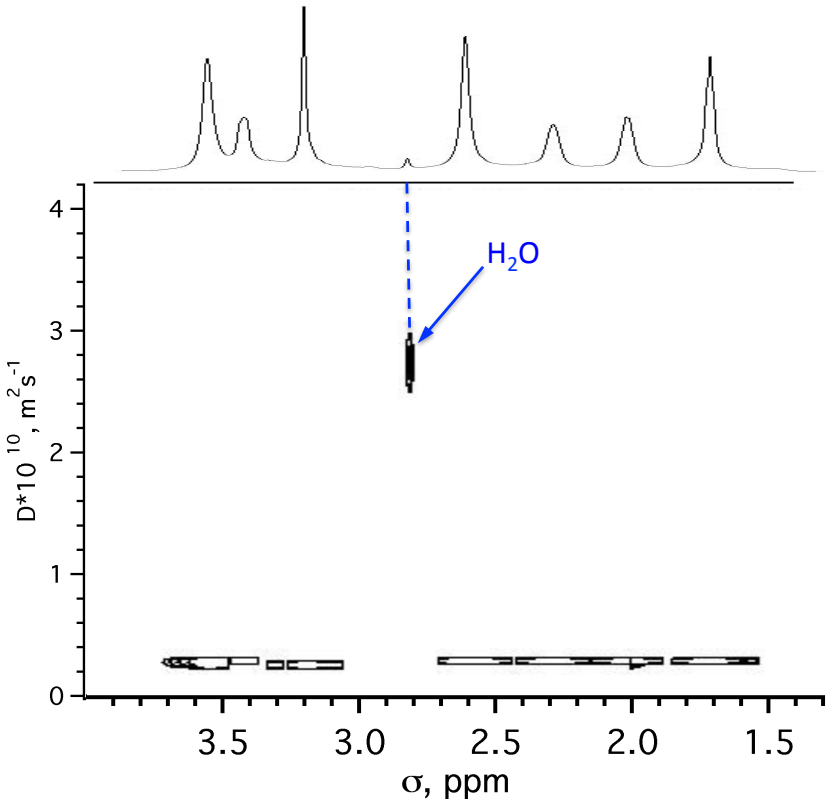

Figure 4.2.2.2 Top: Plot of ^{1}H NMR spectrum of $Pyrr_{14}^{+}/NTf_2^{-}$, x_{H2O} = 0.112. Bottom: Contour plot illustrating the difference between self-diffusion coefficients for the $Pyrr_{14}^{+}$ cation and for water.

The rough prediction for diffusivity in the IL can be done using the hydrodynamic theory of the Stokes-Einstein equation, which relates diffusivity with the radius of diffusing species, viscosity of the liquid and temperature as shown in equation 4.2.2.2.

$$D = \frac{K_B T}{c\pi\eta r} \qquad (4.2.2.2)$$

where D is self-diffusion coefficient, K_B is Boltzmanns constant, T is temperature (K), c is a "stick"or "slip" constant varying between 4 and 6, η is viscosity and r is radius of diffusing ion or molecule.

The Stokes-Einstein model (S-E) assumes the molecule is a spherical rotor and does not iclude the chemical interaction between molecules and ions. For this reason, the measured self-diffusion coefficient in the real liquid can be expected to deviate from the S-E predictions.[19]

In order to estimate diffusion coefficients using the S-E model we have estimated the radii for all diffusing species. The radii of ions r were calculated from the volume assuming a spherical shape. The volume was estimated by the Van der Waals atomic increment method.[20, 21] Atomic radii and volumes of diffusing species are found in table 4.2.2.1.

Table 4.2.2.1 Calculated molecular volumes and effective radii of diffusing species.

Ion or molecule	Volume ($Å^3$)	Radius (Å)
NTf_2^-	158.8	3.360
OTf^-	85.9	2.738
$Pyrr_{14}^+$	169	3.430
H_2O	20.6	1.700

The self-diffusion coefficients were measured for seven samples: three samples of ($Pyrr_{14}^+/NTf_2^-$)/water mixtures with water concentrations $x_{H2O} = 0.00023$, $x_{H2O} = 0.112$ and $x_{H2O} = 0.176$, and four samples of ($Pyrr_{14}^+/OTf^-$)/water mixtures with water concentrations $x_{H2O} = 0.00065$, $x_{H2O} = 0.078$, $x_{H2O} = 0.126$ and $x_{H2O} = 0.204$. For each IL, one sample was kept as dry as possible, namely the sample of $Pyrr_{14}^+/NTf_2^-$ with $x_{H2O} = 0.00023$ and sample of $Pyrr_{14}^+/OTf^-$ with $x_{H2O} = 0.00065$. We will refer to these samples as “dry” samples.

4.2.2.2 Temperature dependence of diffusion coefficients for IL cations and anions

The temperature dependence of the self-diffusion coefficients for ILs cations and anions was investigated over the range of temperatures from 278 K to 318 K. Fig. 4.2.2.3 exhibits the temperature dependence for cation self-diffusion coefficients for all seven samples. The self-diffusion coefficients are higher for less viscous $Pyrr_{14}^{+}/NTf_2^{-}$ than for $Pyrr_{14}^{+}/OTf^{-}$. Also, a dependence of diffusion on the water concentration in IL is observed. The higher self-diffusion coefficients are detected for samples with higher water concentration within samples based on the same IL.

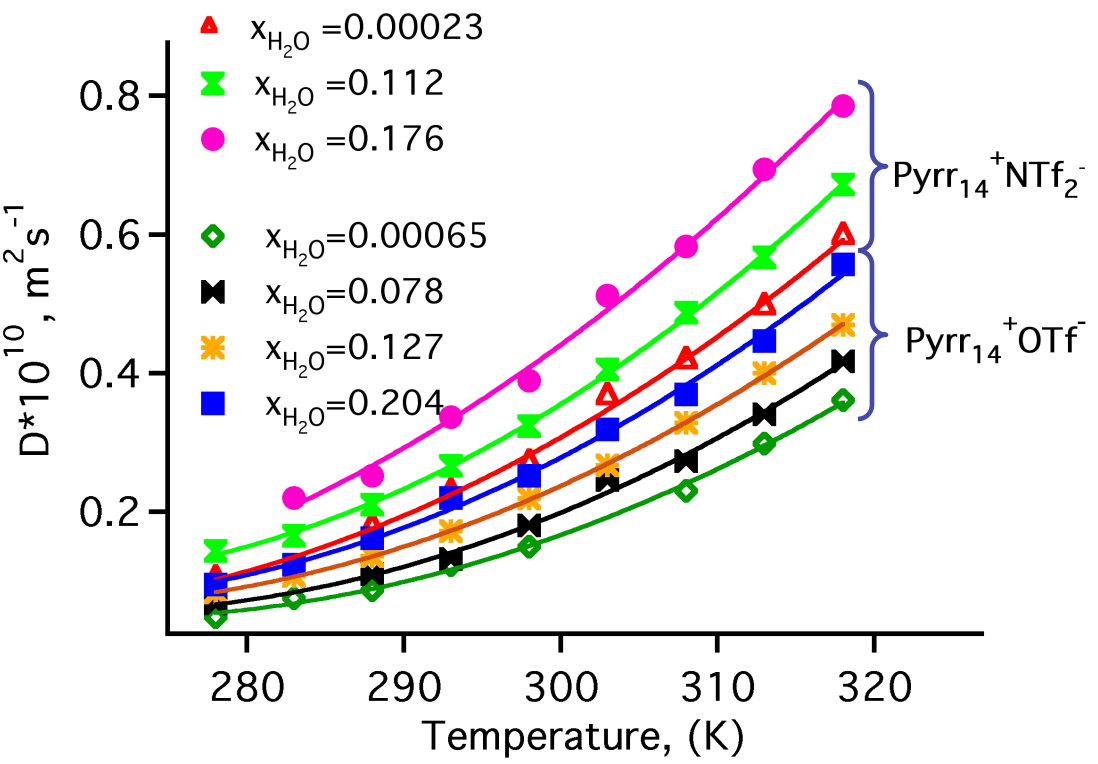

Fig. 4.2.2.3 Temperature dependence of the measured pyrrolidinium-ring-proton self-diffusion coefficients D_{cation} for the IL/water system. The solid lines shown are the VTF fit.

The values of the self-diffusion coefficients for anions are very close to the values for cations. The ratio D_{cation}/D_{anion} is oscillating around 1.1 for all samples at all temperatures as shown in Fig. 4.2.2.4

For $Pyrr_{14}^{+}/NTf_2^{-}$, the anion and the cation have very similar values of effective radii: 3.43 and 3.36 Å correspondingly. Therefore, it is unsurprising that the experimental data of D_{cation}/D_{anion} coincide with the theoretical prediction of Stokes-Einstein model. Whereas for $Pyrr_{14}^{+}/OTf^{-}$, the anion is 1.25 times smaller than the cation, but experimental data for D_{cation}/D_{anion} are approximately 1.1, as was the case for the $Pyrr_{14}^{+}/NTf_2^{-}$. The same trend was observed by other researchers.[15, 22] The possible explanation of this phenomenon is the different character of electrostatic interactions with neighboring ions in $Pyrr_{14}^{+}/OTf^{-}$ and $Pyrr_{14}^{+}/NTf_2^{-}$

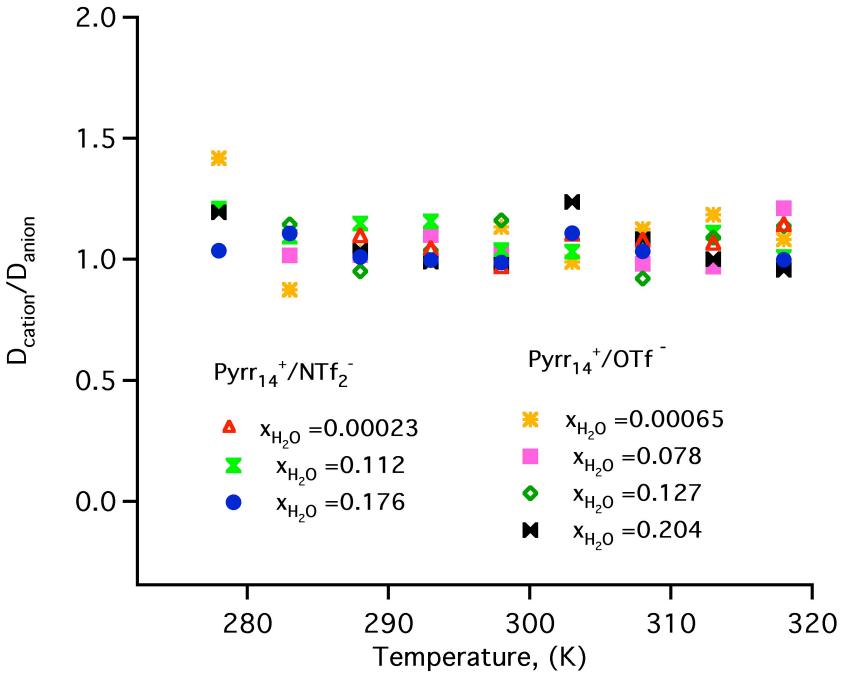

Figure 4.2.2.4 Temperature dependence of the ratio of cation to anion self-diffusion coefficients

4.2.2.3 The hydrodynamic model of self-diffusion in the ILs.

In order to compare experimental data with predictions of hydrodynamic model, we estimated self-diffusion coefficients for "dry" samples of both ILs by equation 4.3. The self-diffusion coefficients estimated from the Stokes-Einstein model are 2.56-1.90 times lower than experimental data for $Pyrr_{14}^{+}/NTf_2^{-}$ and 2.94 – 2.01 times lower for $Pyrr_{14}^{+}/OTf^{-}$. The temperature dependence of D_{cation}/ D_{S-E} is shown in Fig. 3.4.1.2. The deviations from theory were also reported by other authors. Song Chung, et al., reported a difference between experimental data and the S-E prediction of up to 10 times.[23] One of the possible explanations is that the S-E model does not consider interaction between charged particles (ions in the IL).

The ratio of observed to predicted diffusivities D_{cation}/D_{S-E} decrease with increasing temperature.

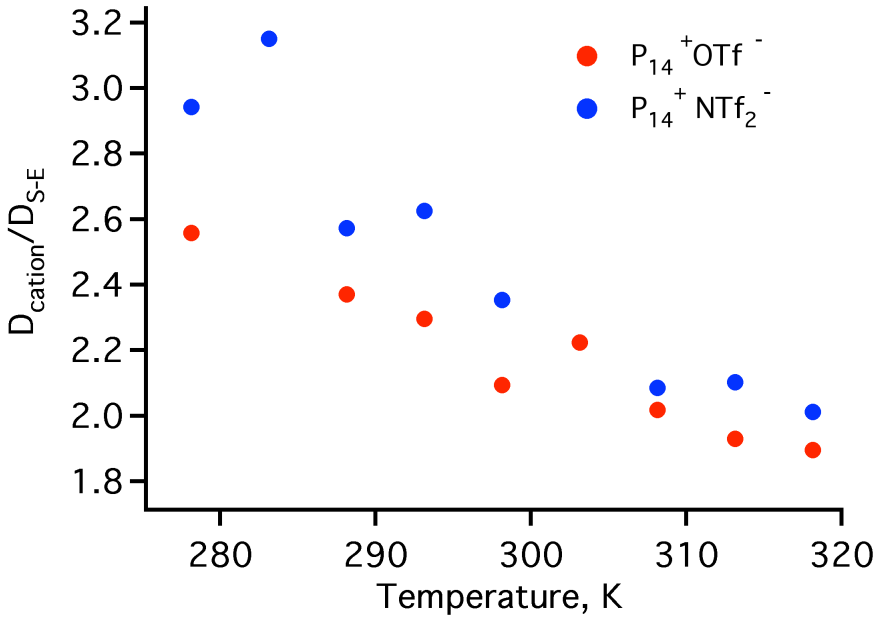

Figure 4.2.2.4 Temperature dependence of ratio between experimental value of self-diffusion coefficient for cation and self-diffusion coefficient estimated by Stokes-Einstein model for $Pyrr_{14}^{+}/NTf_2^{-}$, $x_{H2O} = 0.00023$ and $Pyrr_{14}^{+}/OTf^{-}$, $x_{H2O} = 0.00065$

One of the possible explanations is that the character of translational and rotational movement of cations is changing with growing temperature and the "slip and stick" constant **c** in the Stokes –Einstein equation is drifting from 4 to 6. However. It is difficult to imagine that the interactions becoming "stickier" with increasing temperature.

Despite deviation from the Stokes-Einstein model, the observed self-diffusion coefficients for ILs coefficients are well correlated with T/η according to the NMR study of the Watanabe group.[24] In order to compare diffusion behavior in $Pyrr_{14}^{+}/NTf_2^{-}$ and $Pyrr_{14}^{+}/OTf^{-}$ self-diffusion coefficients of cations and anions for both ILs were plotted against T/η as shown in Fig. 2.4.4.5. $Pyrr_{14}^{+}/NTf_2^{-}$ and $Pyrr_{14}^{+}/OTf^{-}$ share the same cation $Pyrr_{14}^{+}$, and it is not surprising that the self-diffusion coefficient of the cation exhibit very similar deviation from Stokes-Einstein model for both ILs. Plots of self-diffusion coefficients for the NTf_2^{-} and OTf^{-} anions reveal that OTf^{-} deviates slightly less from the S-E model than NTf_2^{-} does.

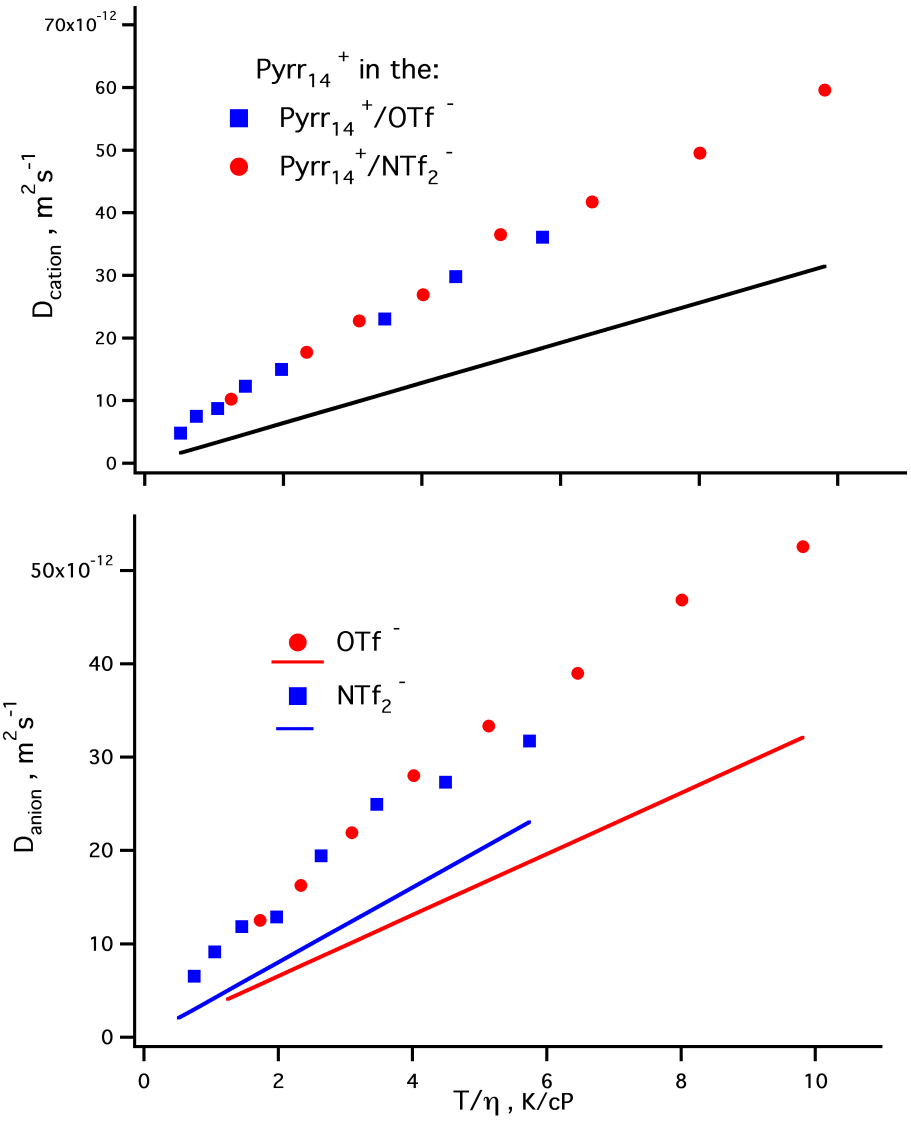

Figure 4.2.2.5 Self-diffusion coefficients of a) cations and b) anions plotted versus T/η illustrating deviation from Stokes-Einstein model. Solid line represents diffusion estimated from the S-E model.

$$D \propto \left(\frac{T}{\eta}\right)^{m} \qquad (4.4)$$

where $m \leq 1$

As for supercooled liquids, the diffusional behavior of ILs can be fit with a fractional S-E model as shown in equation 4.4.[19, 23] The best fit can be achieved with

c = 6 and m = 0.95. The fact that m is close to unity testifies that deviation from the Stokes–Einstein model is not substantial, as it is expected at the temperatures above 1.3 T_g .

4.2.2.6 Diffusion of $Pyrr_{14}^+$, NTf_2^- and OTf^- at infinite dilution in water at 296 K

Observing the deviation from the Stokes-Einstein model for diffusion in the pure ILs, we wonder about diffusional behavior of component cations and anions dissolved in the water. We measured self-diffusion coefficients for cations and anions of ILs dissolved in D_2O for concentrations close to the infinite dilution: $x_{H2O} = 0.0014$ for $Pyrr_{14}^+/NTf_2^-$ and $x_{H2O} = 0.0011$ for $Pyrr_{14}^+/OTf^-$. It is impossible to use lower concentration, because the NMR signal becomes too small for accurate determination of self-diffusion coefficients by the DOSY experiment. The self-diffusion coefficients were measured at the room temperature, 296 K. In order to avoid convection, we switched off temperature controller, because in the low viscous liquids, such as water, convection can evolve even at the smallest temperature gradient.

Contrary to the diffusion in pure ILs, when self-diffusion coefficients were higher than predicted by Stokes-Einstein model, diffusivity of the ions at the infinite dilution in water is approximately two times lower than predicted. Experimental values of self-diffusion coefficients of the cation are practically the same for both IL's, as it was expected from the fact that both liquids have the same cation. Diffusion of the smaller OTf^- anion is faster than for NTf_2^-. The values of self-diffusion coefficients and ratio between coefficients of different species, are presented in tables 4.2.2.2. and 4.2.2.3.

Table 4.2.2.2 Self-diffusion coefficients of the cation and anion measured at infinite dilution of ILs in the D_2O and estimated from Stokes-Einstein model.

Ion	radius (Å)	D_{ion} (m^2 s^{-1})		D_{S-E} (m^2 s^{-1})*
		water with ($Pyrr_{14}^+$ / NTf_2^-)	water with ($Pyrr_{14}^+$ / OTf^-)	
$Pyrr_{14}^+$	3.43	$4.4*10^{-10}$	$4.3*10^{-10}$	$6.2*10^{-10}$
NTf_2^-	3.36	$4.6*10^{-10}$		$6.4*10^{-10}$
OTf^-	2.74		$6.1*10^{-10}$	$7.9*10^{-10}$

*The self-diffusion coefficient was calculated for c=6.

Table 4.2.2.3 Ratio between self-diffusion coefficients of ions for ILs at infinite dilution.

	Ratio of radii	Inverse D_{ion} ratio
$Pyrr_{14}^+$/ $Pyrr_{14}^+$	1	1.02
$Pyrr_{14}^+$/ NTf_2^-	1.02	0.96
$Pyrr_{14}^+$/ OTf^-	1.25	1.39
NTf_2^-/ OTf^-	1.23	1.32

4.2.2.5 Activation energies for diffusion of anions and cations

In order to calculate the activation energies for diffusion we plot the self-diffusion coefficients vs. inverse temperature for all our samples. The logarithmic plot of self-diffusion coefficients for cations is presented in Fig. 4.2.2.6. A logarithmic plot of diffusion coefficients vs. inverse temperature does not show significant VTF character probably because the temperature range in our measurements was not large

enough. The semi-log plot of self-diffusion coefficients for anions in all the different samples fit to a straight line that allows the calculation of activation energies E_a from the Arrhenius equation, shown as equation 4.5,

$$D = D_0 \exp\left(\frac{-E_a}{RT}\right) \tag{4.5}$$

where D is self-diffusion coefficient, R is universal gas constant, T is temperature (K), and E_a is activation energy.

Activation energies for all samples for diffusion of the cation and anion are presented in the Table 4.2.2.4. As expected, activation energies of diffusion are smaller for less viscous $Pyrr_{14}^{+}NTf_2^{-}$ than for $Pyrr_{14}^{+}OTf^{-}$. Also, activation energies are higher for samples with larger water concentration.

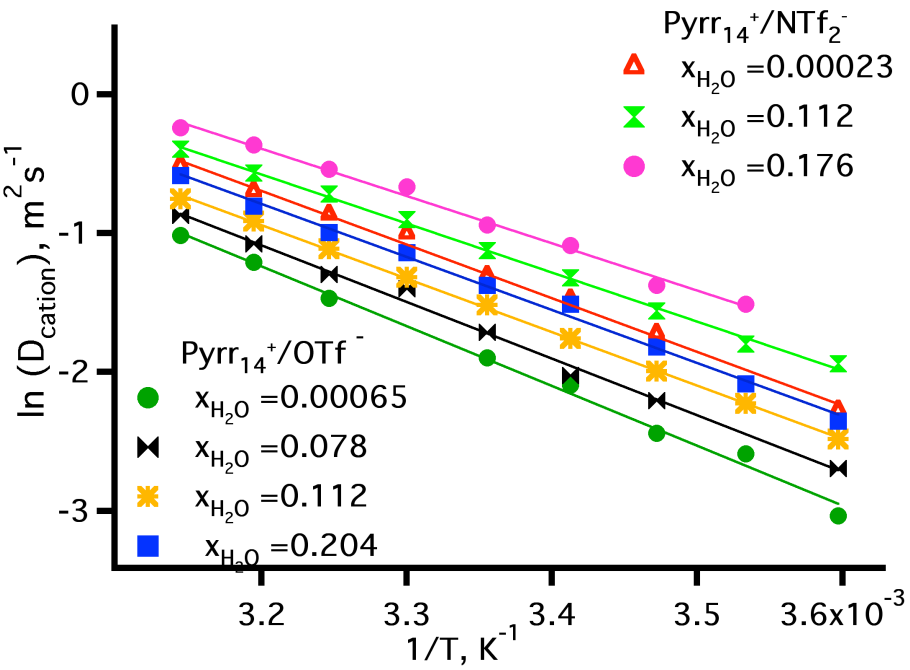

Figure 4.2.2.6 Temperature dependence of the self-diffusion coefficients D_{cation} for the IL/water system. The solid lines show are the linear fit.

Table. 4.2.2.4 Activation energies of diffusion for cation, anion and water in the IL/water system.

Ionic Liquid	$E_{a,\ cation}$ (kJ mol^{-1})	$E_{a.anion}$ (kJ mol^{-1})	$E_{a,water}$ (kJ mol^{-1})
$Pyrr_{14}^{+}$ / OTf^{-}			
x_{H2O}=0.00065	35.8	34.2	(dry)
x_{H2O}=0.078	34.0	34.5	*
x_{H2O}=0.127	32.0	32.4	*
x_{H2O}=0.204	31.8	32.2	25.3
$Pyrr_{14}^{+}$ / NTf_2^{-}			
x_{H2O}=0.00023	32.2	30.8	(dry)
x_{H2O}=0.112	30.0	31.7	29.3
x_{H2O}=0.176	29.8	30.4	23.3

4.2.2.7 Temperature dependence of diffusion coefficient of water

We have investigated diffusion of water for two samples of $Pyrr_{14}^{+}$ /NTf_2^{-} with water concentrations x_{H2O} = 0.112 and x_{H2O} = 0.176 and three samples of $Pyrr_{14}^{+}$/OTf^{-} with water concentrations x_{H2O} = 0.078, x_{H2O} = 0.127 and x_{H2O} = 0.204 in the range of temperatures 278.2 -318.2 K. The temperature dependence of self-diffusion coefficients for water is shown in Fig. 4.2.2.7.

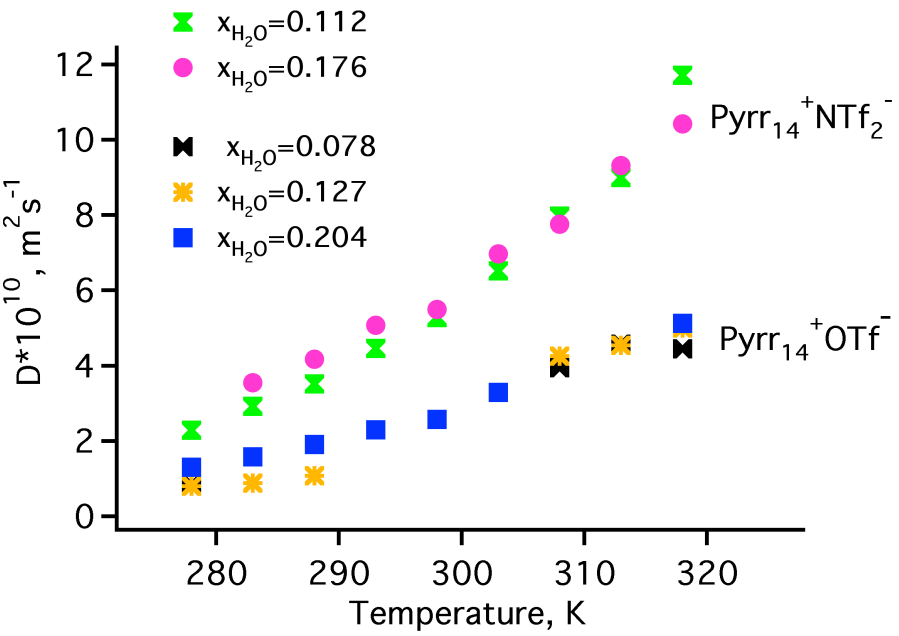

Figure 4.2.2.7 Temperature dependence of the water proton self-diffusion coefficients D_{H2O} in the IL/water system.

The water exhibits higher self-diffusion coefficients than the cation and anion of the ILs. According to the Stokes-Einstein equation, diffusion is inversely proportional to the radii of diffusing species as shown in equation 4.3. The effective radius of $Pyrr_{14}^{+}$ cation is 2.02 times larger than that of the water molecule. Thus it would be reasonable to expect that the water self-diffusion coefficient should be equal to about two larger than for the cation. But the experimental data exhibit much faster diffusivity of water in both ILs. The self-diffusion coefficient of the water is about 20 times larger than D_{cation} in the $Pyrr_{14}^{+}/NTf_2^{-}$, and 15 times larger in the $Pyrr_{14}^{+}/OTf^{-}$ as it is shown in Fig. 4.2.2.7 and Fig 4.2.2.8. Anomalously high diffusivity of water dissolved in ILs was also reported by other researchers.[22, 25] One possible explanation is that the microviscosity experienced by a water molecule is lower than the microviscosity experienced by ions of IL. Water present in the IL in a small amount is associated with anions.[6, 26] Therefore, if interaction between water and the anion is weaker than the interaction between ions of IL, then a water molecule experience less “friction” during diffusion.

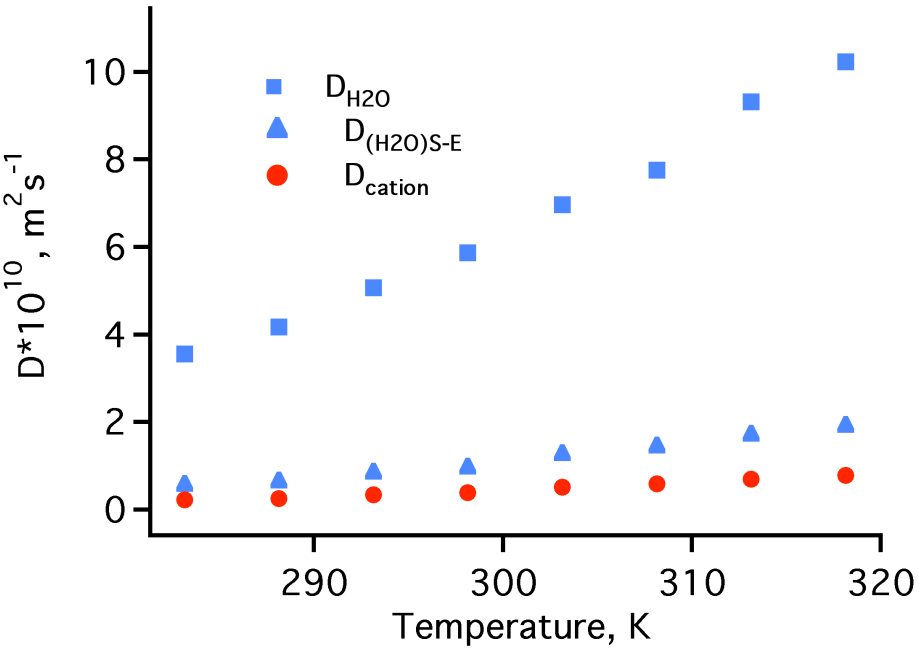

Figure 4.2.2.7 Temperature dependence of measured self-diffusion coefficients for the sample of $Pyrr_{14}^{+}/NTf_2^{-}$, $x_{H2O} = 0.176$. The data are shown for measured D_{cation} (red circles), for measured D_{H2O} (blue circles) and for $D_{(H2O)S-E}$ (self-diffusion coefficient of water proton estimated from Stokes-Einstein equation).

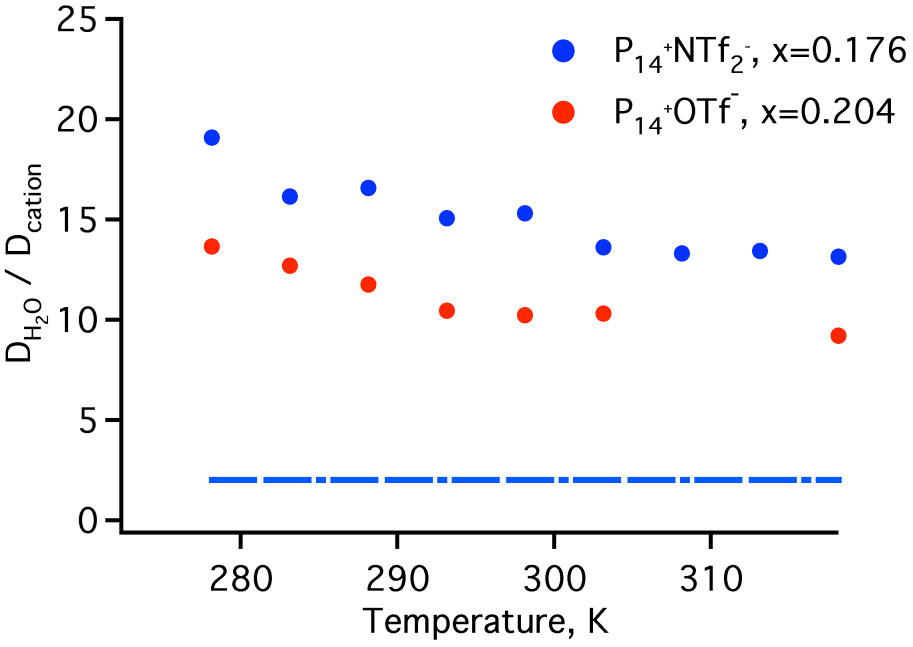

Figure 4.2.2.8 Temperature dependence of the ratio of self-diffusion coefficients for water and cation (D_{H2O}/D_{cation}). The dot-dashed line is D_{H2O}/D_{cation} predicted by S-E model.

The ratio D_{H2O} / D_{cation} is collinear for both ILs and slightly decreases with increasing temperature as shown in Fig 4.2.2.8. A possible explanation is that effective microviscosity for the water molecule decreases slower with increasing temperature than the effective microviscosity for the cation $Pyrr_{14}^{+}$.

The difference in the ratio D_{H2O} / D_{cation} for two ILs reflects the different interactions between water and the anions of these ILs. The interaction of the more hydrophobic NTf_2^- anion with water is weaker than the interaction of the less hydrophobic OTf^- anion[6] and as a consequence, the ratio D_{H2O} / D_{cation} in the $Pyrr_{14}^{+}$ NTf_2^- is higher than in the $Pyrr_{14}^{+}$/ OTf^-.

The E_a values for diffusion of water were calculated from the logarithmic plot of self-diffusion coefficients vs. inverse temperature. Activation energies E_a are shown in table 4.2.2.4 for samples $Pyrr_{14}^{+}$ / NTf_2^- with $x_{H2O} = 0.176$ and $x_{H2O} = 0.112$ and for $Pyrr_{14}^{+}$ / OTf^- with $x_{H2O} = 0.204$. A high experimental error for the determination of self-diffusion coefficient for samples with a small water concentration makes impossible determination of E_a for samples $Pyrr_{14}^{+}$ / OTf^- with $x_{H2O} = 0.078$ and $x_{H2O} = 0.127$. The activation energy E_a for water in the $Pyrr_{14}^{+}$ / NTf_2^- with $x_{H2O} = 0.176$ is slightly lower than E_a for water in the $Pyrr_{14}^{+}$ / OTf^- with $x_{H2O} = 0.204$. It can possibly be explained by weaker H-bonds formed by water with the anion of more hydrophobic $Pyrr_{14}^{+}$ / NTf_2^-.This coincides with the fact that the concentration and temperature dependence of diffusivity are evidence for a weaker water-anion interaction for more hydrophobic $Pyrr_{14}^{+}$ / NTf_2^-. The activation energy E_a for water in the $Pyrr_{14}^{+}$ / NTf_2^- with $x_{H2O} = 0.112$ is unexpectedly higher than both activation energies: E_a for the $Pyrr_{14}^{+}$ / NTf_2^- with $x_{H2O} = 0.176$ and E_a for $Pyrr_{14}^{+}$ / OTf^- with $x_{H2O} = 0.204$. It cannot be explained by convection in the sample, which would be the first guess for unreasonably high diffusivity. The cation and anion in that sample (the $Pyrr_{14}^{+}$ / NTf_2^-

with $x_{H2O} = 0.112$) does not show significant deviation from the general pattern. I believe that the high activation energy of water diffusion is due to experimental error that is higher for samples with a small water concentration.

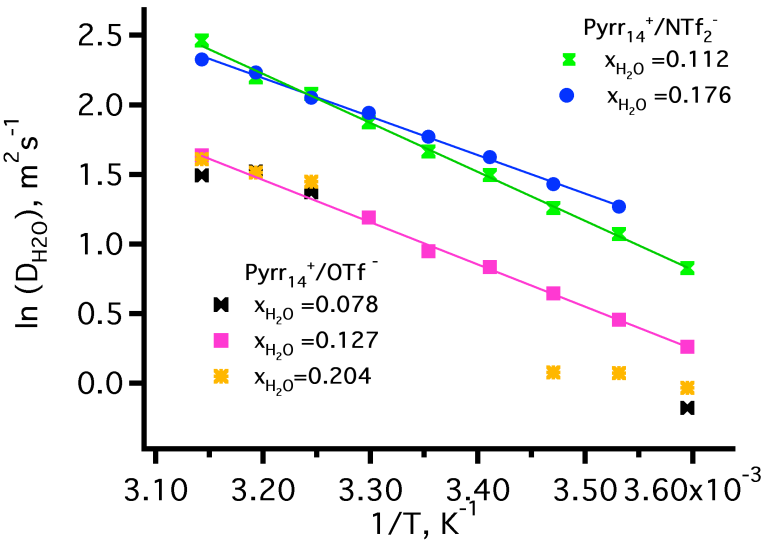

Figure 4.2.2.8 Log plot of self-diffusion coefficients of water vs. inverse temperature Solid lines shows the best fit. $Pyrr_{14}^+ / NTf_2^-$: $x_{H2O} = 0.112$ (green symbols); $x_{H2O} = 0.176$ (blue circles). $Pyrr_{14}^+ / OTf^-$: $x_{H2O} = 0.078$ (black symbols); $x_{H2O} = 0.127$ (yellow symbols) and $x_{H2O} = 0.204$ (pink squares).

4.3 Conclusions

The interaction between water and the IL was characterized by concentration dependence and temperature dependence of the chemical shift of the water proton δ_{H2O}. The water proton exhibits downfield shift of δ_{H2O} with increasing concentration of water in IL. The linear dependence of δ_{H2O} vs. concentration expressed as M_{H2O}/ M_{IL} has a different slope for $Pyrr_{14}^+/OTf^-$ and $Pyrr_{14}^+/NTf_2^-$ that reflects different water-anion interaction in these ILs[-].

The IL/water systems studied exhibit linear temperature dependence of δ_{H2O}. The increase in the values of the slope with increasing water concentration most likely

results from the higher fraction of water-water hydrogen bonds instead of water-anion bonds.

The diffusion properties were investigated in the system IL/water by pulse gradient DOSY experiments. The diffusional behavior of cations and anions is very similar whereas water exhibits an anomalously high diffusion rate.

The self-diffusion coefficients of anions and cations are similar to each other, with the ratio D_{cation}/D_{anion} oscillating around 1.1. Self-diffusion coefficients for both species are higher for less viscous $Pyrr_{14}^{+}/NTf_2^{-}$ than for $Pyrr_{14}^{+}/OTf^{-}$ and also higher for samples with a higher water concentration.

Comparison of diffusional behavior of "dry" samples of IL (samples with negligibly small water concentration) with predictions of Stokes-Einstein model reveal that diffusion of ions in ILs is approximately twice as fast; that can be explained by specificity of electrostatic interaction in the IL. Though, deviation from the S-E model is not substantial, the fit of experimental data to a fractional S-E equation exhibit $m = 0.95$, which is not far from unity.

Water exhibits anomalously high diffusion in the ILs. The ratio between self-diffusion coefficients of water and ions estimated by the S-E model is around 2, whereas this ratio from experimental data is around 20 for $Pyrr_{14}^{+}/NTf_2^{-}$, and it is around 15 for $Pyrr_{14}^{+}/OTf^{-}$.

The difference in the ratio D_{H2O} / D_{cation} for two ILs evidences that diffusional properties of water in ILs are connected with macroscopic hydrophobicity. Both macroscopic properties, hydrophobicity and rate of diffusion, are linked with a strength of interaction between water and anion that explains higher D_{H2O} / D_{cation} ratio for more hydrophobic $Pyrr_{14}^{+}/NTf_2^{-}$.

Activation energies of diffusion were calculated for the cation, anion and water. As expected, activation energies of faster diffusing species are lower. The E_a for water is lower than for anions and cations, E_a for less viscous $Pyrr_{14}^+/NTf_2^-$ is lower than for $Pyrr_{14}^+/OTf^-$ and E_a is lower for samples with higher water concentration.

References

1. R. P. Swatloski, S. K. Spear, J. D. Holbrey, R. D. Rogers, , *Dissolution of Cellulose with Ionic Liquids.* J. Am. Chem. Soc., 2002. **124**: p. 4974.
2. D. A. Fort, R. C. Remsing, R. P. Swatloski, P. Moyna, G. Moyna, R. D. Rogers, , *Can ionic liquids dissolve wood? Processing and analysis of lignocellulosic materials with 1-n-butyl-3-methylimidazolium chloride.* Green Chem., 2007. **9**: p. 63-69.
3. P. J. Dyson, T. J. Geldbach, *Applications of ionic liquids in synthesis and catalysis.* Electrochem. Soc. Interface, 2007. **16**: p. 50.
4. J. Dupont, R. F. de Souza, P. A. Z. Suarez, *Ionic Liquid (Molten Salt) Phase Organometallic Catalysis.* Chem. Rev., 2002. **102**: p. 3667.
5. K. Mizuno, Y. Miyashita, Y. Shindo, H. Ogawa, *NMR and FT-IR Studies of Hydrogen Bonds in Ethanol-Water Mixtures?* J. Phys. Chem., 1995. **99**: p. 3225.
6. L. Cammarata, S. G. Kazarian, P. A. Salter, T. Welton, *Molecular states of water in room temperature ionic liquids,.* Phys. Chem. Chem. Phys., 2001. **3**: p. 5192.
7. J. Cavanagh, W. J. Fairbrother, A. G. Palmer, N. Skelton, *Protein NMR Spectroscopy, Academic Press, San Diego, CA*1996.
8. W. Xu, E. I. Cooper, C. A. Angell, *Ionic Liquids: Ion Mobilities, Glass Temperatures, and Fragilities.* J. Phys. Chem. B, 2003. **107**: p. 6170.
9. A. M. Funston, T. A. Fadeeva, J. F. Wishart, E. W. Castner, Jr., *Fluorescence Probing of Temperature-Dependent Dynamics and Friction in Ionic Liquid Local Environments.* J. Phys. Chem. B, 2007. **111**: p. 4963.
10. W. S. Price, *NMR studies of translational motion* 2009.
11. R. Giernoth, D. Bankmann, N. Schlosrer, *High performance NMR in ionic liquids.* Green Chem., 2005. **7**: p. 279.
12. K. Hayamizu, S. Tsuzuki, S. Seki, Y. Ohno, H. Miyashiro, Y. Kobayashi,, *Quaternary Ammonium Room-Temperature Ionic Liquid Including an Oxygen Atom in Side Chain/Lithium Salt Binary Electrolytes: Ionic Conductivity and 1H, 7Li, and 19F NMR Studies on Diffusion Coefficients and Local Motions.* J. Phys. Chem. B, 2008. **112**: p. 1189.
13. K. Hayamizu, S. Tsuzuki, S. Shiro, *Molecular Motions and Ion Diffusions of the Room-Temperature Ionic Liquid 1,2-Dimethyl-3-propylimidazolium Bis(trifluoromethylsulfonyl)amide (DMPImTFSA) Studied by 1H, 13C, and 19F NMR.* J. Phys. Chem. A, 2008. **112**: p. 12027.
14. A. Wulf, K. Fumino, D. Michalik, R. Ludwig, *IR and NMR Properties of Ionic Liquids: Do They Tell Us the Same Thing?* European Journal of Chemical Physics and Physical Chemistry 2007. **8**: p. 2265.
15. H. Tokuda, K. Hayamizu , K. Ishii, M. A. B. H. Susan , M. Watanabe, *Physicochemical Properties and Structures of Room Temperature Ionic Liquids 2. Variation of Alkyl Chain Length in Imidazolium Cation.* J. Phys. Chem. B, 2005. **109**: p. 6103.
16. J. Keeler, *Understanding NMR spectroscopy* 2005: Wiley.
17. J. B. Lambert, E. P. Mazzola, *Nuclear Magnetic Resonance 5pectroscopy An Introduction to Principles, Applications, and Experimental methods.*2004: Pearson Education, Inc.

18. T. D. W. Claridge, *High-Resolution NMR Techniques in Organic Chemistry*, ed. J. E. Backvall, J.E. Baldwin, and R.M. Williams 2009: Elsevier.
19. K. R. Harris, *The fractional Stokes-Einstein equation: Application to Lennard-Jones,<p>molecular, and ionic liquids.* J. Chem. Phys., 2009. **131**: p. 054503.
20. J. T. Edward, *Molecular volumes and the Stokes-Einstein equation.* Journal of Chemical Education, 1970. **47(4)**: p. 261.
21. A. Bondi, *Van der Waals volumes and radii.* J. Phys. Chem., 1964. **68**: p. 441.
22. A. Menjoge, J. Dixon, J. F. Brennecke, E. J. Maginn, S. Vasenkov, *Influence of Water on Diffusion in Imidazolium-Based Ionic Liquids: A Pulsed Field Gradient NMR study.* J. Phys. Chem. B, 2009. **113**(18): p. 6353.
23. S. H. Chung, R. Lopato, S. Greenbaum, H. Shirota, E. W. Castner Jr., J. F. Wishart, *Nuclear Magnetic Resonance Study of the Dynamics of Imidazolium Ionic Liquids with CH2Si(CH3)3 vs CH2C(CH3)3 Substituents,.* J. Phys. Chem. B, 2007. **111**(18): p. 4885.
24. A. Noda, K. Hayamizu, M. Watanabe, *Pulsed-Gradient Spin−Echo 1H and 19F NMR Ionic Diffusion Coefficient, Viscosity, and Ionic Conductivity of Non-Chloroaluminate Room-Temperature Ionic Liquids.* J. Phys. Chem. B, 2001. **105**: p. 4603.
25. A. L. Rollet, P. Porion, V. Michel, B. Isabelle, D. Michael, B. Catherine, J. Laurence, *Anomalous Diffusion of Water in [BMIM][TFSI] Room-Temperature Ionic Liquid.* J. phys. Chem. B, 2007. **111**: p. 11888.
26. B. Fazio, A. Triolo, G. Di Marco, *Local organization of water and its effect on the srtuctural heterogeneities in room-temperature ionic liquid/H2O mixtures.* Journal of Raman Spectroscopy, 2008. **39**: p. 233.

Chapter 5

Future directions

The introduction of Ionic Liquids into the pool of chemical solvents leads to new approaches for engineering laboratory experiments and technology processes. A researcher can design a new solvent having the required properties instead of searching among existing solvents.[1] The use of Ionic Liquids in the processing of cellulose is a vivid example of task-specific solvent design.[2, 3]

The diversity of IL properties encourages their application in many fields such as catalysis, biocatalysis, biomass processing, energy production and many others.[4-12] However, design of ILs with required properties brings the necessity for a detailed understanding of how physico-chemical properties of ILs depend on their structure. The methods of fluorescence and NMR spectroscopies are widely used for investigation of the structure and physico-chemical properties of ILs, particularly for investigation of the solvation dynamics and diffusional properties of ILs.[13-17] Conclusions from the preceding chapters can serve as a starting point for future research of molecular-level scrutiny of ILs.

The investigation of diffusion properties in the framework of this dissertation shows the dependence of the diffusional behavior on the solute/solvent interaction in the systems IL/water. The ratio D_{H2O}/D_{cation} is different in the IL/water systems based on the

$Pyrr_{14}^{+}$ /OTf^{-} and more hydrophobic $Pyrr_{14}^{+}$ /NTf_2^{-}. This difference provides evidence that diffusional properties of water in ILs are connected with macroscopic hydrophobicity. Both macroscopic properties, the hydrophobicity and the rate of diffusion, are linked with strength of interaction between the water molecule and the anion.

The investigation of diffusional properties for solutes other than water can elucidate more general trends in the dependence of diffusion on the solute/IL interaction.

One of possible schemes for research can be investigation of diffusion in the systems solute/IL, where solute will vary from polar to non-polar species and the IL is held fixed. Another possible scheme is to monitor the diffusion in the systems with a fixed solute and ILs with varying polarity and hydrophobicity.

Another important property of ILs as solvents is solvation dynamics. The heterogeneous solvation dynamics in the ILs designates the broader distribution of solvation rates, as was discussed in the Chapter 3. Investigation of the solvation properties of the systems solute/IL for solutes with varying polarity can explain trends in the solvation dynamics.

Also, permutations of solutes and ILs with varying properties can be used for investigation of trends in the solvation and diffusion for solutes that make hydrogen bonds with anion or cation.

The application of ILs in medicine, pharmacy, batteries, bio-engineering and drug-delivery may involve the use of ILs in gel-like form. Investigation of diffusional properties in the IL-based gels can be required for characterization of these systems. Investigation of the diffusion of the ILs anions and cations through a membrane can help in the biological application of ILs.

Another rapidly growing field of ILs application in industry is their use in the processes such as gas storage, selective capture of a particular gas from the mixture, purification of air and other processes involving dissolution of various gases in the ILs.[18] Understanding these processes requires detailed knowledge of gas exchange dynamic, solvation dynamics of gases and diffusion in the systems gas/IL. The broader distribution of solvation rates in ILs described in this dissertation will possibly also be observed in the gas/IL systems. Investigation of dependence of diffusion on the gas/IL interaction can elucidate trends for comparative diffusion of various gases, that is important for selective gas capture processes.

Many applications of ILs such as fuel cells, biomass processing, enzyme catalysis and many others involve the presence of water in ILs. Further investigation of IL/water interaction may elucidate physico-chemical properties of these systems and denote limitations in their application. Among possible research directions can be named the search for ILs with highest possible hydrophobicity. Such ILs will be useful in processes when the presence of water is undesirable, for example for catalysis where even traces of water can deactivate the catalyst.[19]

Water dissolved in the ionic liquids has different properties compared to bulk water. Water molecules make H-bonds to the IL anions instead of H-bonds to other water molecules. The strength of these bonds depend on the structure of the anion, as was discussed in Chapter 4. Investigation of reactive properties of water dissolved in various ILs can suggest new possibilities of application for H_2O/IL systems and expose limitations concerned with side effects of water presence on processes in ILs.

Further investigation of the structure and properties of ILs will make possible their broader application in industrial processes. That will be an important step in the fight of humanity with global energy and ecology crises. Broader introduction of Ionic Liquids in industry will help to surmount many drawbacks of today's industrial technologies. It can, for example, help to avoid loss of solvents in the form of vapor, replace toxic solvents in some industrial processes, make catalysis more effective and find many other interesting solutions for industrial problems.

Multiformity of IL is an answer for daily changing needs of rapidly upcoming technologies.

References

1. A. E. Visser, R. P. Swatloski, W. M. Reichert, R. Mayton, S. Sheff, A. Wierzbicki, J. H. Davis Jr, R. D. Rogers, , *Task-specific ionic liquids for the extraction of metal ions from aqueous solutions.* Chem. Commun., 2001(2): p. 135.
2. R. P. Swatloski, S. K. Spear, J. D. Holbrey, R. D. Rogers, , *Dissolution of Cellulose with Ionic Liquids.* J. Am. Chem. Soc., 2002. **124**: p. 4974.
3. D. A. Fort, R. C. Remsing, R. P. Swatloski, P. Moyna, G. Moyna, R. D. Rogers, , *Can ionic liquids dissolve wood? Processing and analysis of lignocellulosic materials with 1-n-butyl-3-methylimidazolium chloride.* Green Chem., 2007. **9**: p. 63-69.
4. M. Armand, F. Endres, D. MacFarlane, H. Ohno, B. Scrosati, *Ionic-liquid materials for the electrochemical challenges of the future.* Nature mater. , 2009. **8**: p. 621.
5. D.R. Macfarlane, M. Forsyth, P. C. Howlett, J. M. Pringle, G. Annat, W. Neil, E. Izgorodina,, *Ionic Liquids in Electrochemical Devices and Processes: Managing Interfacial Electrochemistry.* Acc. Chem. Res. , 2007. **40**: p. 1165.
6. S. M. Zakeeruddin, M. Graetzel, , *Solvent-Free Ionic Liquid Electrolytes for Mesoscopic Dye-Sensitized Solar Cells.* Adv. Funct. Mater., 2009. **19**: p. 2187.
7. R. F. de Souza, J. C. Padilha, R. S. Gonßcalves, J. Dupont, *Room temperature dialkylimidazolium ionic liquid-based fuel cells.* Electrochem. Comm., 2003. **5**: p. 728.
8. A. P. Abbott, K. J. McKenzie, *Electrodeposition of Metals using ionic Liquids.* Phys. Chem. Chem. Phys., 2006. **8**: p. 4265.
9. A. K. Chakraborti, S. R. Roy, *On Catalysis by Ionic Liquids.* J. Am. Chem. Soc., 2009. **131**: p. 6902.
10. J. Dupont, R. F. de Souza, P. A. Z. Suarez, *Ionic Liquid (Molten Salt) Phase Organometallic Catalysis.* Chem. Rev., 2002. **102**: p. 3667.
11. P. J. Dyson, T. J. Geldbach, *Applications of ionic liquids in synthesis and catalysis.* Electrochem. Soc. Interface, 2007. **16**: p. 50.
12. A. J. Walker, N. C. Bruce, *Cofactor-dependent enzyme catalysis in functionalized ionic solvents.* Chem. Comm., 2004: p. 2570.
13. E. W. Castner Jr., M. Maroncelli, G. R. Fleming, , *Subpicosecond resolution studies of solvation dynamics in polar aprotic and alcohol solvents.* J. Chem. Phys., 1987. **86**: p. 1090.
14. M. Maroncelli, G. R. Fleming, , *Picosecond solvation dynamics of coumarin 153: the importance of molecular aspects of solvation.* J. Chem. Phys., 1987. **86(11)**: p. 6221.
15. H. Tokuda, K. Hayamizu , K. Ishii, M. A. B. H. Susan , M. Watanabe, *Physicochemical Properties and Structures of Room Temperature Ionic Liquids*

2. Variation of Alkyl Chain Length in Imidazolium Cation. J. Phys. Chem. B, 2005. **109**: p. 6103.

16. K. Hayamizu, S. Tsuzuki, S. Shiro, *Molecular Motions and Ion Diffusions of the Room-Temperature Ionic Liquid 1,2-Dimethyl-3-propylimidazolium Bis(trifluoromethylsulfonyl)amide (DMPImTFSA) Studied by 1H, 13C, and 19F NMR.* J. Phys. Chem. A, 2008. **112**: p. 12027.
17. R. Giernoth, D. Bankmann, N. Schlosrer, *High performance NMR in ionic liquids.* Green Chem., 2005. **7**: p. 279.
18. M. J. Muldoon, S. N. V. K. Aki, J. L. Anderson, J. K. Dixon, J. F. Brennecke, *Improving Carbon Dioxide Solubility in Ionic Liquids.* J. Phys. Chem. B, 2007. **111 (30)**: p. 9001.
19. T. Welton, *Room-Temperature Ionic Liquids. Solvents for Synthesis and Catalysis.* Chem. Rev., 1999. **99**: p. 2071.